Immobilized Carbon Nanofibers; a Novel Structured Catalyst Support

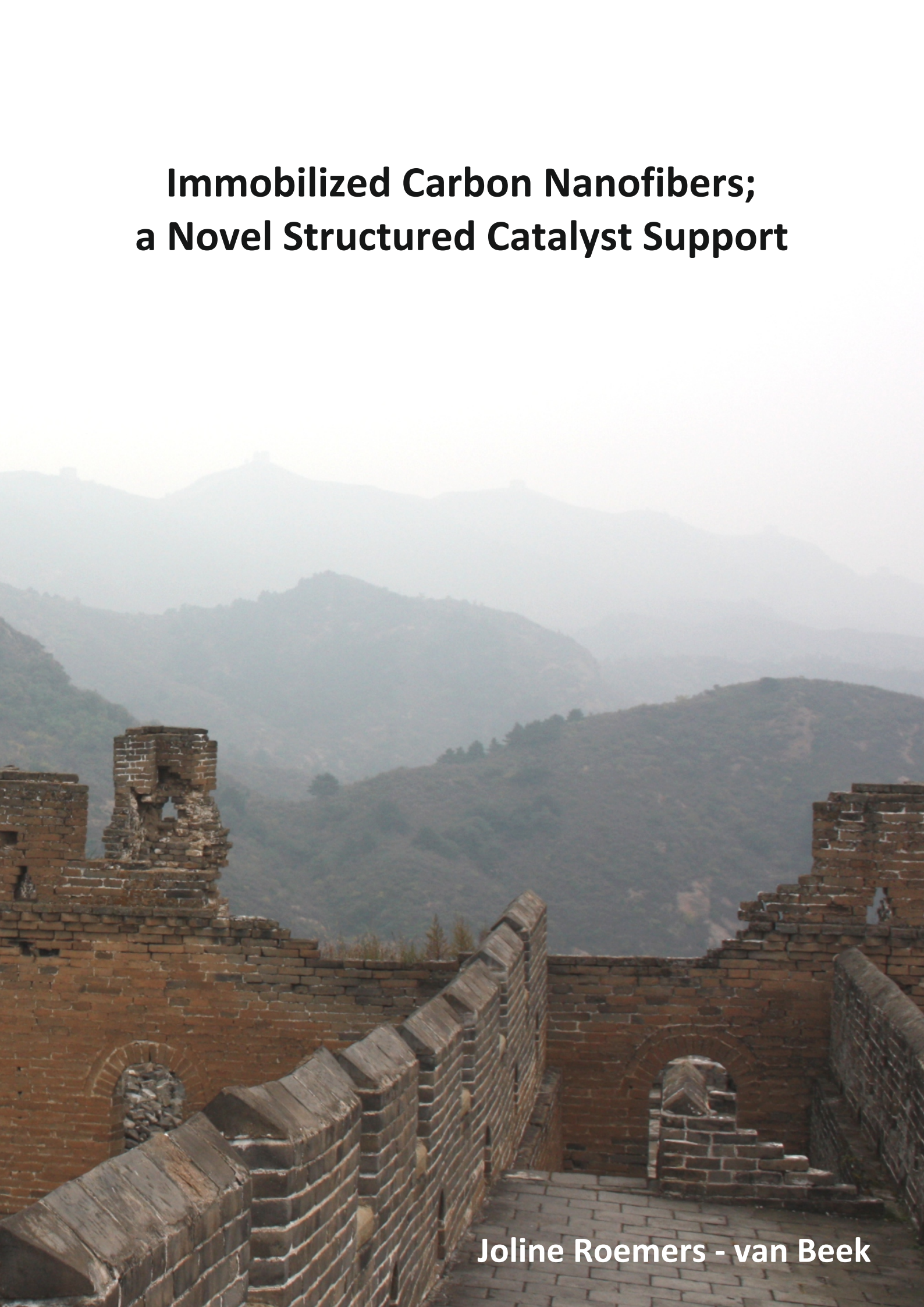

Joline Roemers - van Beek

IMMOBILIZED CARBON NANOFIBERS;

A NOVEL STRUCTURED CATALYST SUPPORT

Promotion committee:

Chairman:	Prof. Dr. Ir. J.W.M. Hilgenkamp	University of Twente
Promotor:	Prof. Dr. Ir. L. Lefferts	University of Twente
Members:	Dr. J.G. van Ommen	University of Twente
	Prof. Dr. Ir. R.G.H. Lammertink	University of Twente
	Prof. Dr. G. Mul	University of Twente
	Dr. M.G. Willinger	Fritz-Haber-Institute of the Max-Planck-Society
	Prof. Dr. F Kapteijn	Technical University of Delft
	Dr. Ir. A.N.R. Bos	Shell

The research described in this thesis was carried out at the Catalytic Processes and Materials group of the MESA+ Institute for Nanotechnology and the Faculty of Science and Technology of the University of Twente, P.O. Box 217, 7500 AE Enschede, The Netherlands.

This project took place within the framework of the Institute for Sustainable Process technology (ISPT).

Cover Design: Joline Roemers - van Beek and Arnout Roemers

ISBN: 978-90-365-4477-1

Printed by: Gildeprint, Enschede, The Netherlands

IMMOBILIZED CARBON NANOFIBERS; A NOVEL STRUCTURED CATALYST SUPPORT

DISSERTATION

to obtain
the degree of doctor at the University of Twente,
on the authority of the rector magnificus,
prof.dr. T.T.M. Palstra,
on account of the decision of the graduation committee,
to be publicly defended
on Friday the 16th of February 2018 at 14.45

by

Joline Miranda Roemers - van Beek

born on 24th of August 1985
in Hengelo, The Netherlands

This dissertation has been approved by:

Supervisor: Prof. Dr. Ir. L. Lefferts

Table of contents

Chapter 1: Introduction **1**

1.1 Commercial reactors 2

1.2 Structured reactors 2

1.3 Carbon Nanofibers 7

1.4 Nitrite Hydrogenation 8

Scope of the thesis 9

References 11

Chapter 2: Initiation of Carbon Nanofiber Growth on Polycrystalline Nickel Foam at low Ethylene Pressure **15**

2.1 Introduction 17

2.2 Experimental 19

2.3 Results and Discussion 22

2.4 General Discussion 33

2.5 Conclusion 35

References 36

Supporting Information 39

Chapter 3: Immobilization of Carbon Nanofibers (CNFs) on a Stainless Steel Filter as a Catalyst Support Layer **41**

3.1 Introduction 43

3.2 Experimental 44

3.3 Results 49

3.4 Discussion 57

3.5 Conclusion 60

References 62

Supporting Information 64

Chapter 4: Hydrogenation of Nitrite on Pd Supported on Immobilized CNF Agglomerates on a Stainless Steel Filter 65

4.1 Introduction 67

4.2 Experimental 68

4.3 Results 72

4.4 Discussion 76

4.5 Conclusions 79

References 80

Chapter 5: Conclusions and Recommendations 83

5.1 CNF Growth Initiation 84

5.2 Reversible Catalyst Loading 86

5.3 Nitrite Hydrogenation 89

References 95

Summary 97

Samenvatting 99

List of Publications 101

Acknowledgements 105

Chapter 1

Introduction

1.1 Commercial reactors

Part of the commercial catalytic chemical reactions are heterogeneous reactions, with three-phase gas-liquid-solid reactions (G-L-S) representing an important part. In three phase reactions reactants in gas and liquid phase are brought into contact with a solid catalyst. These are typically conducted in slurry phase reactors or trickle bed reactors. The advantages of a slurry phase reactor are low pressure drop, relatively small catalyst particles (typically tens of μms), causing low diffusion limitations, good external mass transfer and easy heat control. Drawbacks however are the separation of the products from the catalyst particles and the attrition caused by the needed stirring. In packed bed trickle phase reactors this separation is easy and there is no attrition, but drawbacks are pressure drop over the bed and mass transfer diffusion limitations, due to the large catalyst support particles (typically several mms). The particle size and the pressure drop are a trade-off. Other drawbacks are uneven distribution of reactants, possibly causing hotspots, stagnant zones or channeling [1, 2].

1.2 Structured reactors

For several years now, structured reactors are being studied as an alternative for conventionally used reactors [2-5]. In structured reactors a structured packing is used, which is designed to be the catalyst support while also regulating the liquid/gas flow through its highly regular structure. Structured reactors combine the advantages of slurry and fixed bed reactors [6, 7]. Products are easily separated as the catalyst is immobilized and diffusion limitations can be kept low by fine-tuning the catalyst support structure. Disadvantages are higher catalyst (immobilization) costs, moderate catalyst loading per reactor volume and liquid maldistribution.

To enable sufficient loading of the highly dispersed catalyst particles, high surface areas are necessary for the catalyst support structures. Most commonly used is the monolithic structure (Figure 1a) [6, 8], but also metal structures (Figure 1b), foams (Figure 1c) [9-11], filters, cloth [11] and wires are used.

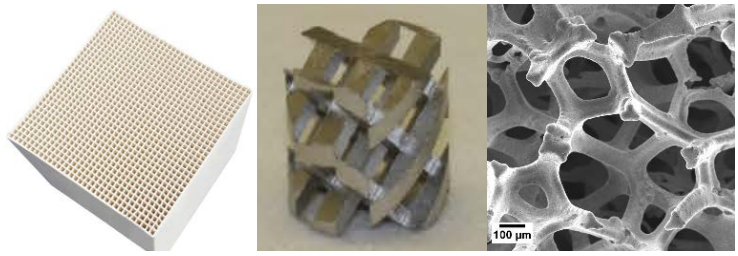

Figure 1: Different structured packings a) Monolith, b) SMX (Sulzer Chemtech Ltd) [12], c) Nickel foam structure

A critical factor for commercial application of structured reactors is the catalyst lifetime. Removal of deactivated catalyst requires the removal of the structured support, therefore the manufacturing costs of the structured support loaded with catalyst are higher. This higher cost can be negated by having a catalyst that is stable for a very long time [13, 14]. An alternative is to develop a procedure to recover the deactivated catalyst particles from the support structure, without removal of the support structure itself from the reactor, lowering the cost of catalyst manufacturing.

1.2.1 Foams/Filters

Foams are very open, three-dimensional structures that can consist of metal, ceramic, carbon or polymer. Foam porosity can range up to 97%, giving it a very open structure and therefore low pressure drop, while having a higher external surface area compared to for instance the external surface of spherical pellets used for conventional packed beds. Foams consist of highly irregular structures, but exhibit great accessibility to the external surface and low pressure drop; characteristics typical for structured reactors. Therefore we consider them structured reactors.

1.2.2 Washcoat

Many structured reactors, *e.g* based on monoliths and foams, have suitable external surface area, but insufficient surface area on a microscale for supporting active metal particles because of the absence of micropores. An increase in surface area available for supporting the active phase is required to increase the amount of active

sites available for the reaction to ensure competitive capacity per m^3 reactor volume compared with conventional reactors. This is commonly achieved by applying a washcoat. Washcoats consist of a highly porous support layer in which the catalyst nanoparticles can be loaded, as can be seen from Figure 2. A typical example of a washcoat material is alumina. Increasing the layer thickness of washcoats gives a trade-off between additional surface area and increasing internal diffusion limitation. This is especially the case in liquid phase operation, as D_{mol} for liquids is much lower than for gases, which increases the Thiele modulus, as can be seen from Equation 1. An optimal layer thickness is usually found at 10-100 µm.

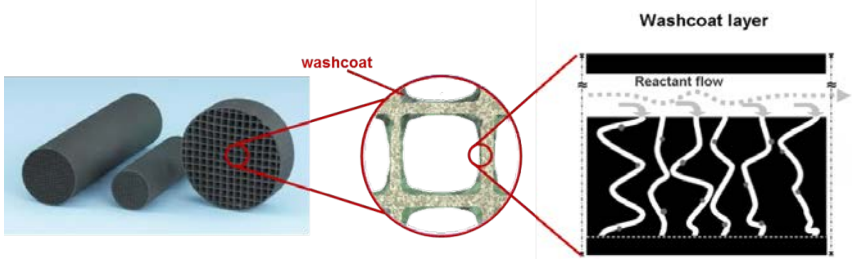

Figure 2: Inside a monolithic structure a washcoat is used to increase the available surface area on which catalyst particles can be deposited [15]

1.2.2.1 Diffusion limitations

There are seven steps occurring in heterogeneous catalytic reactions, as can be seen from Figure 3. First the reactants, both liquid and solid, need to diffuse through the stagnant or boundary layer on the outside of the catalyst particle. Second the reactants need to diffuse into the catalyst particle, in conventional catalysts this means diffusion into the pores of the support, for the suggested Carbon Nanofiber (CNF) layer it means diffusion into the void space between the CNFs. Thirdly the reactants adsorb at the catalytic site. Fourth is the reaction to products. Then the products need to desorb from the surface (step 5), diffuse out of the catalyst particle (step 6) and through the stagnant layer (step 7) [1, 16].

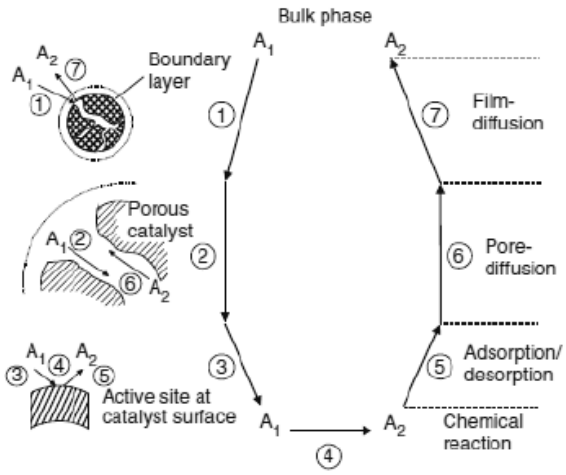

Figure 3: Seven steps of heterogeneous catalytic reaction on a porous catalyst [17]

Internal diffusion limitations can be reduced by decreasing the diffusion length R (smaller particles), increasing the porosity ε (more open particles) and decreasing the tortuosity τ (less winding pores). A commonly used factor to evaluate the presence of internal diffusion limitations is the Thiele modulus, φ (Equation 1) [1, 16, 18]. If the Thiele modulus approaches zero there are no internal diffusion limitations. If the Thiele modulus is large there are strong internal diffusion limitations, up to the extreme case where the reactants do not diffuse into the particle at all and the reaction will take place at the external surface of the catalyst particle.

$$\varphi = R\sqrt{\frac{kC_{As}^{n-1}\tau}{D_{mol}\,\varepsilon}} \qquad \textbf{Equation 1}$$

Where R = diffusion length (catalyst particle radius), k = rate constant, C_{AS} = reactant concentration at the catalyst surface, n = reaction order, ε = porosity, τ = tortuosity and D_{mol} = molecular diffusion coefficient.

To evaluate the internal diffusion limitations starting from an observed reaction rate, the Weisz-Prater criterion (C_{wp}) is used (Equation 2).

$$C_{WP} = \frac{r_{obs}\,\rho_p\,R_p^2}{\frac{\varepsilon\,D_{AB}}{\tau}\,C_A} \qquad \textbf{Equation 2}$$

Where r_{obs} = observed reaction rate, ρ_p = particle density, R_p = catalyst particle radius, ε = porosity, D_{AB} = molecular diffusion coefficient, τ = tortuosity and C_A = reactant concentration.

For $C_{WP} << 1$ internal diffusion limitations can be neglected, when $C_{WP} >> 1$ the internal diffusion limitations are significant.

A similarly used factor for evaluation of external diffusion limitations is the Carberry number, Ca (Equation 3) [1].

$$Ca = \frac{r_{v,p}^{obs}}{a' k_f C_b} = \frac{C_b - C_s}{C_b} \qquad \textbf{Equation 3}$$

Where C_b = reactant concentration in the bulk, C_s = reactant concentration at the catalyst surface, $r_{v,p}$ = reaction rate per volume of catalyst particle (obs = observed), a' = volumetric external surface area and k_f = mass transfer coefficient.

If the Carberry number approaches zero there are no external diffusion limitations. If the Carberry number approaches 1 there are external diffusion limitations.

Thiele modulus, Weisz-Prater criterion and Carberry number are applicable under isothermal conditions.

1.3 Carbon nanofibers

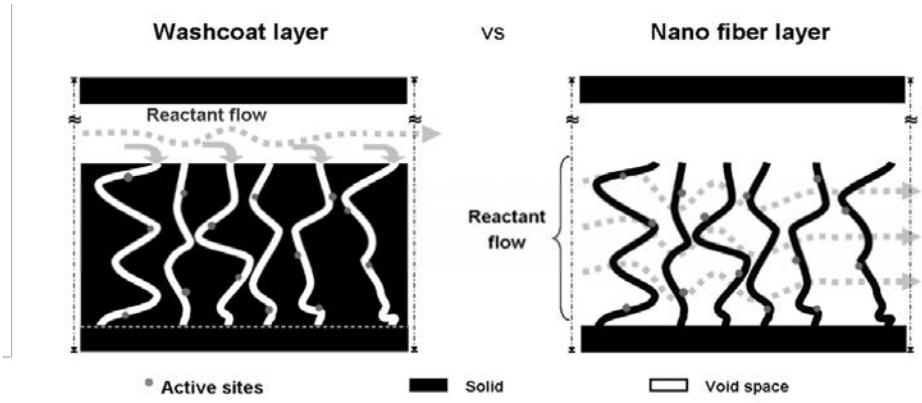

Figure 4: Schematic representation of washcoat layer and CNF layer, inverse of the washcoat [15]

In our work, as well as previous work in our group, carbon nanofibers (CNFs) are considered as an alternative support layer to replace the washcoat layer. CNFs exhibit a very open structure which resembles the inverse structure compared to the conventional washcoat layer [10], see Figure 4. The inverse structure shows that the solid of the washcoat is substituted by open space, increasing porosity ε and decreasing tortuosity τ, therefore the catalytic sites become more easily available. This means it reduces the diffusion limitations as exhibited in washcoat layers, thereby enabling thicker support layers as compared to conventional washcoat layers. Previous work in our group has explored these CNF layers as catalyst support on monoliths [19], foams [9, 20], cloth, thin layers [21], microchannels [21] and metal foils [22].

1.3.1 What are carbon nanofibers (CNFs)?

Carbon nanofibers were first discovered as a nuisance in chemical reactors while converting hydrocarbons, damaging catalyst and reactor and deactivating the catalyst. Carbon nanofibers are a type of carbon nanostructures that consists of stacks of graphitic carbon. These graphitic layers are commonly arranged in either a fishbone of a platelet structure, as can be seen from Figure 5 [23, 24]. Carbon nanofibers have been studied for many years now for applications ranging from hydrogen storage [25], heat transfer [26], electrodes for fuel cells [27, 28], hydrophobic surfaces [29, 30] to catalyst supports [9, 31].

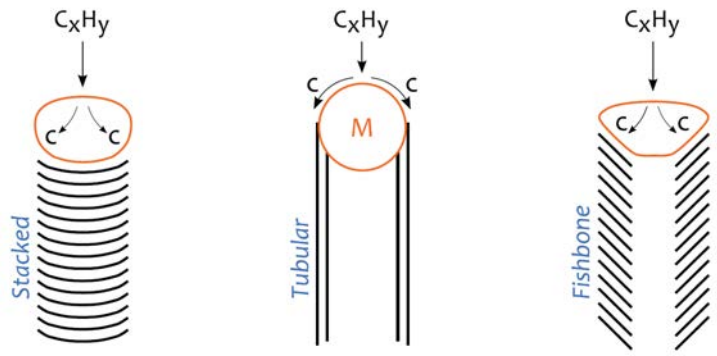

Figure 5: Schematic representation of different structures observed for carbon nanofibers [24]

1.3.2 Synthesis of CNFs

Carbon nanofiber and carbon nanotube growth is generally achieved using arc discharge [25, 32], catalytic chemical vapor deposition (C-CVD) [11, 21, 22, 33-35] and plasma enhanced chemical vapor deposition [11, 36, 37]. Synthesis can be achieved from pre-formed metal nanoparticles of different metals [38] *e.g.* nickel, iron, cobalt [10, 23, 39, 40], on thin metal layers on flat model supports [21, 41, 42] or polycrystalline bulk metal, like we will study further in this thesis. Previous studies on CNF synthesis on bulk metal have explored nickel [43, 44], iron [22] and stainless steel [22] of different shape and macro-structure (foams [43], filters [31], foils [22]) as supports.

In catalytic chemical vapor deposition, CNF growth consists of three steps, shown in Figure 5. In the first step the carbon containing gas (e.g. methanol, ethylene, syn gas) decomposes on the surface of a transition metal particle. During Step 2 dissolved carbon diffuses through and/or over the surface of the metal particle. And finally the dissolved carbon precipitates on one side of the metal particle to form a carbon nanofiber [23, 45].

1.4 Nitrite hydrogenation

Nitrite and nitrate are pollutants in drinking water, which can cause serious health issues like methemoglobinemia (affecting the oxygen-carrying ability of haemoglobin)

also known as blue-baby syndrome and hypertension [46, 47]. Therefore a limit of nitrate and nitrite concentrations in drinking water of 50 and 0.1 mg/L respectively has been imposed by the European Environmental Agency (EEA) [46]. The removal of nitrite can be achieved by nitrite hydrogenation, a very fast liquid phase reaction [48]. Nitrite hydrogenation is conducted in aqueous environment over a noble metal catalyst, e.g. Pd or Pt. Two reactions, shown in Equation 4 and Equation 5, occur forming both di-nitrogen, the preferred product, and ammonium, an undesired product. Ammonium is also under strict regulations by the EEA (0.5 mg/L), due to its toxicity in large quantities.

$$2NO_2^- + 3H_2 + 2H^+ \overset{Pd}{\rightarrow} N_2 + 4H_2O \qquad \textbf{Equation 4}$$

$$NO_2^- + 3H_2 + 2H^+ \overset{Pd}{\rightarrow} NH_4^+ + 2H_2O \qquad \textbf{Equation 5}$$

Selectivity of these reactions is known to be influenced by diffusion limitations and internal concentration gradients. Increasing pH has been shown to result in decreasing activity and increasing ammonium selectivity [49, 50], whereas decreasing temperatures favor the formation of di-nitrogen [51].

Scope of the thesis

In this work we explore the design of a novel catalyst support structure enabling stable operation under operational conditions, in combination with allowing removal of the catalyst particles after deactivation. This would allow recovery of deactivated catalyst particles from the structured support, without necessitating the removal of the support structure itself from the reactor. We use CNF agglomerates, supporting Pd nanoparticles as catalyst particles on the structured support. These CNF agglomerates are immobilized on structured supports that allow mechanical attachment. An additional binder layer of grown CNFs on the structural support is explored. In this work nitrite hydrogenation is used as a model reaction to demonstrate the functionality of the immobilized CNF agglomerates layer on a structured support.

In Chapter 2 we start with a more fundamental question. The idea of using a CNF layer directly grown on a structured support raised questions about the manipulation of

the characteristics of this CNF layer. Insight in the initiation of CNF growth directly on bulk polycrystalline metal is generally lacking in literature. We study the initiation of CNF growth on polycrystalline nickel foam. Nickel foam is chosen instead of stainless steel filter because there is previous knowledge on initiation of CNF growth on nickel foam under atmospheric conditions, additionally nickel foam can also be used as a structured catalyst in its own right. Under atmospheric conditions this initiation is too fast to observe, therefore to observe the CNF growth initiation, the (partial) pressure of the carbon containing gas is extremely reduced. This gives us insight in the production of CNF layers directly on polycrystalline Ni metal, *e.g.* foam and metal filters, like the layer studied as a binder layer in Chapter 3.

Chapter 3 demonstrates the immobilization of CNF agglomerates upon a stainless steel filter. This is a first step in producing a catalyst support that can be reversibly loaded with catalyst particles. In our work we use sintered stainless steel filters as structured support for the immobilized CNF layer. Filters are used here because thin layers of catalysts can be easily obtained via formation of a filter cake. A range of parameters (pressure drop, particle size, layer thickness, densification) are varied to find the most stable layer under operational conditions and to study the adhesion of the CNF agglomerates layer. An additional CNF layer grown directly on the stainless steel filter is explored as binder layer for the CNF agglomerates. The growth of this CNF layer directly from the stainless steel filter caused the previously discussed questions about the initiation of CNF growth, as described in detail in Chapter 2.

In Chapter 4 the catalyst support structures as synthesized in Chapter 3 are used in a model reaction; nitrite hydrogenation. Pd loaded CNF agglomerates are used for this extremely fast reaction. The thin layers of this catalyst on the Ni foam were exposed to the reactant both by flowing the liquid over, as well as through the thin layer. The results will be discussed in terms of mass transfer in the catalyst layer.

Chapter 5 summarizes the results of this thesis and adds some concluding thoughts and recommendations.

[1] B. Averill, J. Moulijn, R. van Santen, and P. van Leeuwen, *Catalysis: An Integrated Approach: An Integrated Approach* vol. 123: Elsevier, 1999.

[2] F. Kapteijn, T. A. Nijhuis, J. J. Heiszwolf, and J. A. Moulijn, "New non-traditional multiphase catalytic reactors based on monolithic structures," *Catalysis Today,* vol. 66, pp. 133-144, 3/30/ 2001.

[3] K. Pangarkar, T. J. Schildhauer, J. R. van Ommen, J. Nijenhuis, F. Kapteijn, and J. A. Moulijn, "Structured Packings for Multiphase Catalytic Reactors," *Industrial & Engineering Chemistry Research,* vol. 47, pp. 3720-3751, 2008/05/01 2008.

[4] T. Boger, A. K. Heibel, and C. M. Sorensen, "Monolithic Catalysts for the Chemical Industry," *Industrial & Engineering Chemistry Research,* vol. 43, pp. 4602-4611, 2004/08/01 2004.

[5] M. Grasemann, A. Renken, M. Kashid, and L. Kiwi-Minsker, "A novel compact reactor for three-phase hydrogenations," *Chemical Engineering Science,* vol. 65, pp. 364-371, 2010.

[6] T. A. Nijhuis, M. T. Kreutzer, A. C. J. Romijn, F. Kapteijn, and J. A. Moulijn, "Monolithic catalysts as efficient three-phase reactors," *Chemical Engineering Science,* vol. 56, pp. 823-829, 2// 2001.

[7] S. Roy, T. Bauer, M. Al-Dahhan, P. Lehner, and T. Turek, "Monoliths as multiphase reactors: a review," *AIChE journal,* vol. 50, pp. 2918-2938, 2004.

[8] N. Jarrah, J. G. van Ommen, and L. Lefferts, "Development of monolith with a carbon-nanofiber-washcoat as a structured catalyst support in liquid phase," *Catalysis Today,* vol. 79–80, pp. 29-33, 4/30/ 2003.

[9] N. A. Jarrah, F. Li, J. G. van Ommen, and L. Lefferts, "Immobilization of a layer of carbon nanofibres (CNFs) on Ni foam: A new structured catalyst support," *Journal of Materials Chemistry,* vol. 15, pp. 1946-1953, 2005.

[10] P. W. A. M. Wenmakers, J. van der Schaaf, B. F. M. Kuster, and J. C. Schouten, ""Hairy Foam": carbon nanofibers grown on solid carbon foam. A fully accessible, high surface area, graphitic catalyst support," *Journal of Materials Chemistry,* vol. 18, pp. 2426-2436, 2008.

[11] M. Cantoro, V. B. Golovko, S. Hofmann, D. R. Williams, C. Ducati, J. Geng*, et al.*, "Wet catalyst assisted growth of carbon nanofibers on complex three-dimensional substrates," *Diamond and Related Materials,* vol. 14, pp. 733-738, 3// 2005.

[12] Sulzer Chemtech Ltd. Available: http://www.sulzer.com/el/Products-and-Services/Mixpac-Cartridges-Applications-Static-Mixers/Static-Mixers/General-Purpose-Mixers/SMX-plus

[13] R. M. Machado, R. R. Broekhuis, A. F. Nordquist, B. P. Roy, and S. R. Carney, "Applying monolith reactors for hydrogenations in the production of specialty chemicals—process and economic considerations," *Catalysis Today,* vol. 105, pp. 305-317, 2005/08/15/ 2005.

[14] M. T. Kreutzer, F. Kapteijn, and J. A. Moulijn, "Shouldn't catalysts shape up?: Structured reactors in general and gas–liquid monolith reactors in particular," *Catalysis Today,* vol. 111, pp. 111-118, 2006/01/15/ 2006.

[15] D. B. Thakur, "Catalytic Microreactors for Aqueous Phase Reactions – Carbon Nano Fibers as Catalyst Support," PhD Thesis, University of Twente, Enschede, The Netherlands, 2010.

[16] R. Klaewkla, M. Arend, and W. F. Hoelderich, "A Review of Mass Transfer Controlling the Reaction Rate in Heterogeneous Catalytic Systems," in *Mass Transfer - Advanced Aspects*, ed, 2011, pp. 667-684.

[17] R. Dittmeyer and G. Emig, "Simultaneous Heat and Mass Transfer and Chemical Reaction," in *Handbook of Heterogeneous Catalysis*, ed: Wiley-VCH Verlag GmbH & Co. KGaA, 2008.

[18] H. S. Fogler, *Elements of chemical reaction engineering*: Prentice-Hall, 1992.

[19] N. A. Jarrah, J. G. van Ommen, and L. Lefferts, "Growing a carbon nano-fiber layer on a monolith support; effect of nickel loading and growth conditions," *Journal of Materials Chemistry,* vol. 14, pp. 1590-1597, 2004.

[20] J. Chinthaginjala, D. Thakur, K. Seshan, and L. Lefferts, "How carbon-nano-fibers attach to Ni foam," *Carbon,* vol. 46, pp. 1638-1647, 2008.

[21] R. M. Tiggelaar, D. B. Thakur, H. Nair, L. Lefferts, K. Seshan, and J. G. E. Gardeniers, "Influence of thin film nickel pretreatment on catalytic thermal chemical vapor deposition of carbon nanofibers," *Thin Solid Films,* vol. 534, pp. 341-347, 5/1/ 2013.

[22] S. Pacheco Benito and L. Lefferts, "The production of a homogeneous and well-attached layer of carbon nanofibers on metal foils," *Carbon,* vol. 48, pp. 2862-2872, 8// 2010.

[23] K. P. De Jong and J. W. Geus, "Carbon Nanofibers: Catalytic Synthesis and Applications," *Catalysis Reviews,* vol. 42, pp. 481-510, 2000/11/30 2000.

[24] T. Taha, B. Mojet, L. Lefferts, and T. H. van der Meer, "Effect of carbon nanofiber surface morphology on convective heat transfer from cylindrical surface: Synthesis, characterization and heat transfer measurement," *International journal of thermal sciences,* vol. 105, pp. 13-21, 2016.

[25] C. Liu, Y. Y. Fan, M. Liu, H. T. Cong, H. M. Cheng, and M. S. Dresselhaus, "Hydrogen Storage in Single-Walled Carbon Nanotubes at Room Temperature," *Science,* vol. 286, pp. 1127-1129, 1999-11-05 00:00:00 1999.

[26] P. K. Schelling, L. Shi, and K. E. Goodson, "Managing heat for electronics," *Materials Today,* vol. 8, pp. 30-35, 6// 2005.

[27] C. A. Bessel, K. Laubernds, N. M. Rodriguez, and R. T. K. Baker, "Graphite Nanofibers as an Electrode for Fuel Cell Applications," *The Journal of Physical Chemistry B,* vol. 105, pp. 1115-1118, 2001/02/01 2001.

[28] K. Lee, J. Zhang, H. Wang, and P. D. Wilkinson, "Progress in the synthesis of carbon nanotube- and nanofiber-supported Pt electrocatalysts for PEM fuel cell catalysis," *Journal of Applied Electrochemistry,* vol. 36, pp. 507-522, 2006.

[29] P. Tsai, S. Pacheco, C. Pirat, L. Lefferts, and D. Lohse, "Drop Impact upon Micro- and Nanostructured Superhydrophobic Surfaces," *Langmuir,* vol. 25, pp. 12293-12298, 2009/10/20 2009.

[30] H. Gelderblom, Á. G. Marín, H. Nair, A. van Houselt, L. Lefferts, J. H. Snoeijer*, et al.*, "How water droplets evaporate on a superhydrophobic substrate," *Physical Review E,* vol. 83, p. 026306, 02/17/ 2011.

[31] P. Tribolet and L. Kiwi-Minsker, "Palladium on carbon nanofibers grown on metallic filters as novel structured catalyst," *Catalysis Today,* vol. 105, pp. 337-343, 8/15/ 2005.

[32] Y. S. Park, K. S. Kim, H. J. Jeong, W. S. Kim, J. M. Moon, K. H. An*, et al.*, "Low pressure synthesis of single-walled carbon nanotubes by arc discharge," *Synthetic Metals,* vol. 126, pp. 245-251, 2/14/ 2002.

[33] H. Amara, C. Bichara, and F. Ducastelle, "Understanding the Nucleation Mechanisms of Carbon Nanotubes in Catalytic Chemical Vapor Deposition," *Physical Review Letters,* vol. 100, p. 056105, 02/08/ 2008.

[34] R. T. K. Baker, M. A. Barber, P. S. Harris, F. S. Feates, and R. J. Waite, "Nucleation and growth of carbon deposits from the nickel catalyzed decomposition of acetylene," *Journal of Catalysis,* vol. 26, pp. 51-62, 1972/07/01 1972.

[35] N. A. Jarrah, "Studying the influence of process parameters on the catalytic carbon nanofibers formation using factorial design," *Chemical Engineering Journal,* vol. 151, pp. 367-371, 8/15/ 2009.

[36] V. I. Merkulov, D. H. Lowndes, Y. Y. Wei, G. Eres, and E. Voelkl, "Patterned growth of individual and multiple vertically aligned carbon nanofibers," *Applied Physics Letters,* vol. 76, pp. 3555-3557, 2000.

[37] S. Hofmann, G. Csányi, A. C. Ferrari, M. C. Payne, and J. Robertson, "Surface Diffusion: The Low Activation Energy Path for Nanotube Growth," *Physical Review Letters,* vol. 95, p. 036101, 07/12/ 2005.

[38] I. Kvande, Z. Yu, T. Zhao, M. Rønning, A. Holmen, and D. Chen, "Towards large scale production of CNF for catalytic applications," *Chem. Sustainable Dev,* vol. 14, p. 583, 2006.

[39] M. Kumar and Y. Ando, "Chemical Vapor Deposition of Carbon Nanotubes: A Review on Growth Mechanism and Mass Production," *Journal of Nanoscience and Nanotechnology,* vol. 10, pp. 3739-3758, // 2010.

[40] N. M. Rodriguez, "A review of catalytically grown carbon nanofibers," *Journal of Materials Research,* vol. 8, pp. 3233-3250, 1993.

[41] A. Gohier, T. M. Minea, S. Point, J. Y. Mevellec, J. Jimenez, M. A. Djouadi*, et al.*, "Early stages of the carbon nanotube growth by low pressure CVD and PE-CVD," *Diamond and Related Materials,* vol. 18, pp. 61-65, 1// 2009.

[42] D. B. Thakur, R. M. Tiggelaar, J. G. E. Gardeniers, L. Lefferts, and K. Seshan, "Carbon nanofiber based catalyst supports to be used in microreactors: Synthesis and characterization," *Chemical Engineering Journal,* vol. 160, pp. 899-908, 6/15/ 2010.

[43] N. A. Jarrah, J. G. van Ommen, and L. Lefferts, "Mechanistic aspects of the formation of carbon-nanofibers on the surface of Ni foam: A new microstructured catalyst support," *Journal of Catalysis,* vol. 239, pp. 460-469, 4/25/ 2006.

[44] A. Romero, A. Garrido, A. Nieto-Márquez, A. R. de la Osa, A. de Lucas, and J. L. Valverde, "The influence of operating conditions on the growth of carbon nanofibers on carbon nanofiber-supported nickel catalysts," *Applied Catalysis A: General,* vol. 319, pp. 246-258, 3/1/ 2007.

[45] M. L. Toebes, J. H. Bitter, A. J. van Dillen, and K. P. de Jong, "Impact of the structure and reactivity of nickel particles on the catalytic growth of carbon nanofibers," *Catalysis Today,* vol. 76, pp. 33-42, 11/1/ 2002.

[46] N. Barrabés and J. Sá, "Catalytic nitrate removal from water, past, present and future perspectives," *Applied Catalysis B: Environmental,* vol. 104, pp. 1-5, 2011.

[47] S. Hörold, T. Tacke, and K. D. Vorlop, "Catalytical removal of nitrate and nitrite from drinking water: 1. Screening for hydrogenation catalysts and influence of reaction conditions on activity and selectivity," *Environmental Technology,* vol. 14, pp. 931-939, 1993/10/01 1993.

[48] S. Hörold, K. D. Vorlop, T. Tacke, and M. Sell, "Development of catalysts for a selective nitrate and nitrite removal from drinking water," *Catalysis Today,* vol. 17, pp. 21-30, 1993/05/26/ 1993.

[49] J. K. Chinthaginjala and L. Lefferts, "Support effect on selectivity of nitrite reduction in water," *Applied Catalysis B: Environmental,* vol. 101, pp. 144-149, 2010/11/22/ 2010.

[50] S. D. Ebbesen, B. L. Mojet, and L. Lefferts, "Effect of pH on the Nitrite Hydrogenation Mechanism over Pd/Al2O3 and Pt/Al2O3: Details Obtained with ATR-IR Spectroscopy," *The Journal of Physical Chemistry C,* vol. 115, pp. 1186-1194, 2011/02/03 2011.

[51] V. Höller, K. Rådevik, I. Yuranov, L. Kiwi-Minsker, and A. Renken, "Reduction of nitrite-ions in water over Pd-supported on structured fibrous materials," *Applied Catalysis B: Environmental,* vol. 32, pp. 143-150, 2001.

Chapter 2

Initiation of Carbon Nanofiber Growth on Polycrystalline Nickel Foam at low Ethylene Pressure

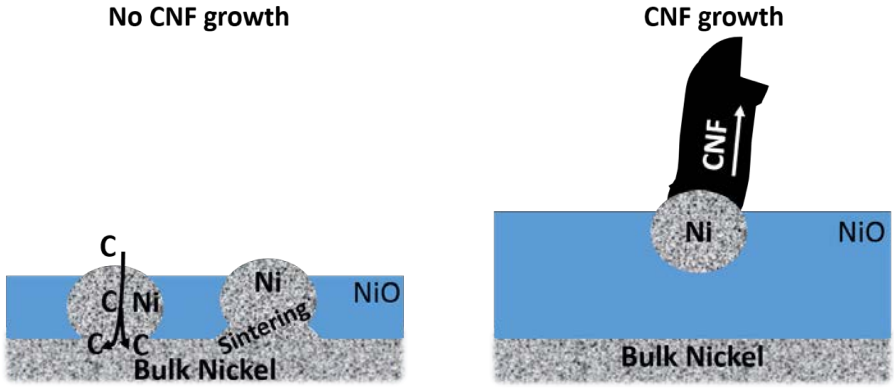

Chapter published as:

J.M. Roemers-van Beek, Z.J. Wang, A. Rinaldi, M.G. Willinger, L. Lefferts, Initiation of Carbon Nanofiber Growth on Polycrystalline Nickel Foam at low Ethylene Pressure (Submitted to ChemCatChem)

Abstract

The initiation of carbon nanofiber (CNF) growth on polycrystalline Ni foam was investigated by a combination of *ex*- and *in-situ* methods, including scanning electron microscopy, X-ray diffraction and Raman spectroscopy. Experiments were performed at low hydrocarbon partial pressure in order to slow down the initiation process. Very little to no CNFs were observed on reduced samples, which is caused by diffusion of C to the bulk of the Ni foam. At low hydrocarbon partial pressure, this prevents formation of Ni_3C as a precursor of Ni nanoparticles acting as active particles for CNF formation. CNF growth was significant on oxidized samples and the initiation was slowed down by using extremely low ethylene pressure. Ni-nanoparticles are capable of catalyzing CNF growth, provided these are isolated from the Ni bulk by unreduced NiO, resulting from incomplete reduction of the NiO layer.

2.1 Introduction

Carbon nanofibers (CNFs) and carbon nanotubes (CNTs) are a novel class of materials that are studied for various applications ranging from hydrogen storage [1], heat transfer [2], electrodes for fuel cells [3, 4], hydrophobic surfaces [5, 6] to catalyst supports [7, 8]. While CNTs consist of rolled-up sheets of graphitic carbon, CNFs can consist of amorphous carbon or stacks of graphitic carbon in which graphitic layers are arranged in so-called fishbone or platelet structures [9].

CNT and CNF growth is generally achieved using arc discharge [1, 10], catalytic chemical vapour deposition (C-CVD) [11-16] and plasma enhanced chemical vapour deposition [16-18]. Depending on the growth conditions, i.e. temperature and pressure, as well as the catalyst (type of metal and morphology [19]) and the reactive gas used as carbon source [19, 20], the formation of CNFs or CNTs is favoured.

C-CVD on catalysts with pre-formed metal nanoparticles has been studied in detail for different metals [20] i.e. nickel, iron, cobalt [9, 21-23]. Also studies on thin metal layers on flat model supports have been reported [15, 24, 25], in which the thin layer first fragmentises, forming metal nanoparticles, just before CNFs start growing. In-situ TEM [26, 27] experiments have been reported on CNF growth on pre-shaped transition-metal particles as well as on thin layers of transition metal. Based on these observations, a generally accepted picture of CNF growth was developed. It involves three main steps [19] which basically consist of the decomposition of the carbon containing gas on the metal catalyst particle, carbon diffusion through or over the surface of the metal particle and finally, carbon precipitation at a specific side of the particle [9, 19].

In contrast to the rich literature on CNF and CNT growth on small metal particles, insight in the formation, and especially the initiation, of CNF growth on polycrystalline bulk metal samples is lacking to an important extent. Carbon nanofiber growth on bulk metal has been studied for *e.g.* nickel [28, 29], iron [14] and stainless steel [14] with different shape and morphology, including foams [28], filters [7] and foils [14]. A wide range of parameters have been looked at for these materials, including the type of carbon containing gas (C_2H_4, C_2H_2, CH_4, C_2H_6, $CO + H_2$) [20], the growth temperature

(440 °C-1000 °C) [8], and pre-treatments of the material (oxidation, reduction, combinations of these) [14].

CNF and CNT growth on polycrystalline bulk metal catalysts is essentially different from the case of supported nano-particles, because the micrometer-sized grains of the polycrystalline surface have to first break up into smaller nano-particles in order to enable CNF growth. In the case of growth at atmospheric pressures, it has been shown that carbon diffuses into the nickel bulk and accumulates at grain boundaries and defects. Precipitation induced disintegration can occur in relatively low-carbon activity environment, resulting in particles of the same size as crystallites in the original material, which are usually still too large to directly catalyse CNF and CNT formation [8]. Thus, further fragmentation is required to form Ni particles that are small enough to subsequently catalyse CNF growth, which can be induced by an environment with higher carbon activity. Both these processes result in corrosive degradation that is known as metal-dusting [30, 31].

In previous work by Jarrah et al., CNF growth initiation on reduced bulk Ni foams was studied as a function of exposure time to a mixture of 25% C_2H_4 in N_2 at atmospheric pressure by *ex-situ* SEM and XRD [8, 28]. It was postulated that CNF growth starts with formation of meta-stable Ni_3C, which subsequently decomposes into nickel particles and carbon precipitates. The resulting nickel nanoparticles have proper dimensions (20-70 nm) to catalyse CNF growth. Based on this, a new type of catalyst support was developed (*hairy foam*) consisting of a thin layer of entangled CNFs on the surface of Ni-foam with an extraordinary high porosity and low tortuosity. These support materials allow very efficient internal mass transport, which has been demonstrated with Pd supported on hairy foam for catalytic hydrogenation of nitrite in aqueous phase [32, 33].

A similar study on growth initiation, based on *ex-situ* characterization, was impossible on oxidized Ni foam due to very rapid formation of CNFs. Presence of a NiO layer increases both the initiation rate as well as the rate of CNF formation by one order of magnitude, as compared to slower formation on reduced metallic Ni substrates. It was proposed that the reducing conditions when growing CNFs first cause reduction of the nickel oxide layer and consequently *in-situ* formation of nickel nanoparticles,

facilitating the growth of CNFs much more rapidly than *via* formation and decomposition of Ni_3C.

The goal of this work is to determine the mechanism of initiation of catalytic-CNF growth on reduced polycrystalline nickel, as well as to confirm or challenge the proposed mechanism of initiation of CNF growth on polycrystalline nickel covered with a nickel oxide layer. *In-situ* characterization during CNF growth initiation was performed in an environmental scanning electron microscope (ESEM) in mixtures of C_2H_4 and H_2 at pressures between 10 to 100 Pa. *Ex-situ* techniques, i.e. Raman Spectroscopy, SEM and XRD, were used for characterization after exposing Ni foam at atmospheric pressure to highly diluted gas mixtures with similar partial pressures of C_2H_4 and H_2 as in the ESEM experiments.

2.2 Experimental

2.2.1 Materials

The nickel foam used for this study was obtained from RECEMAT bv [34]. This foam consists of hollow strands of nickel that are typically 15 μm thick (Figure 1). The foam is highly porous (typically 95%) with typical pore-sizes of 0.4 mm. The specific surface area of the nickel is 5400 m^2/m^3. The nickel foam is 99,5% pure, containing traces of Fe (0.2%), Cu (0.1%) and Zn (0.1%). Cylinders with a diameter of 4,3 mm and length of 5 mm were cut from the as-received foam sheet, using Electrical Discharge Machining (Agiecut Challenge 2).

Ethylene/nitrogen (1000 ppm C_2H_4 in N_2, Praxair), hydrogen (99,999%, Linde), compressed air (in-house production) and nitrogen (99,999%, Linde) were used for carbon nanofiber growth and pre-treatments of the foam.

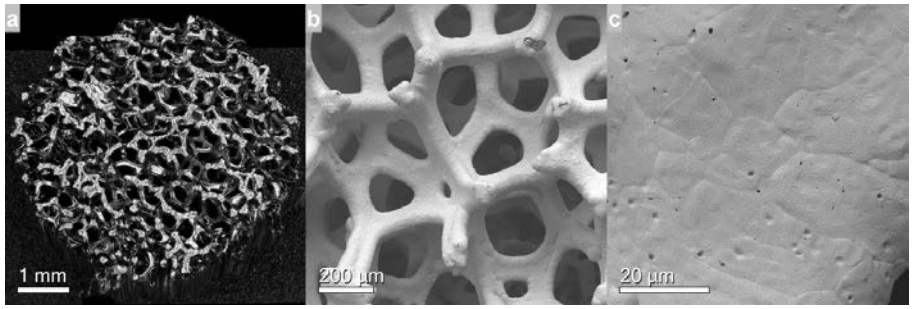

Figure 1: Optical (a) and scanning electron microscopic image (b), (c) of an as-received metallic nickel foam sample at different magnifications

2.2.2 Pre-treatment

As-received nickel foam was cleaned in acetone by ultra-sonication for 15 minutes. In the case of atmospheric growth experiments, metallic foams were additionally pre-treated by *in-situ* reduction at 440 °C for 1 hour in a 20 vol% H_2 in N_2 atmosphere, right before switching to carbon nanofiber growth. For the growth experiments on oxidized foams, a treatment at 600 °C for 1 hour in 4 vol% O_2 in N_2 at ambient pressure was applied. For ESEM experiments, the same nickel foam cylinders were used.

2.2.3 Carbon nanofiber growth

Carbon nanofibers were grown directly on nickel foam cylinders in a home-build quartz reactor with a diameter of 42 mm. The reactor containing the nickel foam was heated in a vertical furnace [8, 35] under a flow of 100 ml/min N_2 with a ramp of 5 °C/min. The actual growth of CNFs was conducted at 440 °C at atmospheric pressure in a total flow of 100 ml/min feeding gas containing N_2, 0,5 vol‰ C_2H_4 and 1 vol‰ H_2 during times varying from 1 minute up to 27 hours. The concentrations of C_2H_4 and H_2 were chosen such that the partial pressures of, respectively, 50 Pa and 100 Pa were the same range as the ones used in the ESEM. CNF growth was stopped by flushing the reactor with N_2. Samples were allowed to cool down to room temperature before exposition to ambient air. These experiments are termed “atmospheric” experiments.

For the real-time observation in the ESEM, a FEI Quantum 200 instrument with a field emission gun, oil-free vacuum pre-pumps and a home-built laser heating stage

was used. The instrument is equipped with a set of mass-flow controllers that allow introducing desired amounts of gas mixtures directly into the chamber of the microscope. In the high-vacuum operation mode, the instrument reaches a base-pressure of around $5x10^{-5}$ Pa. In a typical experiment, the chamber is purged and pumped several times with N_2 after introducing the sample. All samples were initially annealed under 20 Pa H_2 for 15 minutes to 1 hour at 600 °C in order to remove surface oxides and carbon contaminations. In the case of experiments on oxidized foams, the samples were oxidized under 30 Pa O_2 for different times. Each time before changing the gas composition, the sample was cooled down to room temperature. After the gas atmosphere was changed, the sample was reheated to the desired temperature. The composition of the chamber atmosphere was monitored using a mass spectrometer that is directly connected to the chamber. For CNF growth, the atmosphere was set to 8 Pa C_2H_4 and 22 Pa H_2. The sample was heated by direct illumination with infrared laser light of a wavelength of 800 nm. A K-type thermocouple was inserted into the foam in order to directly measure the temperature of the foam. The temperature can be changed at relatively fast rates in the range of several 100 °C/minute due to the small mass of the heated sample. The laser heating current was manually controlled on the basis of feedback from the thermocouple. In order to reach the desired experimental conditions as fast as possible and to reduce the time during which observation is hindered by thermal drift, temperature changes were applied at rates of several 10 °C/sec.

2.2.4 Characterization

The atmospheric samples were analyzed and characterized *ex-situ*, *i.e.*, after exposure to ambient air, by high-resolution SEM (HR-SEM), X-ray diffraction (XRD), Raman Spectroscopy, thermo gravimetric analysis (TGA), N_2 adsorption and elemental analysis (CHN analysis). HR-SEM pictures were obtained in a Zeiss Merlin Scanning Electron Microscope equipped with an EDX detector. Statistical analysis of the diameters of the produced CNFs was conducted by analyzing HR-SEM pictures using ImageJ.

XRD patterns were recorded using a Panalytical X'Pert PRO operated with a Cu source. Raman spectra were recorded with a Bruker Senterra instrument that is equipped with an Infinity 1 camera using an excitation wavelength of 532 nm (5 mW).

Spectra were averaged from 5 spots to compensate for any inhomogeneity of the sample, with 20 individual spectra per spot and an accumulation time of 2 s. TGA was performed in a TGA/SDTA851e, Mettler Toledo. The surface area was determined by N_2 physisorption in a QuantaChrome Autosorb-1 using the BET isotherm, using multiple samples because of the low absolute surface area. CHN analysis was performed in a Flash 2000 Organic Elemental Analyzer (Interscience), repeating the measurement five times and averaging the result.

Additional characterization of samples grown in the ESEM was done *ex-situ* using a Hitachi S4800-SEM and a JEOL ARM transmission electron microscope. EDX was recorded in the ESEM (FEI Quantum 200) using a Bruker Si(Li) EDX detector.

2.3 Results and Discussion

2.3.1 Growth on metallic Ni foams.

Reduced nickel shows mild morphological change upon exposure to diluted ethylene feed at atmospheric pressure for several hours (Figure 2b,c,d). The dominant change that is observed with increasing exposure time is the formation of carbon deposits or precipitates, which give rise to islands of particularly dark contrast in the SEM images. Very small amount of CNFs can be observed only after prolonged exposure to ethylene during 15 minutes and 3 hours (Figure 2c,d).

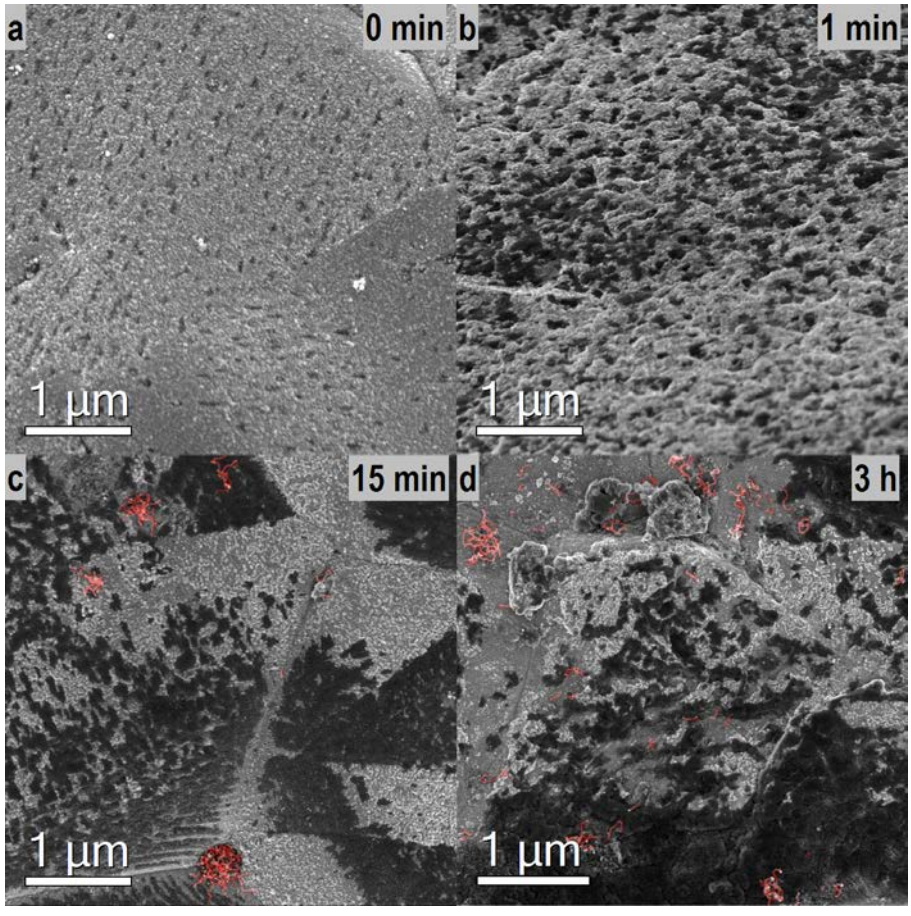

Figure 2: *Ex-situ* SEM images recorded after exposing metallic Ni foams (*in-situ* reduced, 440 °C, 1 h) to growth conditions at ambient pressure with 50 Pa C_2H_4 and 100 Pa H_2 for different times of exposure; CNFs are highlighted in red to improve visibility

Similar observations were made in the ESEM. Exposure of the reduced Ni foam to both pure C_2H_4 (Figure 3) and mixtures of C_2H_4 and H_2 (SI Movie 1) at pressures between 10^{-2} Pa and 100 Pa for extended times of up to several hours resulted in the formation of carbon precipitates on the surface of the foam. Carbon deposits become visible after decreasing either temperature or ethylene pressure, inducing segregation of dissolved carbon to the surface of the Ni foam. No CNF formation on the reduced Ni foam was observed in the ESEM.

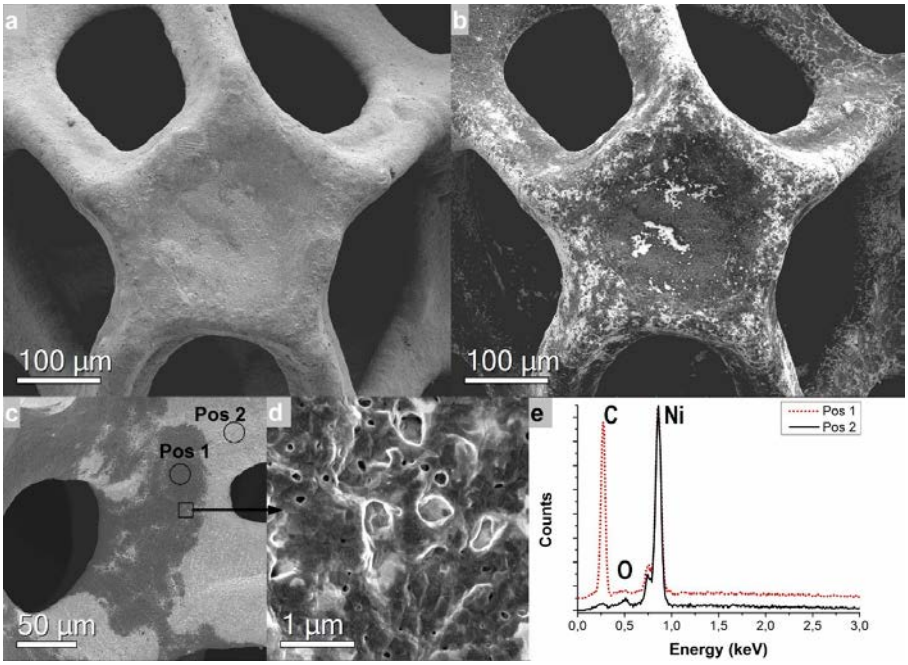

Figure 3: Precipitation of carbon on reduced nickel foam upon exposure to pure C_2H_4 at temperatures between 450 °C and 800 °C and pressures of up to 100 Pa. Images (a) and (b) were recorded in the high vacuum mode at ~10^{-2} Pa. (a) shows the initial state of the Ni foam, (b) was recorded after carbon deposits appeared at the surface after decreasing the pressure. (c) and (d) show higher magnified images of the surface with precipitates. In (e) two EDX spectra are shown that were recorded from positions 1 and 2 in (c)

In summary, exposure of reduced Ni to diluted amounts of C_2H_4 and H_2 in atmospheric conditions results in the growth of scattered CNFs after prolonged exposure time and formation of carbon precipitates on the surface if the exposure time is sufficiently long. This finding is in line with observations reported by Weatherup et al. [36, 37]. This is in clear contrast to the results of Jarrah et al. [8], who showed that CNF can be grown on reduced Ni at significantly higher ethylene pressure.

2.3.2 Growth on oxidized Ni foams at atmospheric pressure

2.3.2.1 Oxidation Ni foam

The effect of the oxidative pre-treatments on the surface morphology is shown in Figure 4. Figure 4a and b show the as-received nickel foam at two different magnifications with a very thin layer of NiO on the surface resulting from exposure to ambient. The as-received nickel foam consists of nickel grains of about 1 to 10 µm in size. Significant surface structure differences are observed after oxidation during 1 hour at 600 °C (Figure 4c) and 700 °C (Figure 4d). Oxidation at 600 °C results in a heterogeneous layer of NiO particles of about 30 nm as estimated based on XRD line-broadening (see below). This sample contains 8,5 wt% NiO as determined by TGA (SI Figure 1). Unfortunately, the very low surface area of the foam cannot be easily determined experimentally. Therefore, it is estimated to be about 0.03 m^2/g [8], assuming the foam consists of cylindrical nickel strands of typically 16 µm. Based on the bulk density of NiO (7.78 g/cm^3), it can be estimated that this corresponds to a NiO layer of about 500 nm. This estimated NiO layer thickness indicates that the NiO layer is polycrystalline as the crystallite size is significantly smaller. Oxidation at 700 °C results in a more homogeneous coverage of the surface with larger and structurally more defined NiO crystals, with a NiO content of 9.2 wt% according to TGA.

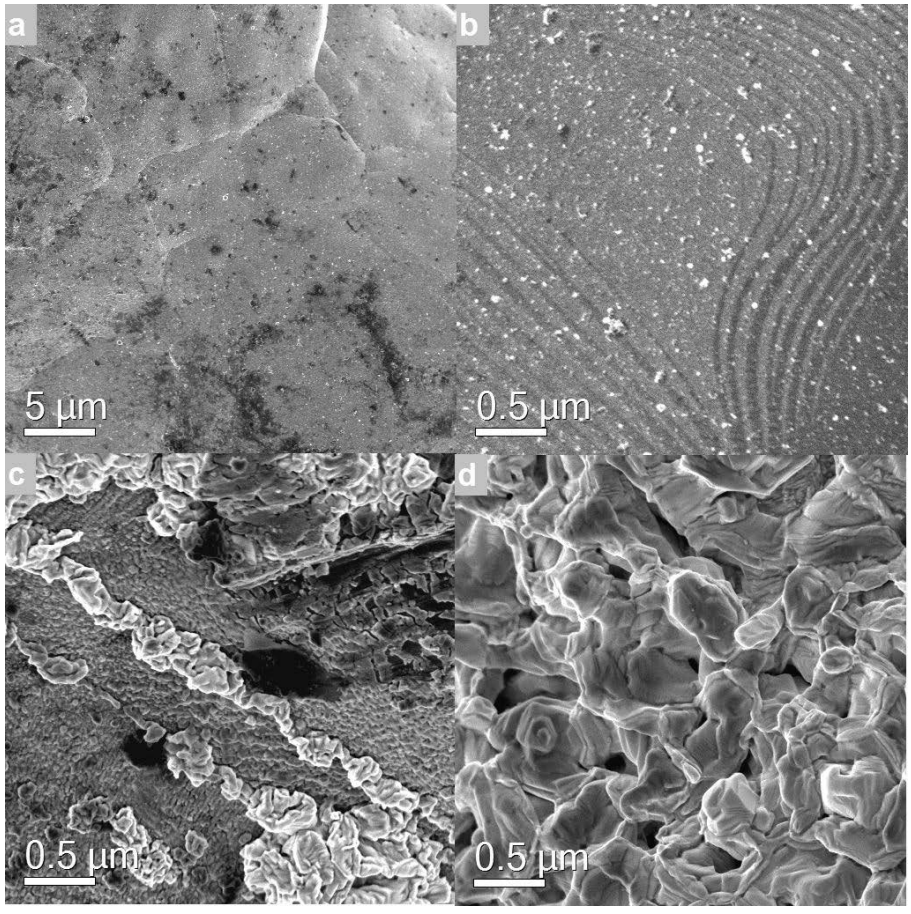

Figure 4: *Ex-situ* SEM images of nickel foam as-received at two different magnifications (a, b); oxidized under 4% O_2 in He for 1 h at, respectively, 600 °C (c) and 700 °C (d)

2.3.2.2 Growth on the oxidized Ni foams at atmospheric pressures (*ex-situ*)

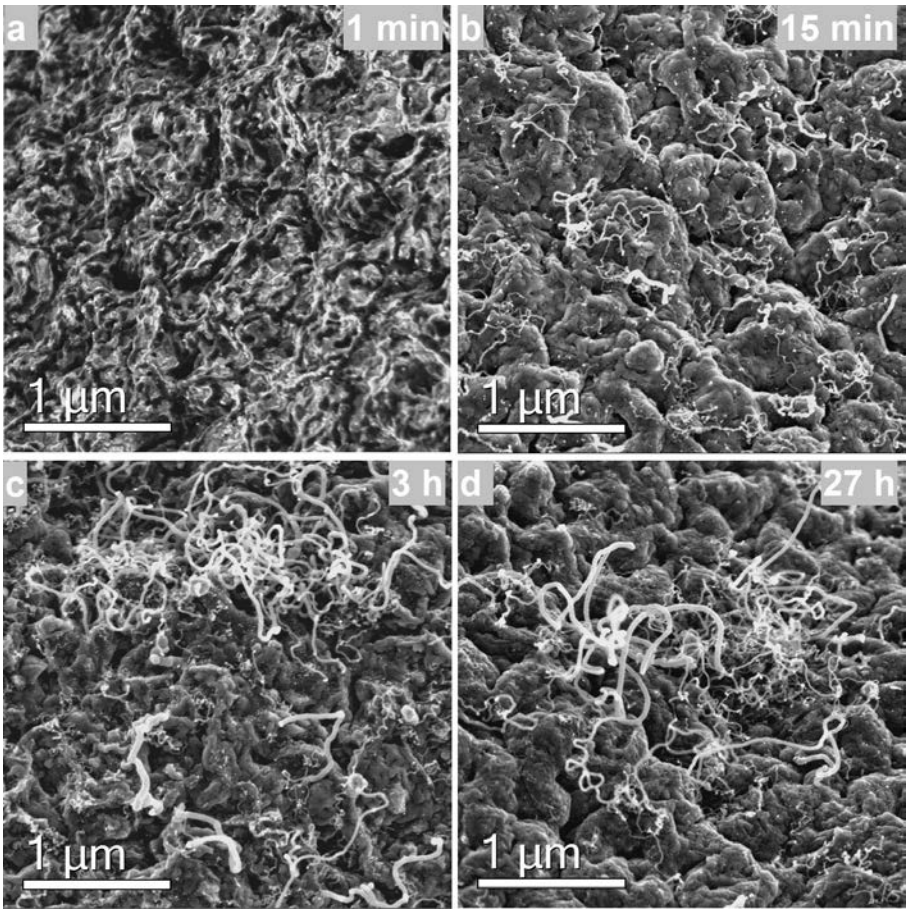

Figure 5: *Ex-situ* SEM images of pre-oxidized (600 °C, 1 h, 4% O_2, *ex-situ*); after growth under exposure to 50 Pa C_2H_4 + 100 Pa H_2 for 1 min (a), 15 min (b), 3 h (c) and 27 h (d)

Exposure to ethylene-hydrogen in N_2 gives rise to CNF growth on the surface of the oxidized Ni foam, although no CNFs are visible yet after 1 minute (Figure 5b). As can be seen in Figure 5c, some CNFs are clearly visible after 15 minutes whereas the structure of the Ni surface flattened slightly due to continued reduction and slight sintering. Further extension of the growth time leads to increasing CNF growth and the morphology of the foam surface does not show significant changes (Figure 5d and 5e). The resulting CNFs have diameters ranging from a few nm to ~35 nm.

CHN analysis shows that CNF growth on nickel oxidized at 600 °C results in a C content of 2,9 wt% after 27 hours of growth. Note that the C concentration of the oxidized sample (Figure 4c), before CNF growth, is below the detection limit (<0.1 wt%). Further experiments were performed with samples oxidized at 600 °C.

Figure 6 shows XRD diffraction pattern in the 2θ-region centered around the main diffraction peak of nickel oxide at 2θ = 43,3°. Oxidation at 600 °C during 1 hour clearly causes the formation of a NiO layer (Figure 6, curve b) containing particles of about 30 nm, as estimated from the peak width of the NiO diffraction peak using the Scherrer equation. This is in reasonable agreement with NiO structures observed in Figure 5a. The oxidized nickel foam as well as the sample after 1 minute CNF-growth clearly contain NiO according the diffraction peak at 2θ = 43.3°, whereas CNF-growth during 27 hours clearly reduces NiO completely, i.e. to a level below the detection limit of XRD. There is no sign of formation of any Ni_3C which would induce diffraction peaks at 2θ values 39.1° and 41.6°, as was observed previously using significantly higher ethylene concentrations [28].

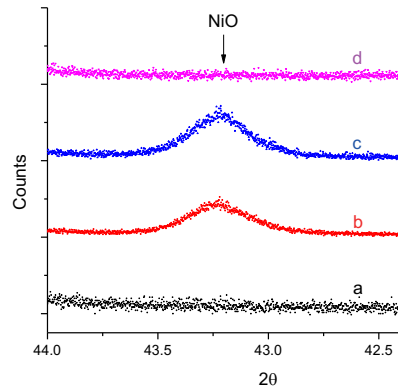

Figure 6: NiO peak in XRD spectra of nickel foam a) as-received, b) after oxidation (600 °C, 1 h, 4% O_2) c) after 1 min of CNF growth and d) after 27 h of CNF growth. Both growth experiments were performed at 440 °C, with partial pressures of 50 Pa for C_2H_4 and 100 Pa for H_2, respectively

Figure 7 shows Raman spectra of nickel foam after oxidation and after 1 and 15 minutes of CNF growth. The peaks in the solid line at 1100 cm^{-1} and 1500 cm^{-1} are attributed to the NiO bulk. The peak at 520 cm^{-1} is the most pronounced NiO peak [38], well separated from the peaks assigned to graphitic deposits as detected in the other two spectra. This NiO peak is clearly detectable on the sample after growing CNFs during 1 minute, though the intensity decreased significantly. The spectra obtained after CNF growth during 1 minute and 15 minutes clearly show double peaks around 1500 cm^{-1} and 2800 cm^{-1}, attributed to graphitic material and characteristic for CNFs [39, 40]. The spectrum measured after CNF growth for 1 minute, clearly demonstrates that CNF growth is already initiated before NiO is completely reduced.

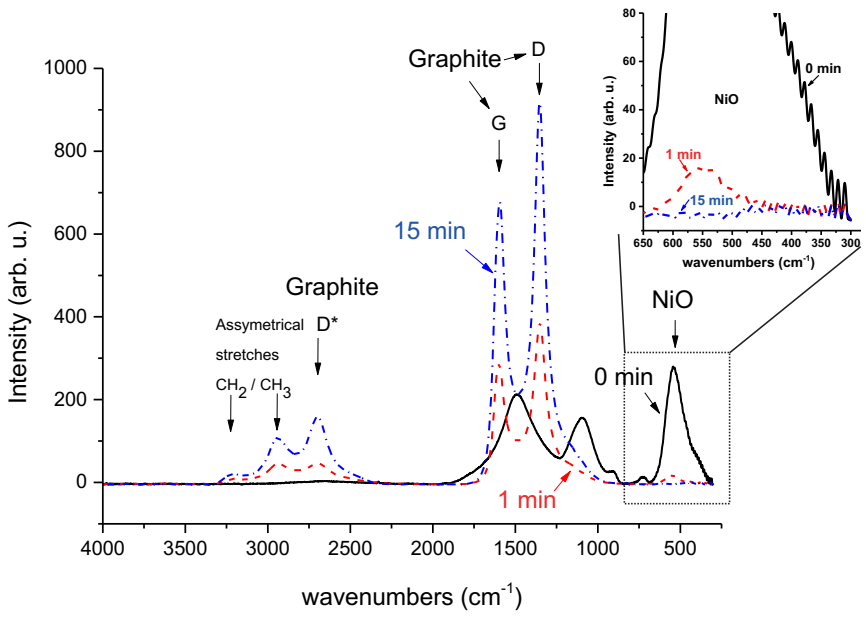

Figure 7: Raman spectra of oxidized nickel foam (600 °C, 1 h, 4% O_2, solid line) and after subsequent CNF growth under 50 Pa C_2H_4 + 100 Pa H_2 for 1 min (dashed line) and 15 min (dashed-dotted line) respectively

Although after 1 minute of CNF growth, CNFs are not visible yet in SEM (Figure 5b), Raman analysis shows there is already graphitized carbon present, indicative of CNFs. Both Raman and XRD confirm the presence of nickel oxide after growing CNFs for 1 minute. Raman shows a clear decrease in oxide content compared to the initial

nickel oxide sample, whereas XRD shows similar NiO content. Since Raman is more surface sensitive than XRD, this confirms that the surface of the NiO is reduced first, as expected, simultaneously with the formation of the first CNFs.

2.3.3 In-situ growth on oxidized Ni foams in ESEM

2.3.3.1 *In-situ* oxidation

ESEM enables *in-situ* observation of the oxidation process (Figure 8). Note that the resulting surface features are similar to the surface features obtained under atmospheric pressure, although oxidation in the ESEM results in a more uniform coverage. This might well be caused by the difference in the O_2 pressure *i.e.* 4000 Pa in the atmospheric experiments *versus* 40 Pa in the ESEM, or differences in the pre-reduction treatment in the atmospheric and ESEM experiments.

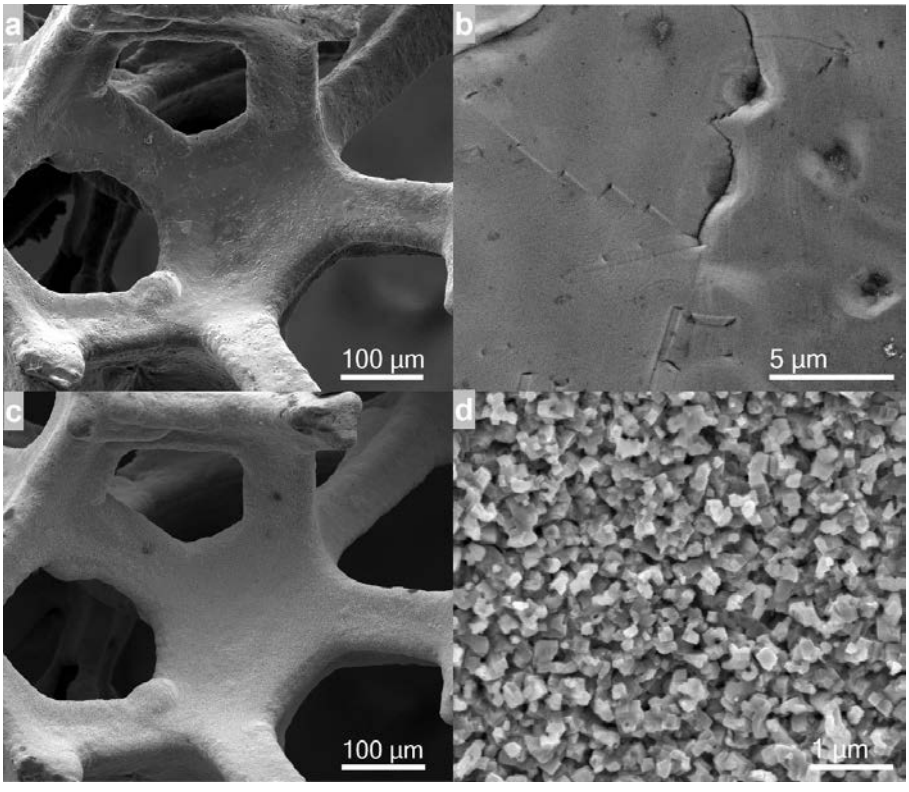

Figure 8: Nickel foam reduced at 600 °C, 1 h, 20 Pa H_2 (a,b); subsequently oxidized at 700 °C for 1 h at 30 Pa O_2 (c,d)

2.3.3.2 In-situ growth on oxidized Ni foams in ESEM

Switching from oxidizing conditions to conditions for CNF growth was performed by first cooling the sample to room temperature, exchanging the oxygen with 8 Pa C_2H_4/20 Pa H_2 mixture and then heating back to 600 °C. Due to the high drift of the sample during the heating step, no undistorted scanning images could be recorded during heating until the sample has reached the final temperature and drift has stopped. The unfortunate consequence is that the initiation cannot be observed directly. SI Movie 2, which is provided in the supporting information, shows changes in the surface and formation of Ni nanoparticles. At the same time, some surface movement due to CNF-cluster growth can be observed. The formation of some individual CNFs is visible in real time at intermediate magnification as can be seen in SI Movie 3.

Figure 9a shows a part of an oxidized Ni foam, Figure 9b shows the same sample, after reduction, causing slight morphological changes. CNFs are observed in Figure 9c (top view), as well as in side-view at higher magnification (Figure 9f). The cross-section view, obtained by mechanically cracking the foam, reveals a brighter layer underneath the darker top-layer that is covered by a carpet of CNFs. According to EDX analysis, the bright layer is due to nickel oxide.

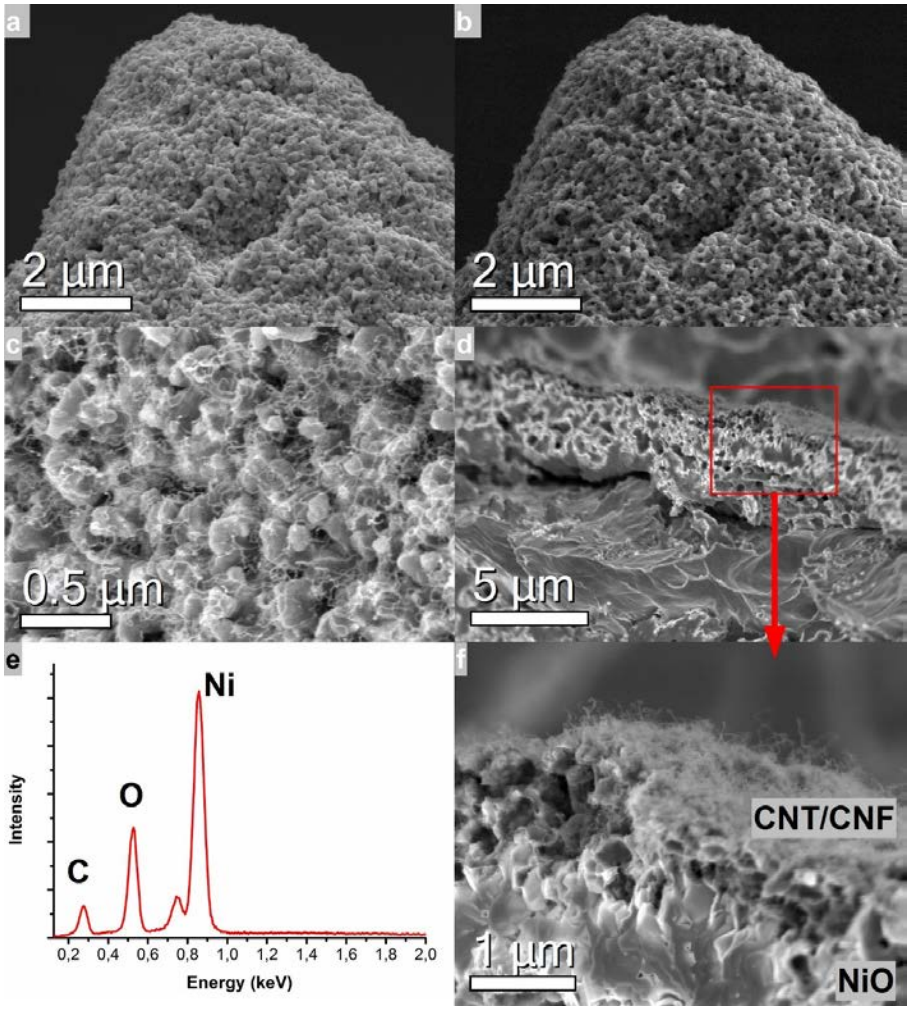

Figure 9: (a) Nickel foam oxidized at 700 °C, 1 h, 30 Pa O_2; (b) subsequently reduced at 400 °C for 15 min in 20 Pa H_2 and (c) after growth at 600 °C for 15 min under 8 Pa C_2H_4 and 20 Pa H_2 (top view); (d) same sample in cross section; (f) a zoom in of the CNFs layer on the NiO layer; (e) EDX spectrum of the layer cross-section shown in (f).

2.4 General discussion

As would be expected, the extreme low ethylene concentration used in this study retarded the formation of CNFs as compared to the previous study on the same materials of Jarrah *et al.* [28], operating at much higher ethylene concentrations. Nevertheless, the enhancing effect of NiO on CNF formation is observed at low concentration, similar to the previous results at high ethylene concentration. Reduced samples show CNFs at low ethylene concentration only after very long exposure time, while no CNF growth was observed in the ESEM (not shown).

ESEM experiments reveal that carbon diffuses into the Ni bulk (Figure 3b and SI Movie 1). Carbon deposits are not visible during exposure to 100 Pa ethylene within the time during which *in-situ* observation in the ESEM was performed. However, carbon segregates to the surface after decreasing temperature or reduction of the ethylene pressure in the ESEM chamber, demonstrating that exposure to ethylene caused significant carbon dissolution.

2.4.1 CNF growth on reduced nickel foam

CNF growth on reduced nickel foam in this study is observed after 15 min of growth; the amount of CNFs is very small and the surface contains only scattered CNFs even after 27 hrs. This demonstrates much slower initiation at low ethylene concentration (50 Pa) compared to the observation of massive CNF-growth under 25000 Pa ethylene, reported previously by Jarrah *et al.* [28].

A possible cause for this phenomenon is the lack of formation and subsequent decomposition of Ni_3C, as proposed by Jarrah *et al.* [28], based on detection of such a meta-stable phase with XRD and SEM. This result was obtained when exposing the reduced Ni foam to 25000 Pa ethylene. Apparently, the same mechanism does not occur significantly in 50 Pa ethylene pressure. As the *in-situ* SEM data clearly confirm dissolution of C in Ni under the conditions in this study, it is clear that ethylene is decomposing on the Ni surface, generating C. It seems reasonable to assume that the decomposition reaction is slow at low ethylene pressure and we speculate that under these conditions the diffusion of C into the bulk of the Ni foam is so fast that Ni_3C

cannot form on the surface of the Ni foam. Hence, initiation of CNF formation is strongly suppressed.

2.4.2 CNF growth on oxidized nickel foam

Clearly, the initiation of CNF growth can be observed on oxidized nickel when the growth is tempered by decreasing the ethylene pressure. This is in clear contrast to earlier results at high ethylene pressure by Jarrah *et al* [28], reporting extremely fast CNF growth. Only massive CNF growth could be observed, even after very short exposure to ethylene-hydrogen mixtures at higher pressure and no information could be obtained on the initiation process. Our investigations demonstrate that CNF growth initiates while NiO is still present. For atmospheric tests, Raman analysis shows the presence of NiO as well as CNFs (graphitized carbon) after 1 min CNF growth (Figure 7). XRD confirms the presence of NiO after 1 min CNF growth (Figure 6). ESEM results with EDX measurements clearly show that a NiO layer is still present after CNF growth was initiated (Figure 9e and f). The averaged thickness of the initial NiO layer is in the order of 500 nm, according to TGA. This is in line with the original hypothesis [28] that reduction of NiO provides a fast route to form Ni nanoparticles. The new observations allow us to further detail the effect of the NiO layer.

A first explanation assumes NiO is responsible for preventing C diffusion from the Ni nanoparticles to the bulk of the Ni foam. Ni particles grow on top of the NiO layer at the external surface where H_2 is offered. If the growing Ni nanoparticles are isolated from the Ni bulk by the NiO layer, C diffusion to the bulk is not possible. Therefore, the carbon concentration in the Ni nanoparticles can increase, allowing initiation of CNF growth.

Alternatively it can be assumed that the presence of a NiO layer prevents sintering and merging of *in-situ* formed Ni nanoparticles with the polycrystalline bulk, via separating the Ni nanoparticles from the bulk. Ni nanoparticles need to be small in order to enable CNF growth. Sintering and merging of the Ni nanoparticles with the bulk of the polycrystalline Ni is detrimental to CNF growth. The isolation of the small Ni nanoparticles by the NiO layer results in CNF growth similar to growth on pre-shaped nanoparticles supported on *e.g.* alumina, silica and carbon.

The critical size of the Ni nanoparticles for CNF formation is in the order of tenths of nm, based on the diameters of the resulting fibers. Apparently, a 500 nm NiO layer is able to induce CNF growth whereas native oxide layers fail. Obviously, the thickness of the NiO layer (500nm) needs to be significantly larger than the size of the Ni nanoparticles (typically 50 nm) growing CNFs, in order to isolate the nanoparticles from the bulk. The observations support both explanations and at this time it is not possible to decide if one of the hypotheses is dominant, or possibly both effects are necessary to induce CNF-growth.

2.5 Conclusion

CNF growth is slowed down and the initiation is retarded by using extremely low ethylene concentrations. Reduced samples show few CNFs at low ethylene concentration after long exposure time, or in the ESEM not at all. This is attributed to diffusion of C to the bulk of the Ni foam, preventing formation of Ni_3C as a precursor in the formation of Ni-nanoparticles. On oxidized samples, it is shown that CNF growth initiates when NiO is still present to isolate the Ni nanoparticles, forming during reduction of the NiO layer, from the bulk Ni. This isolation prevents C diffusion to the bulk and/or inhibits sintering of the Ni nanoparticles with the polycrystalline nickel in the foam.

Acknowledgments

This work took place within the framework of the Institute for Sustainable Process Technology (ISPT). The authors gratefully acknowledge M.A. Smithers for HR-SEM measurements, B.J. Wylie-van Eerd for XRD measurements. This work was supported by the Max Planck−EPFL center for molecular nanoscience and technology, and the European Research Council under the ERC Grant Agreement 278213.

References

[1] C. Liu, Y. Y. Fan, M. Liu, H. T. Cong, H. M. Cheng, and M. S. Dresselhaus, "Hydrogen Storage in Single-Walled Carbon Nanotubes at Room Temperature," *Science,* vol. 286, pp. 1127-1129, 1999-11-05 00:00:00 1999.

[2] P. K. Schelling, L. Shi, and K. E. Goodson, "Managing heat for electronics," *Materials Today,* vol. 8, pp. 30-35, 6// 2005.

[3] C. A. Bessel, K. Laubernds, N. M. Rodriguez, and R. T. K. Baker, "Graphite Nanofibers as an Electrode for Fuel Cell Applications," *The Journal of Physical Chemistry B,* vol. 105, pp. 1115-1118, 2001/02/01 2001.

[4] K. Lee, J. Zhang, H. Wang, and P. D. Wilkinson, "Progress in the synthesis of carbon nanotube- and nanofiber-supported Pt electrocatalysts for PEM fuel cell catalysis," *Journal of Applied Electrochemistry,* vol. 36, pp. 507-522, 2006.

[5] P. Tsai, S. Pacheco, C. Pirat, L. Lefferts, and D. Lohse, "Drop Impact upon Micro- and Nanostructured Superhydrophobic Surfaces," *Langmuir,* vol. 25, pp. 12293-12298, 2009/10/20 2009.

[6] H. Gelderblom, Á. G. Marín, H. Nair, A. van Houselt, L. Lefferts, J. H. Snoeijer*, et al.*, "How water droplets evaporate on a superhydrophobic substrate," *Physical Review E,* vol. 83, p. 026306, 02/17/ 2011.

[7] P. Tribolet and L. Kiwi-Minsker, "Palladium on carbon nanofibers grown on metallic filters as novel structured catalyst," *Catalysis Today,* vol. 105, pp. 337-343, 8/15/ 2005.

[8] N. A. Jarrah, F. Li, J. G. van Ommen, and L. Lefferts, "Immobilization of a layer of carbon nanofibres (CNFs) on Ni foam: A new structured catalyst support," *Journal of Materials Chemistry,* vol. 15, pp. 1946-1953, 2005.

[9] K. P. De Jong and J. W. Geus, "Carbon nanofibers: catalytic synthesis and applications," *Catalysis Reviews,* vol. 42, pp. 481-510, 2000.

[10] Y. S. Park, K. S. Kim, H. J. Jeong, W. S. Kim, J. M. Moon, K. H. An*, et al.*, "Low pressure synthesis of single-walled carbon nanotubes by arc discharge," *Synthetic Metals,* vol. 126, pp. 245-251, 2/14/ 2002.

[11] H. Amara, C. Bichara, and F. Ducastelle, "Understanding the Nucleation Mechanisms of Carbon Nanotubes in Catalytic Chemical Vapor Deposition," *Physical Review Letters,* vol. 100, p. 056105, 02/08/ 2008.

[12] R. T. K. Baker, M. A. Barber, P. S. Harris, F. S. Feates, and R. J. Waite, "Nucleation and growth of carbon deposits from the nickel catalyzed decomposition of acetylene," *Journal of Catalysis,* vol. 26, pp. 51-62, 1972/07/01 1972.

[13] N. A. Jarrah, "Studying the influence of process parameters on the catalytic carbon nanofibers formation using factorial design," *Chemical Engineering Journal,* vol. 151, pp. 367-371, 8/15/ 2009.

[14] S. Pacheco Benito and L. Lefferts, "The production of a homogeneous and well-attached layer of carbon nanofibers on metal foils," *Carbon,* vol. 48, pp. 2862-2872, 8// 2010.

[15] R. M. Tiggelaar, D. B. Thakur, H. Nair, L. Lefferts, K. Seshan, and J. G. E. Gardeniers, "Influence of thin film nickel pretreatment on catalytic thermal chemical vapor deposition of carbon nanofibers," *Thin Solid Films,* vol. 534, pp. 341-347, 5/1/ 2013.

[16] M. Cantoro, V. B. Golovko, S. Hofmann, D. R. Williams, C. Ducati, J. Geng*, et al.*, "Wet catalyst assisted growth of carbon nanofibers on complex three-dimensional substrates," *Diamond and Related Materials,* vol. 14, pp. 733-738, 3// 2005.

[17] V. I. Merkulov, D. H. Lowndes, Y. Y. Wei, G. Eres, and E. Voelkl, "Patterned growth of individual and multiple vertically aligned carbon nanofibers," *Applied Physics Letters,* vol. 76, pp. 3555-3557, 2000.

[18] S. Hofmann, G. Csányi, A. C. Ferrari, M. C. Payne, and J. Robertson, "Surface Diffusion: The Low Activation Energy Path for Nanotube Growth," *Physical Review Letters,* vol. 95, p. 036101, 07/12/ 2005.

[19] M. L. Toebes, J. H. Bitter, A. J. van Dillen, and K. P. de Jong, "Impact of the structure and reactivity of nickel particles on the catalytic growth of carbon nanofibers," *Catalysis Today,* vol. 76, pp. 33-42, 11/1/ 2002.

[20] I. Kvande, Z. Yu, T. Zhao, M. Rønning, A. Holmen, and D. Chen, "Towards large scale production of CNF for catalytic applications," *Chem. Sustainable Dev,* vol. 14, p. 583, 2006.

[21] M. Kumar and Y. Ando, "Chemical Vapor Deposition of Carbon Nanotubes: A Review on Growth Mechanism and Mass Production," *Journal of Nanoscience and Nanotechnology,* vol. 10, pp. 3739-3758, // 2010.

[22] N. M. Rodriguez, "A review of catalytically grown carbon nanofibers," *Journal of Materials Research,* vol. 8, pp. 3233-3250, 1993.

[23] P. W. A. M. Wenmakers, J. van der Schaaf, B. F. M. Kuster, and J. C. Schouten, ""Hairy Foam": carbon nanofibers grown on solid carbon foam. A fully accessible, high surface area, graphitic catalyst support," *Journal of Materials Chemistry,* vol. 18, pp. 2426-2436, 2008.

[24] A. Gohier, T. M. Minea, S. Point, J. Y. Mevellec, J. Jimenez, M. A. Djouadi*, et al.*, "Early stages of the carbon nanotube growth by low pressure CVD and PE-CVD," *Diamond and Related Materials,* vol. 18, pp. 61-65, 1// 2009.

[25] D. B. Thakur, R. M. Tiggelaar, J. G. E. Gardeniers, L. Lefferts, and K. Seshan, "Carbon nanofiber based catalyst supports to be used in microreactors: Synthesis and characterization," *Chemical Engineering Journal,* vol. 160, pp. 899-908, 6/15/ 2010.

[26] S. Helveg, C. Lopez-Cartes, J. Sehested, P. L. Hansen, B. S. Clausen, J. R. Rostrup-Nielsen*, et al.*, "Atomic-scale imaging of carbon nanofibre growth," *Nature,* vol. 427, pp. 426-429, 01/29/print 2004.

[27] H. Yoshida, S. Takeda, T. Uchiyama, H. Kohno, and Y. Homma, "Atomic-Scale In-situ Observation of Carbon Nanotube Growth from Solid State Iron Carbide Nanoparticles," *Nano Letters,* vol. 8, pp. 2082-2086, 2008/07/01 2008.

[28] N. A. Jarrah, J. G. van Ommen, and L. Lefferts, "Mechanistic aspects of the formation of carbon-nanofibers on the surface of Ni foam: A new microstructured catalyst support," *Journal of Catalysis,* vol. 239, pp. 460-469, 4/25/ 2006.

[29] A. Romero, A. Garrido, A. Nieto-Márquez, A. R. de la Osa, A. de Lucas, and J. L. Valverde, "The influence of operating conditions on the growth of carbon nanofibers on carbon nanofiber-supported nickel catalysts," *Applied Catalysis A: General,* vol. 319, pp. 246-258, 3/1/ 2007.

[30] Z. Zeng and K. Natesan, "Relationship between the Growth of Carbon Nanofilaments and Metal Dusting Corrosion," *Chemistry of Materials,* vol. 17, pp. 3794-3801, 2005/07/01 2005.

[31] C. Chun, G. Bhargava, and T. Ramanarayanan, "Metal dusting corrosion of nickel-based alloys," *Journal of the Electrochemical Society,* vol. 154, pp. C231-C240, 2007.

[32] J. K. Chinthaginjala, J. H. Bitter, and L. Lefferts, "Thin layer of carbon-nano-fibers (CNFs) as catalyst support for fast mass transfer in hydrogenation of nitrite," *Applied Catalysis A: General,* vol. 383, pp. 24-32, 2010.

[33] J. K. Chinthaginjala and L. Lefferts, "Support effect on selectivity of nitrite reduction in water," *Applied Catalysis B: Environmental,* vol. 101, pp. 144-149, 2010/11/22/ 2010.

[34] b. v. RECEMAT. Available: http://www.recemat.nl/eng/datasheets/datasheet_nickel.pdf

[35] J. Chinthaginjala, D. Thakur, K. Seshan, and L. Lefferts, "How carbon-nano-fibers attach to Ni foam," *Carbon,* vol. 46, pp. 1638-1647, 2008.

[36] A. Cabrero-Vilatela, R. S. Weatherup, P. Braeuninger-Weimer, S. Caneva, and S. Hofmann, "Towards a general growth model for graphene CVD on transition metal catalysts," *Nanoscale,* vol. 8, pp. 2149-2158, 2016.

[37] R. S. Weatherup, B. C. Bayer, R. Blume, C. Ducati, C. Baehtz, R. Schlögl*, et al.*, "In Situ Characterization of Alloy Catalysts for Low-Temperature Graphene Growth," *Nano Letters,* vol. 11, pp. 4154-4160, 2011/10/12 2011.

[38] N. Dharmaraj, P. Prabu, S. Nagarajan, C. H. Kim, J. H. Park, and H. Y. Kim, "Synthesis of nickel oxide nanoparticles using nickel acetate and poly(vinyl acetate) precursor," *Materials Science and Engineering: B,* vol. 128, pp. 111-114, 3/15/ 2006.

[39] Y. Liu, C. Pan, and J. Wang, "Raman spectra of carbon nanotubes and nanofibers prepared by ethanol flames," *Journal of Materials Science,* vol. 39, pp. 1091-1094, 2004.

[40] F. Tuinstra and J. L. Koenig, "Raman Spectrum of Graphite," *The Journal of Chemical Physics,* vol. 53, pp. 1126-1130, 1970.

Supporting Information

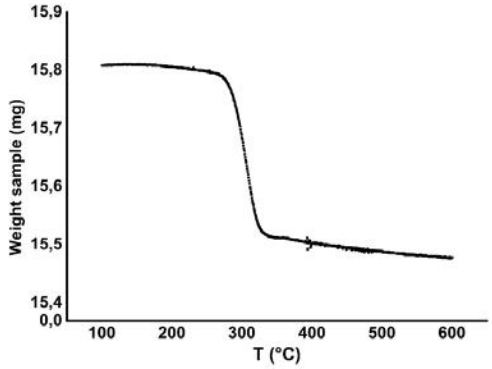

SI Figure 1: TGA graph (ΔT 5 °C/min, 20 vol% H_2 in Ar) of pre-oxidized nickel foam; oxidized at 600 °C for 1 h under 4 vol% O_2 in N_2 at ambient pressure

(Snapshots from movies)

Movies can be found at https://www.utwente.nl/en/tnw/cpm/supporting_movies

SI Movie 1: ESEM movie showing carbon precipitation on the surface of the Ni foam after prolonged exposure at 600 °C of the reduced Ni foam to C_2H_4 and H_2 at pressures between 10^{-2} Pa and 100 Pa followed by decreasing ethylene pressure to below 10^{-2} Pa

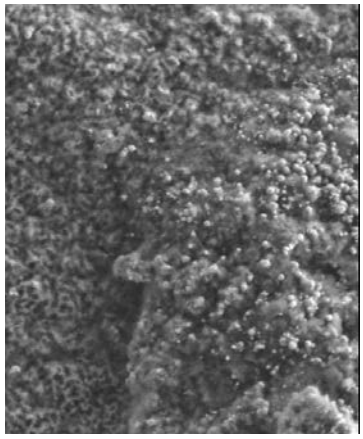

SI Movie 2: ESEM movie of NiO at 440 °C under 10 sccm C_2H_4 and 10 sccm H_2 with a total pressure of 60 Pa, showing formation of Ni nanoparticles in the range of tens of nanometers over the entire NiO surface; in the bottom right corner a NiO fragment is moving due to CNF-cluster growth

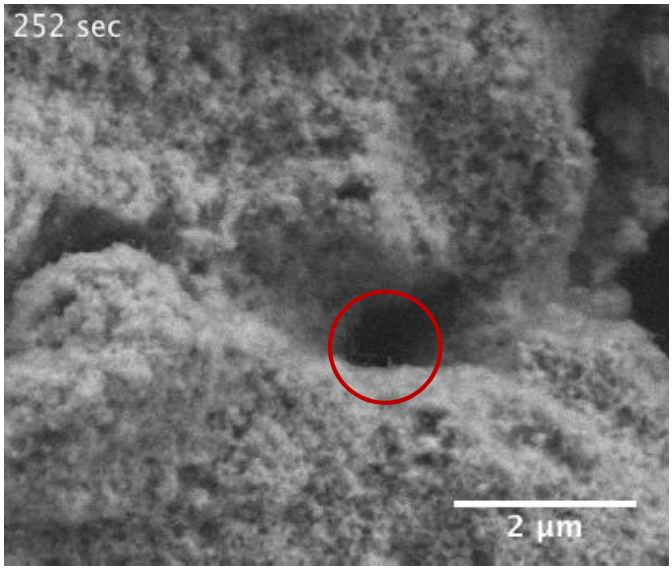

SI Movie 3: Zoom in of an ESEM movie showing individual CNF growth in-situ (clear example of this in the red circle), at 440 °C during exposure to 10 sccm C_2H_4 and 10 sccm H_2 with a total pressure of 60 Pa

Chapter 3

Immobilization of Carbon Nanofibers (CNFs) on a Stainless Steel Filter as a Catalyst Support Layer

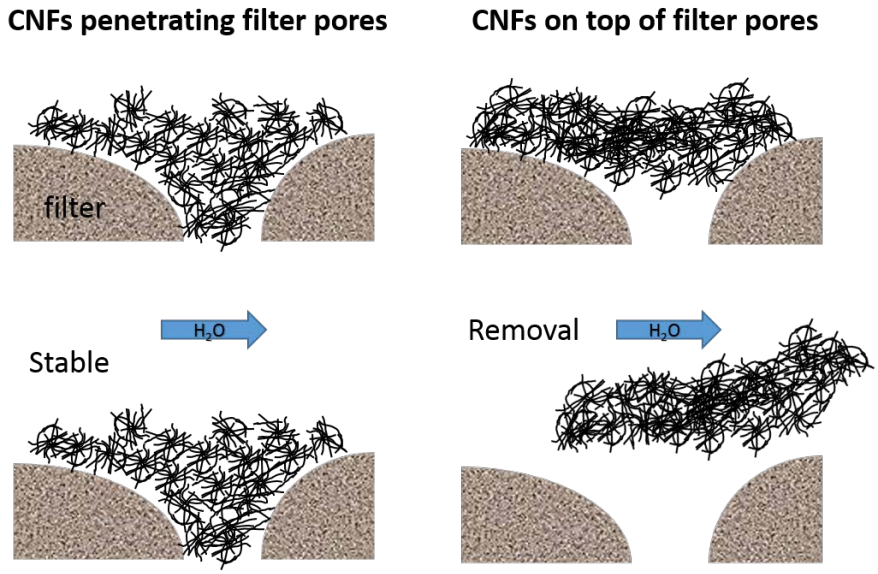

Chapter published as:

J.M. Roemers-van Beek, J.G. van Ommen, L. Lefferts, Immobilization of Carbon Nanofibers (CNFs) on a Stainless Steel Filter as a Catalyst Support Layer, Catalysis Today, vol. 301, pp 134-140, 2018

Abstract

A layer of carbon nanofiber (CNF) agglomerates is used to produce a catalyst support layer that can be immobilized on a stainless steel filter and that can be removed when desired. For immobilization a filtration procedure is developed that produces a stable CNF layer at relatively low shear force flows (<0.18 m/s). Under these conditions the device can be used as a chemical reactor. Increasing the shear force flow rate enables removal of the CNF layer. The interaction between the CNF agglomerates within the immobilized layer is stronger than the attachment of the entire layer to the surface of the stainless steel filter. The weaker interaction between the layer of CNF agglomerates and the filter surface therefore determines the stability of the layer. High surface roughness of the filter on micro-scale as well as deep penetration of CNF agglomerates in the pore mouths of the stainless steel filter both enhance stability of the CNF layer.

3.1 Introduction

The majority of commercially applied chemical processes uses heterogeneous reactions, where one important reaction-type is three-phase gas-liquid-solid reactions (G-L-S). Typical reactors used for these are trickle bed reactors or slurry phase reactors, with respective pros and cons. The main drawback of packed bed trickle phase reactors is internal diffusion limitations whereas separation of catalyst and product is much more facile compared to slurry phase operation [1, 2]. Structured reactors [2-5] are an alternative for slurry and trickle-bed reactors, which has been an active research field for many years. In structured reactors good external mass transfer, short diffusion distances and good temperature control can be achieved in combination with low pressure drop. Disadvantages, compared to trickle bed or slurry phase reactors, are the moderate catalyst loading, higher catalyst (immobilization) costs and challenging liquid distribution [1].

In structured reactors the surface area, needed to support highly dispersed active particles, is usually provided by using a washcoat, as structured packings like monoliths [6, 7], foams and filters [8] usually provide insufficient surface area. This washcoat layer needs to be thin (10-100μm) to minimize diffusion limitations, however this is a trade-off with the higher available surface area that would result from a thicker layer. Washcoats need maximal porosity and minimal tortuosity. Another important drawback of washcoats on structured packings is catalyst recycling and replacement. Replacement of the catalyst necessitates removal of the entire structured packing from the reactor, increasing costs significantly.

A layer consisting of carbon nanofibers has been proposed as an alternative to washcoat layers. These carbon nanofibers constitute a much more open structure than the conventional washcoat layer, the structure mimicking the inverse structure of the washcoat [9]. Carbon nanofibers can be produced *e.g.* through arc discharge, catalytic chemical vapour deposition [10, 11] and plasma enhanced chemical vapour deposition [10]. For catalytic chemical vapour deposition a carbon containing gas (*e.g.* ethylene [12], ethyn [10], methane [12], acetylene [8], syngas, CO) is flowed over transitions metal particles (*e.g.* Ni [10, 13], Fe [14], Co [14]) at elevated temperature. The carbon

containing gas decomposes at the surface on one side of the metal particle and carbon diffuses through or over the metal particle. The carbon then segregates at another side of the metal particle, producing a carbon nanofiber.

Previous work in our group reported on preparation procedures and catalytic applications of thin layers of CNFs on monoliths [15], foam structures [11, 13], metal foils [14], thin layers [16] and in microchannels [17]. The goal of this study is to explore the possibility to prepare a removable support layer on a structured packing using CNFs. This idea is inspired on the observation that particles consisting of entangled CNFs tend to stick together after filtration, so that re-dispersion is sometimes difficult to achieve. It is speculated that this effect is caused by interaction between CNFs sticking out of the individual agglomerates, causing a mechanical interaction similar to the well-known Velcro tape [18]. We explore how attachment between CNF agglomerates, as well as CNF agglomerates with the surface of the structured packing, can be used to achieve reversible immobilization on the surface of the structured packing. In this way, it would be possible to replace only the catalyst in case of deactivation, leaving the structured packing in the reactor. It is proposed that an immobilized CNF layer can combine the advantages of a highly porous catalyst support with the option to load and de-load exclusively the carbon nanofiber supported catalyst. In this study we will be using sintered metal filters as a model for a structured packing in order to explore the concept. Once the concept is successfully produced, this model support will be used in nitrite hydrogenation in future work.

3.2 Experimental

3.2.1 Materials

The stainless steel filter used for this study is a Sika R50, a 1.4404 (316L) steel from GKN Sinter Metals [19], consisting of 65wt% Fe, 19 wt% Cr, 12 wt% Ni, traces of Mo and Si. This filter has average pores of 50 μm and a BET surface area of 0.14 m^2/g (Figure 1a). From the as-received, 5 mm thick stainless steel sheet, rectangles of 16x36 mm are cut, using electrical discharge machining (Agiecut Challenge 2).

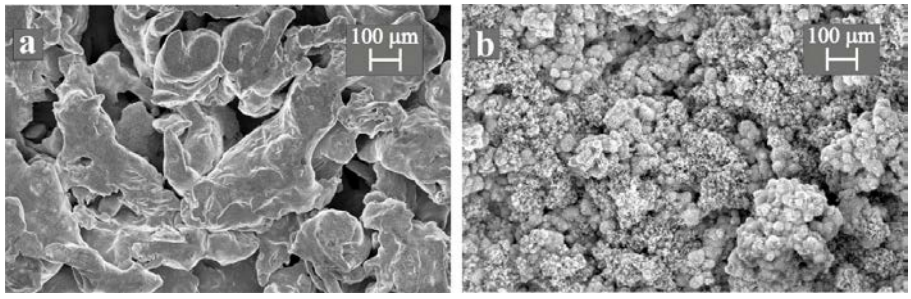

Figure 1: Low magnification SEM pictures of a) as-received stainless steel filter b) stainless steel filter covered with a grown carbon nanofibers layer

Two different types of carbon nanofibers are used in this study. CNF agglomerates (MF-C150, commercially available from Carbon Nanotube & Fibers 21) are used, containing individual fibers of 80-150 nm in diameter and a purity of >80%, with <20% amorphous carbon and <2% Ni/Fe. These CNF agglomerates as-received have an average size of 150 µm. This type CNF agglomerates was selected, despite the relatively low surface area, because of the observation that homogeneous CNF layers were obtained after deposition, in contrast to other types of CNF agglomerates.

The second type of carbon nanofibers is produced in house by growing carbon nanofibers directly on the surface of the stainless steel filter, using ethylene (99.95%, Praxair), hydrogen (99.999%, Linde) and nitrogen (99.999%, Linde). CNFs are grown in a home-designed vertical quartz reactor. The stainless steel filter (16x36x5mm, typically ~12g) is reduced for one hour with 20% H_2 in N_2. Growth is achieved at 600 °C under 100 ml/min flow of 20% C_2H_4 + 20% H_2 in N_2 for 2 hours. This procedure is inspired on previous growth procedures conducted on stainless steel foils in our group [14].

Milli-Q water (Synergy Millipore machine) is used for pressure drop and compressibility testing.

3.2.2 Characterization

The average agglomerate size of CNFs is measured by laser light diffraction in a Mastersizer 2000 from Malvern Instruments. BET surface areas of these CNF

agglomerates have been calculated from N_2 adsorption measured with a Micromeretics Tristar 3000. HR-SEM pictures were obtained in a Zeiss Merlin Scanning Electron Microscope equipped with an EDX detector. Stability of the grown CNF layer is tested by sonicating the layer in an ethanol solution in a VWR USC300TH sonication bath.

3.2.3 Preparation immobilized CNF layers

The CNF agglomerates are separated into three size fractions by dispersing the as-received CNFs in ethanol and using three sieve mesh sizes (80, 150 and 250 μm) for wet sieving.

Formation of layers of immobilized CNF agglomerates is achieved in a home-designed set-up shown in Figure 2. The CNF agglomerates for deposition are suspended in 15 ml ethanol, using 12.5, 25 or 50 mg CNFs. A layer of the CNF agglomerates is formed by filtration, *i.e.* removal of the ethanol through the stainless steel filter (Figure 2) and therefore this equipment is named "filtration set-up".

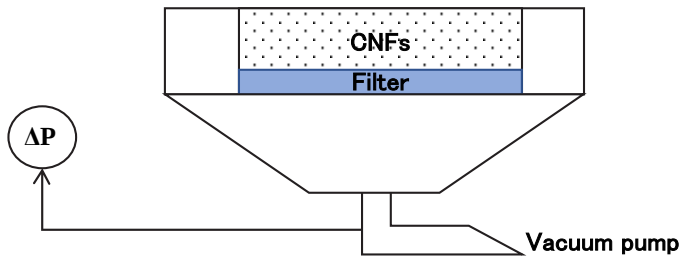

Figure 2: Schematic representation of the filtration set-up for CNF layer formation

The CNF suspension is poured onto the stainless steel filter, while the pump is off, and immediately the pump (capacity 1.7 m^3/h) is started. This pump capacity results in a pressure difference over the empty stainless steel filter smaller than 200 mbar, the lower limit of the pressure indicator. Within typically five seconds the ethanol is removed by filtration with a pressure drop varying between 300-700 mbar. As soon as the ethanol has passed through the filter the pressure drop reverts to less than 200 mbar. When the ethanol is completely removed the pump is turned off.

During the filtration, the CNF layer is compressed by a combination of both the force that is exerted by the pressure drop over the CNF layer, as well as by shear forces of ethanol flowing along the CNF agglomerates. These mechanical forces cause the agglomerates to be pushed together, and/or are pushed against the surface of the filter, with or without a grown CNF layer.

Layer thicknesses of immobilized CNF layers were determined with an analogue thickness meter, with a round plunger with a diameter of 5 mm and an accuracy of 0.01 mm. The CNF layer thickness was calculated by subtracting the thickness of the empty stainless steel filter (experimental variation ±0.025 mm) from the thickness of the filter with the CNF layer (experimental variation ±0.1 mm), each in two spots per individual sample. To determine the layer thickness and its error margin, 3 samples were measured per data point.

A qualitative measure for the density of the immobilized CNF layer is obtained by measuring the permeability to water, by measuring the flow rate of water through the substrate at a fixed pressure drop of ~90 mbar. This experiment is named the "pressure drop test". The same procedure was also used to try to densify the CNF layer, by repetitively applying the 90 mbar pressure drop and using the accumulative time to show the effects of longer exposure times. The immobilized CNF layer is subjected to typically five subsequent tests; in between tests the flow was paused to measure the amount of Milli-Q water flowed through.

3.2.4 Stability of immobilized CNF layers

Stability of the prepared CNF layer is tested in a home-designed set-up, shown in Figure 3. This set-up consists of a holder for the rectangular stainless steel filter with on top a flow chamber, with a height of 11 mm. To minimize mechanical damage during handling, the same holder as used in the filtration set-up is used here, which is transferred from the filtration equipment to the stability testing equipment.

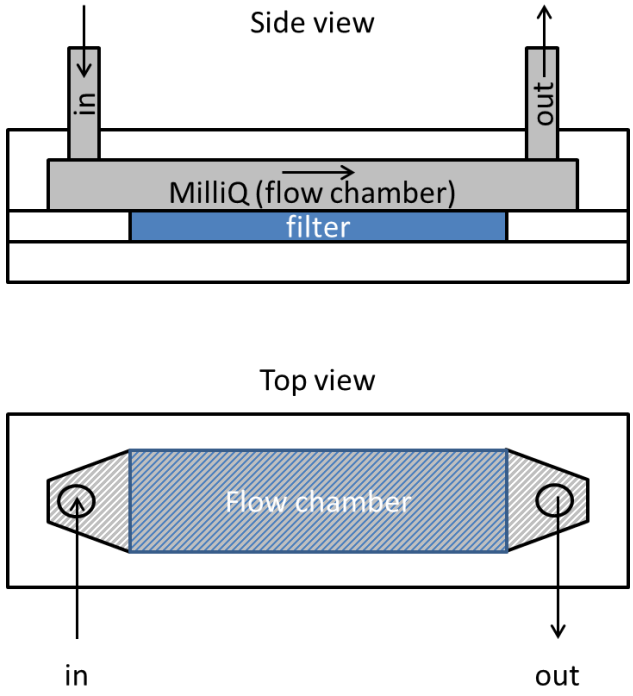

Figure 3: Schematic side- and top view of home designed set-up for CNF layer stability testing

The CNF layer stability is tested by flowing Milli-Q water over the immobilized CNF layer, with flow rates up to 0.6 m/s for typically 10 minutes. The stability of the layer is determined by measuring the amount of CNFs that is removed on basis of weight change of the sample, after thorough drying in a vacuum oven overnight. The top part of the stability testing set-up is made of transparent poly(methyl methacrylate) (PMMA) allowing recording of an *in-situ* movie during CNF removal.

3.3 Results

3.3.1 CNF agglomerates

The CNF agglomerates, as-received, exhibit a (volume) particle size distribution ranging from 7 to 1000 µm (Figure 4), measured in an ethanol suspension with laser light diffraction, with an average size of 150 µm. The as-received CNFs have a BET surface area of 32 m^2/g.

Figure 4 shows the CNF particle size of the as-received CNF agglomerates and the three size fractions separated by wet sieving, resulting in a fraction of smaller particles (average particle size 95 µm), a medium fraction (average particle size 150 µm) and a large fraction (average particle size 400 µm).

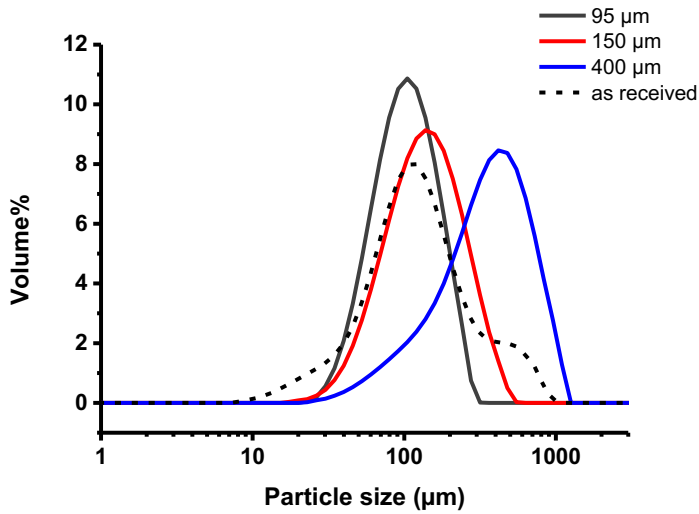

Figure 4: Volume averaged particle size distributions of as-received CNF agglomerates and the three selected size fractions, according to laser light diffraction

As can be seen in Figure 5a, the CNFs agglomerate into apparently dense particles with a smooth surface, at low magnification. Intermediate magnification (Figure 5b) shows however the rough nature of the external surface with some individual CNFs sticking out. The high magnification in Figure 5c however clearly confirms the highly open morphology, generated by entangled CNFs with a typical diameter of 100 nm.

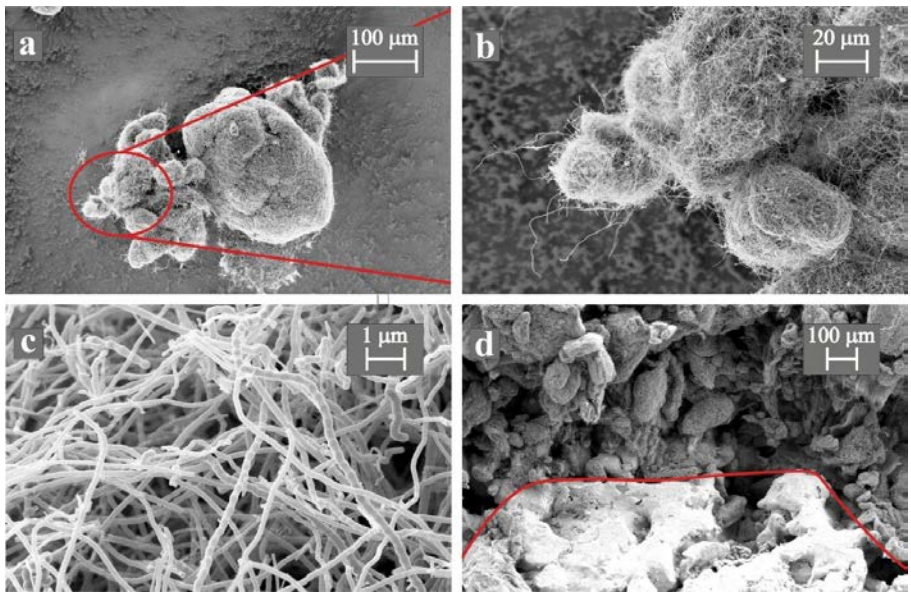

Figure 5: SEM pictures of as-received carbon nanofibers a) at low magnification, b) intermediate magnification and c) high magnification, d) cross-section of a deposited CNF layer (top), making a 90° angle at the line with the bare stainless steel filter below (bottom)

3.3.2 CNF layer synthesis

A CNF layer is grown directly on the stainless steel filter under the conditions described in the experimental section, attempting to generate a binder layer between the CNF agglomerates and the stainless steel. This results in a typical average ethylene conversion of 20% over 2 hours of CNF growth. This CNF layer completely covers the surface of the filter (Figure 1b) with a typical thickness of a few µm, measured in a SEM-picture (shown in SI Figure 1a). The diameter of the CNFs ranges from 5 to 250 nm (SEM-picture, shown in SI Figure 1b). According to N_2 adsorption this results in a

typical BET area of ~290 m^2/g_{carbon}, which corresponds to a CNF diameter of 6.2 nm. This indicates that the smaller CNF diameters are dominant. The grown layer is well attached to the stainless steel, as sonication in ethanol for 15 min removes only 1 wt% of the CNFs and shear force testing (10 min, 0.36 m/s) results in negligible removal of CNFs. Strong attachment of CNFs grown directly on metal substrates was also reported previously [13, 14]. It has been proposed that a thin, microporous carbon layer is formed that closely follows the surface roughness of the metal surface and CNFs are rooted in that layer, explaining the observed mechanical stability [13, 14]. The growth catalyst particles were identified as Fe particles based on EDX analysis.

3.3.3 CNF agglomerates immobilization

The CNF agglomerates are pushed together, which results in a CNF layer in which the individual agglomerates are not distinguishable anymore in SEM (Figure 5d), indicating significant interaction between CNF agglomerates. The filtrate is collected and no CNFs could be detected (with a detection limit of 0.01 mg)

Figure 6 shows the effects of particle size and amounts of CNFs on the resulting layer thickness of the immobilized CNF layer. Figure 6 shows a small effect of particle size, where smaller particles show slightly thinner layers, as would be expected. The increase in layer thickness compared to the amount of CNFs applied is slightly less than proportional, which suggests that thicker layers are slightly more compressed.

A CNF layer of 12.5 mg of CNFs results in a layer thickness of 200-350 μm thickness; when considering the particle size (95, 150 and 400 μm), it is clear that the layer is only 1-3 particles thick, causing partial coverage of the surface of the filter, as visually observed. CNF layers of 25 and 50 mg of CNFs result in fully covering, homogeneous layers, although the 50 mg layer resulted in larger variations in the observed layer thickness.

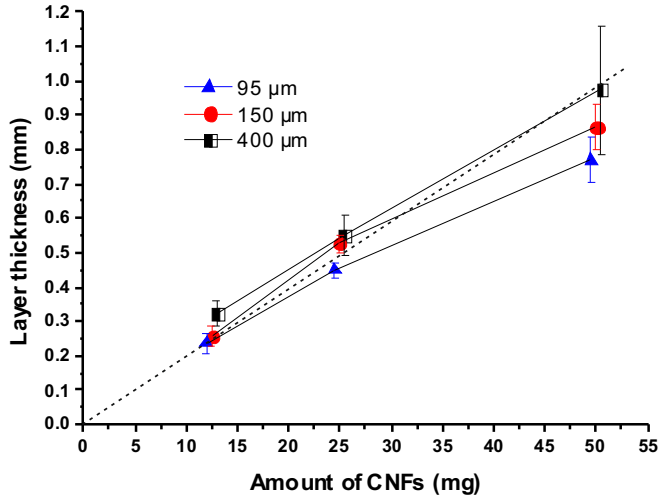

Figure 6: Influence of the particle size and amount of CNFs on the resulting thickness of the CNF layer after immobilization with 400 mbar pressure drop; data points shifted slightly for visualization, dotted guide line to show proportionality related to 95 µm, 12.5 mg layer

The pressure drop during filtration for all experiments in Figure 6 is strongly influenced by the amount of CNFs used for preparation of the immobilized CNF layer, as expected; however, the effect of particle size appears insignificant.

Figure 6 shows reasonably reproducible data for 95 µm particles and with 150 µm particles, in contrast to 400 µm particles showing larger scatter. This is probably caused by poor homogeneity resulting from the fact that the layers thicknesses (300-1200 µm) are typically 1-3 times the average particle size of 400 µm. Wet sieving results in much higher yields for 150 µm particles than for 95 µm particles, therefore the 150 µm particles are selected for further testing.

3.3.4 Densification of the CNF agglomerates layer

The rates of flow through the CNF layers of the three particle size fractions were measured with water at 90 mbar pressure drop for respectively 240, 120 and 90 sec. These CNF layers were immobilized beforehand with 300-400 mbar pressure drop during filtration. On average the 95 µm fraction results in a flow through of 0.04 L/min, 150 µm results in 0.11 L/min and 400 µm results in 0.26 L/min. This shows that the smaller the particles, the higher the resistance of the CNF layer, indicating that the layer becomes denser, as expected.

Repetitive exposure to 90 mbar water pressure results in decreasing flow rates (Figure 7), demonstrating that the forces exerted by the water pressure on the CNF layer cause densification of the CNF layer.

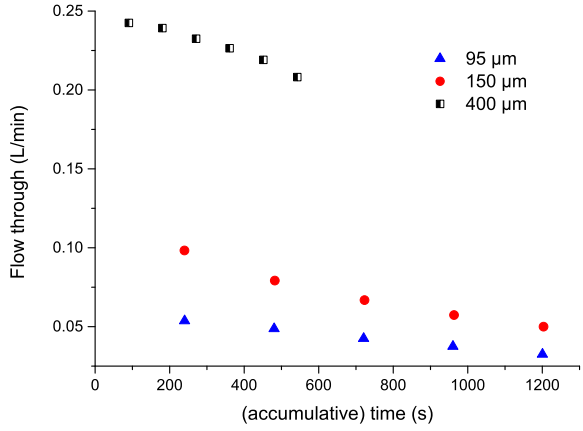

Figure 7: Effect of accumulative time on flow rate of water through a 25 mg CNF layer (90 mbar pressure drop) supported on the stainless steel filter, immobilized with 300-350 mbar

3.3.5 Stability of the CNF agglomerates layer

The deposited layers were exposed to water flowing along the surface during 10 minutes for testing the stability of the CNF layers consisting of 25 mg CNFs agglomerates sized 150 μm. Figure 8 shows the influence of the flow rate on the stability of these CNF layers, immobilized with a pressure drop of 400 mbar and resulting in 0.5 mm thick layers, as described above.

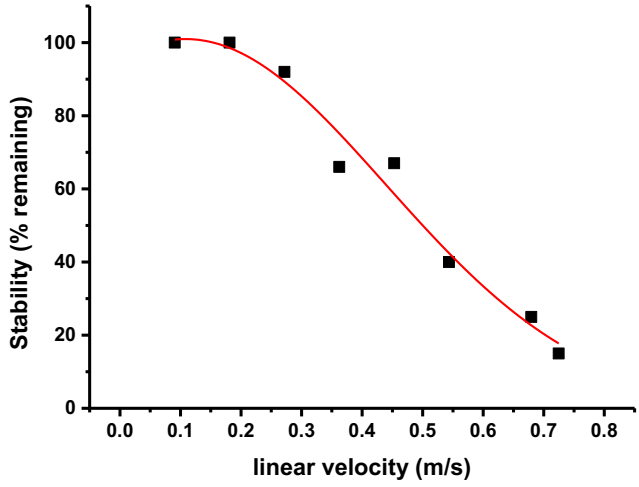

Figure 8: Effect of linear flow velocity in shear force testing on the CNF layer stability for an immobilized CNF agglomerates layer consisting of 25 mg CNFs of the 150μm fraction, immobilized with 400 mbar pressure drop

The removal of CNFs, if any, happens mostly in the first few minutes. For all linear velocities causing removal, removal is observed to occur in pieces starting close to the entrance of the water flow, removing the entire layer locally and thus exposing clean external surface of the metal filter. The relatively sharp boundary between clean and CNF-covered filter moves slowly downstream. Figure 9 shows snapshots from an *in-situ* movie of the removal of CNFs when flowing water with a velocity of 0.45 m/s

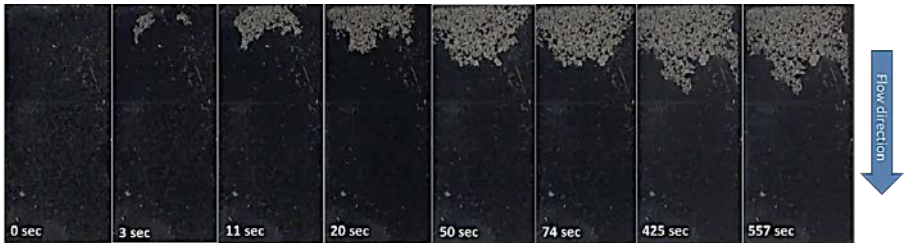

Figure 9: Removal of CNF particles for a layer of 25 mg CNFs (150 µm fraction) during flow over testing, 0.45 m/s linear velocity (flow direction top to bottom), top view of the sample showing the CNF layer (black) with stainless steel filter underneath (grey)

3.3.6 Effect of pressure drop during immobilization

Figure 10 shows the effect of the pressure drop, used during the filtration when immobilizing the CNF agglomerates, on the stability of the CNF layer. For these tests CNF layers (25 mg, 150 µm fraction) were subjected to 0.36 m/s for 10 min.

From Figure 10 (▪) it can be clearly seen that the stability of the immobilized CNF layer increases with increasing pressure drop during filtration. In contrast, densification of the layers after filtration by flowing water at 90 mbar, as shown in figure 7, showed no significant effect on stability of the CNF layer (not shown).

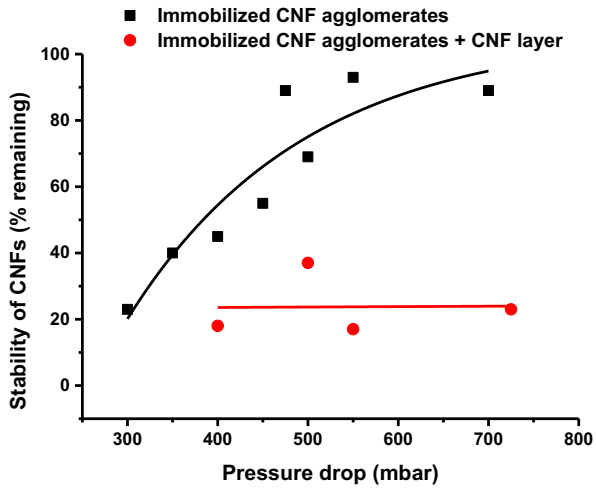

Figure 10: Effect of pressure drop during filtration on the stability of the immobilized CNF agglomerates on CNF-covered filter (•) and on the empty filter (▪), tested at 0,36 m/s linear velocity for 10 min, on an immobilized CNF layer consisting of 25 mg CNFs sized 150 µm

3.3.7 CNF binder layer

Figure 10(•) also shows the stability of the immobilized CNF agglomerates layer when it is immobilized on a CNF layer grown on the surface of the filter. The stability tests are conducted as described above. Surprisingly the resulting stability appears inferior compared to the CNF agglomerates layer on the empty filter. Furthermore, it seems independent of the pressure drop applied during deposition of the agglomerates, as can be seen in Figure 10 (•).

3.4 Discussion

Immobilization of CNF agglomerates is achieved by filtration. The most reproducible procedure was found to be immobilization of 25 mg of CNFs of the 150 μm fraction, by using a pressure drop of 400 mbar during filtration. The immobilized CNF layer was shown to be stable when flowing water over the layer with linear velocity up to 0.18 m/s, whereas removal of CNFs is observed at higher velocities (Figure 8). Also, it can be seen that at high flow rates (>0.7 m/s) almost the entire CNF layer is removed and complete removal is anticipated at even higher flowrates or via back-flushing.

In short, the immobilized CNF layer is stable at intermediate flow rates (till 0.18 m/s) allowing in principle operation as a catalytic reactor. Importantly, the layer can be removed from the structured packing by simply increasing the flow rate, without the need of removing the packing itself from the reactor.

Figure 7 shows that CNF layers with large particles are more permeable for water to flow through the layer, as expected. Figure 7 also shows a decrease in flow rate as a result of repetitive exposure to the pressure drop (90 mbar) when flowing water through the layer. This suggests that the density of the CNF layer increases by pushing the CNF aggregates more into each other.

Figure 10 clearly shows that presence of the grown CNF binder layer decreases the stability of the layer of CNF agglomerates, apparently weakening the interaction between the CNF agglomerates and the stainless steel filter. The lower stability with a CNF binder layer is attributed to the decreasing surface roughness when growing CNFs. This surface roughness decrease is visualized in both SEM pictures in Figure 1 as well as by confocal microscopy shown in SI Figure 2. Both show decreasing micro roughness of the stainless steel surface when growing a CNF layer. On the other hand, the roughness on the nanometer scale clearly increased when CNFs are present. Roughness on micrometer scale is apparently important for creating stable layers.

The results in Figure 9 show that pieces of the entire layer are removed from the filter, indicating that the interaction between the layer of CNF agglomerates and the

filter surface is weaker than the interaction between the CNF agglomerates within the layer. In other words, the interaction between the layer and the filter surface determines the stability of the layer. The stability of the layer of CNF agglomerates on the bare stainless steel filter increases with increasing pressure drop during immobilization (Figure 10). This is attributed to deeper penetration of the CNF agglomerates into the pore mouths of the filter, therefore making better use of the surface micro-roughness, as schematically presented in Figure 11a.

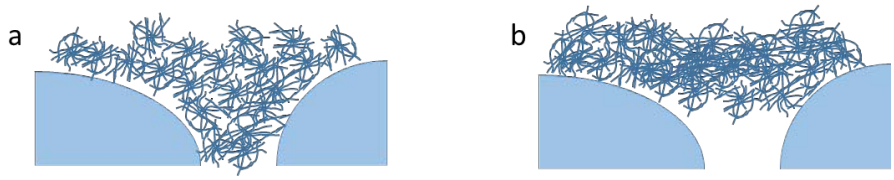

Figure 11: Schematic representation of interaction of the CNF agglomerates with the surface micro-roughness of the stainless steel filter a) CNF agglomerates penetrate into the pore mouth by applying high pressure drop during immobilization via filtration, b) densification, by prolonged exposure to pressure drop, of the layer without pore mouth penetration due to low pressure drop during immobilization via filtration

This proposal can also explain the results of the prolonged pressure drop tests. The observed densification (Figure 7) of the CNF layer increases the interaction between the CNF agglomerates within the layer, but does not influence the stability of the layer. Apparently, the CNF agglomerates are so well attached that the pressure drop provided is not able to push the agglomerates deeper into the pore mouths (Figure 11b). In contrast higher pressure drop during immobilization via filtration increases the stability, as shown in Figure 10▪. During build-up of the CNF layer, the agglomerates are initially not connected and the first agglomerates can penetrate deeper into the pore mouths (Figure 11a), resulting in deeper penetration and better attachment of the entire layer to the surface of the filter.

In this work, metallic filters were used for relatively easy immobilization of CNF agglomerates. However, it is shown that the stability of the CNF layer is mainly determined by the macro-roughness of the filter. The additional CNF layer grown on and attached to the metal filter, aiming at a binder layer, displayed an adverse effect on the CNF layer stability. Therefore, in future also alternative filter materials that do not allow direct CNF growth, such as ceramics or carbon based filters, should be explored. Clearly, additional work would be needed to develop this concept further to enable implementation in practical catalytic reactors. A practical reactor is envisaged consisting of concentric tubes where the inner tube is the porous wall that is considered in this study, as shown in Figure 12. Immobilization of the CNF layer can be done by flowing through the wall from inside to the shell, depositing the CNFs as a filter cake at the inner-surface of the porous tube. The reactor can then be operated either in flow-through mode in which the shell acts as reactor outlet, or in flow-over mode by operating the inner-tube as both inlet and outlet. Removal of deactivated catalyst is then easily achieved by back-flush operation.

The catalytic performance of these CNF layers as catalyst support loaded with Pd have been tested for nitrite hydrogenation for water cleaning, which will be reported in detail in a future paper.

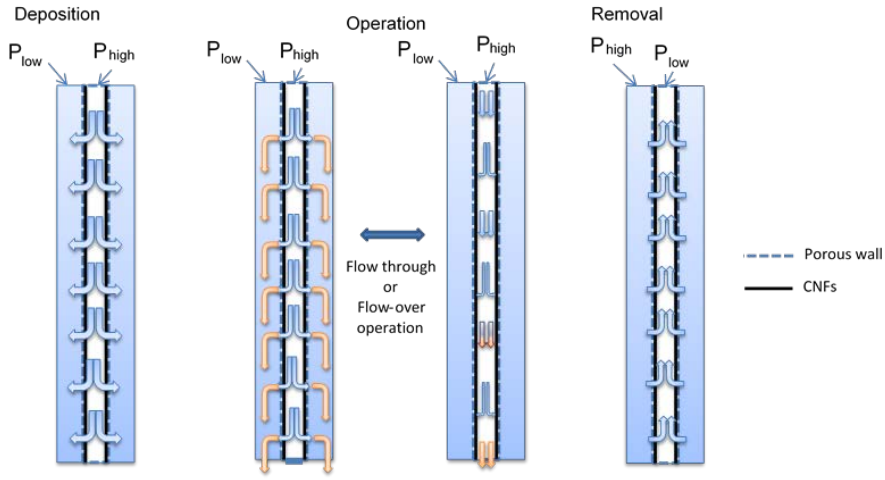

Figure 12: Schematic representation of a possible reactor design using the porous catalyst support structure as developed in this article

3.5 Conclusion

In this study a CNF layer is synthesized as a stable catalyst support layer for operational conditions. This layer is shown to be stable up to 0.18 m/s flow over the layer. This CNF layer can be removed by increasing shear force flow rate.

A CNF agglomerates layer immobilized directly on the stainless steel filter is more stable than the same layer deposited on a stainless steel filter with a grown CNF layer. It is proposed that the grown CNF layer decreases the micro roughness of the stainless steel filter, causing the decrease in stability.

The fact that the layer is removed in pieces of the entire layer during flow tests, leaving behind a bare filter surface, shows that the CNFs layer stability is determined by the interaction of the CNFs layer with the stainless steel filter surface. This is confirmed by the increased stability of the CNFs layer when increasing the pressure drop during immobilization via filtration, increasing the bonding between the surface of the filter and the CNF layer via deep penetration in the pore mouths of the filter.

Acknowledgements

This work took place within the framework of the Institute for Sustainable Process Technology (ISPT). Ing. Bert Geerdink is gratefully acknowledged for essential assistance in designing the set-ups, Mark Smithers for SEM micrographs and Karin Altena-Schildkamp and ing. Cindy Huiskes for performing N_2 adsorption experiments.

References

[1] B. Averill, J. Moulijn, R. van Santen, P. van Leeuwen, Catalysis: An Integrated Approach: An Integrated Approach, Elsevier1999.

[2] F. Kapteijn, T.A. Nijhuis, J.J. Heiszwolf, J.A. Moulijn, New non-traditional multiphase catalytic reactors based on monolithic structures, Catalysis Today, 66 (2001) 133-144.

[3] K. Pangarkar, T.J. Schildhauer, J.R. van Ommen, J. Nijenhuis, F. Kapteijn, J.A. Moulijn, Structured Packings for Multiphase Catalytic Reactors, Industrial & Engineering Chemistry Research, 47 (2008) 3720-3751.

[4] T. Boger, A.K. Heibel, C.M. Sorensen, Monolithic Catalysts for the Chemical Industry, Industrial & Engineering Chemistry Research, 43 (2004) 4602-4611.

[5] M. Grasemann, A. Renken, M. Kashid, L. Kiwi-Minsker, A novel compact reactor for three-phase hydrogenations, Chemical Engineering Science, 65 (2010) 364-371.

[6] T.A. Nijhuis, M.T. Kreutzer, A.C.J. Romijn, F. Kapteijn, J.A. Moulijn, Monolithic catalysts as efficient three-phase reactors, Chemical Engineering Science, 56 (2001) 823-829.

[7] S. Roy, T. Bauer, M. Al-Dahhan, P. Lehner, T. Turek, Monoliths as multiphase reactors: a review, AIChE journal, 50 (2004) 2918-2938.

[8] L.Kiwi.-Minsker. P. Tribolet, Palladium on carbon nanofibers grown on metallic filters as novel structured catalyst, Catalysis Today, 2005 (2005) 337-343.

[9] P.W.A.M. Wenmakers, J. van der Schaaf, B.F.M. Kuster, J.C. Schouten, "Hairy Foam": carbon nanofibers grown on solid carbon foam. A fully accessible, high surface area, graphitic catalyst support, Journal of Materials Chemistry, 18 (2008) 2426-2436.

[10] M. Cantoro, V.B. Golovko, S. Hofmann, D.R. Williams, C. Ducati, J. Geng, B.O. Boskovic, B. Kleinsorge, D.A. Jefferson, A.C. Ferrari, B.F.G. Johnson, J. Robertson, Wet catalyst assisted growth of carbon nanofibers on complex three-dimensional substrates, Diamond and Related Materials, 14 (2005) 733-738.

[11] N.A. Jarrah, F. Li, J.G. van Ommen, L. Lefferts, Immobilization of a layer of carbon nanofibres (CNFs) on Ni foam: A new structured catalyst support, Journal of Materials Chemistry, 15 (2005) 1946-1953.

[12] N.A. Jarrah, J.G. van Ommen, L. Lefferts, Growing a carbon nano-fiber layer on a monolith support; effect of nickel loading and growth conditions, Journal of Materials Chemistry, 14 (2004) 1590-1597.

[13] J.K. Chinthaginjala, D.B. Thakur, K. Seshan, L. Lefferts, How Carbon-Nano-Fibers attach to Ni foam, Carbon, 46 (2008) 1638-1647.

[14] S. Pacheco Benito, L. Lefferts, The production of a homogeneous and well-attached layer of carbon nanofibers on metal foils, Carbon, 48 (2010) 2862-2872.

[15] N. Jarrah, J.G. Van Ommen, L. Lefferts, Development of monolith with a carbon-nanofiber-washcoat as a structured catalyst support in liquid phase, Catalysis Today, 79-80 (2003) 29-33.

[16] R.M. Tiggelaar, D.B. Thakur, H. Nair, L. Lefferts, K. Seshan, J.G.E. Gardeniers, Influence of thin film nickel pretreatment on catalytic thermal chemical vapor deposition of carbon nanofibers, Thin Solid Films, 534 (2013) 341-347.

[17] D.B. Thakur, R.M. Tiggelaar, J.G.E. Gardeniers, L. Lefferts, K. Seshan, Carbon nanofiber based catalyst supports to be used in microreactors: Synthesis and characterization, Chemical Engineering Journal, 160 (2010) 899-908.

[18] G. De Mestral, Velvet type fabric and method of producing same, 1955.

[19] G.S. Metals: http://www.gkngroup.com/sintermetals/media/Brochures Library/ Capabilities - Porous Metal Filters/GKN Filter Technology SIKA-R AX EN.pdf, last Accessed November 2016.

Supporting Information

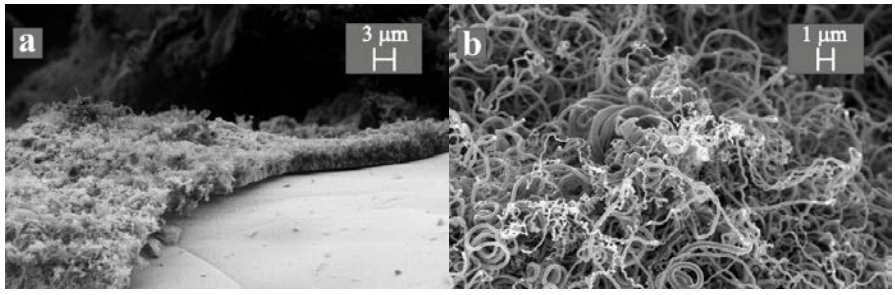

SI Figure 1: SEM pictures of a CNF layer grown on a stainless steel filter a) cross section of the CNFs layer b) CNFs showing variation in diameter

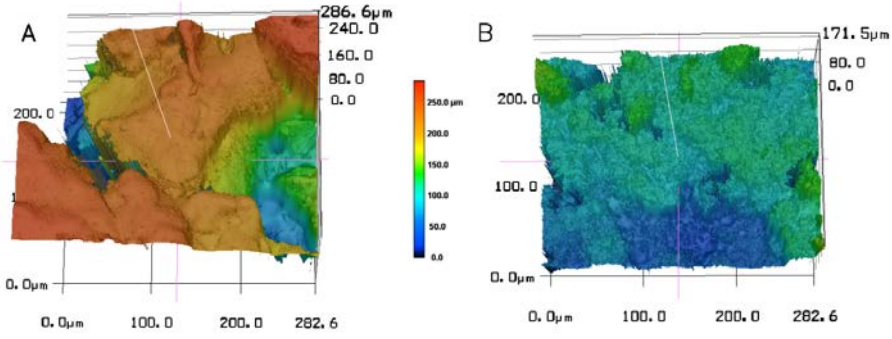

SI Figure 2: 3D profile of stainless steel filter measured with confocal microscopy a) bare filter, b) filter covered with grown CNFs layer

3D profile captured with confocal microscopy, on a Laser scanning microscope VK 9700 Keyence. The pores in the bare filter (left panel) are too deep to detect the bottom, so that quantification of the roughness is not possible. Laura Vargas is gratefully acknowledged for performing confocal microscopy experiments.

Chapter 4

Hydrogenation of Nitrite on Pd Supported on Immobilized CNF Agglomerates on a Stainless Steel Filter

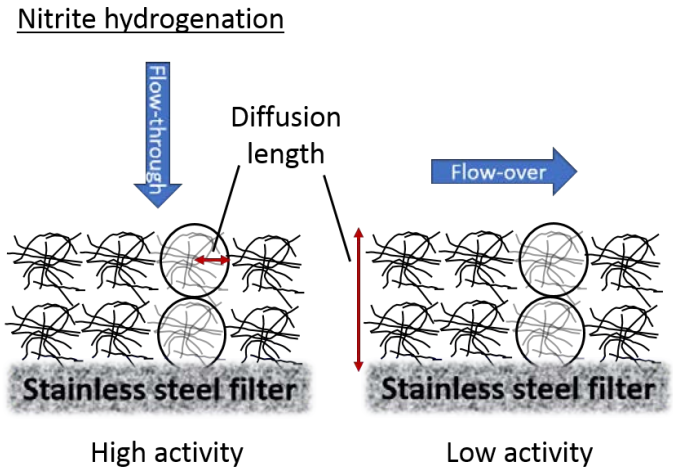

Chapter article in preparation:

J.M. Roemers-van Beek, J. Zhu, J.G. van Ommen, L. Lefferts, Hydrogenation of nitrite on Pd supported on immobilized CNF agglomerates on a stainless steel filter

Abstract

Pd-loaded carbon nanofiber (CNF) agglomerates, a slurry catalyst, are used after immobilization on a stainless-steel filter as a model for a structured reactor allowing reversible loading of catalyst. It is demonstrated that this indeed results in a carbon-based, structured reactor active for hydrogenation of nitrite as a model reaction. Activity was achieved both by flowing the H_2 saturated nitrite solution over the Pd-CNF layer as well as through the layer of immobilized Pd-CNF. Flowing liquid through the Pd-CNF layer results in higher reaction rates, demonstrating that mass transfer limitations affect operation in flow-over mode, caused by the relatively long diffusion distance in the Pd-CNF layer. External diffusion limitations at the surface of the individual CNF agglomerates dominate in flow-through mode.

4.1 Introduction

Structured reactors [1-4] as an alternative for conventionally used trickle bed or slurry reactors are a hot research topic nowadays. These structured reactors combine the advantages of slurry reactors, i.e. the low pressure drop, short diffusion distance, good external mass transfer and good temperature control, with advantages of trickle bed reactors, *i.e.* no attrition and easy separation of catalyst particles [5]. Disadvantages in structured reactors are the moderate catalyst loading per unit of reactor volume, higher catalyst (immobilization) costs and possible liquid maldistribution [5].

Highly dispersed active catalyst particles are used, necessitating high surface areas for the support structure. Since the structured supports like monoliths [6, 7], foams and filters [8] provide insufficient surface area, washcoats are usually employed to ensure sufficient available surface area. For these washcoats a balance needs to be found between additional surface area resulting from thicker layers and the resulting increase in internal diffusion limitations, especially when operating in liquid phase. Therefore washcoats are usually thin layers (10-100 μm).

Previous work in our group proposes an immobilized carbon nanofiber (CNF) layer as an alternative for washcoats. This CNF layer mimics the inverse structure of conventional washcoats [9], offering an open catalyst support structure, reducing diffusion limitations and enabling thicker catalyst support layers compared to conventional washcoats. The preparation and application of these CNF layers have been studied on monoliths [10], foam structures [11, 12], metal foils [13], thin layers [14] and in microchannels [15].

In our work we introduce a layer of immobilized CNF agglomerates using sintered metal filters as a structured packing. In our previous study we explored the stability and possible recyclability of this immobilized CNF layer [16]. CNF agglomerates are immobilized by a filtration procedure. The produced CNF layer is stable at relatively low shear force flows (<0.18 m/s), but can be removed by increasing the shear force flow rate. In this way, catalyst can be reversibly loaded on a structured packing, enabling removal of the catalyst, *e.g.* after deactivation, without the need to remove the structured packing. The stability of this CNF layer under operating conditions is

attributed to both the high surface roughness of the filter on micro-scale and the penetration of CNF agglomerates in the pore mouths of the stainless steel filter, in combination with strong attachment between CNF agglomerates. It is also shown that increased layer thickness leads to CNF layer densification.

In this study we present the catalytic testing of Pd particles deposited on these CNF agglomerates in nitrite hydrogenation, in order to test the ability of this novel catalyst support design to enable efficient (internal) mass transfer. Nitrite hydrogenation is ideal to detect diffusion limitations, because it is a very fast liquid phase reaction. In addition, diffusion limitation and development of internal concentration gradient is also known to influence the selectivity of the reaction, forming both the preferred product di-nitrogen (Equation 1) as well as the undesired product ammonium (Equation 2).

$$2NO_2^- + 3H_2 + 2H^+ \xrightarrow{Pd} N_2 + 4H_2O \qquad \text{Equation 1}$$

$$NO_2^- + 3H_2 + 2H^+ \xrightarrow{Pd} NH_4^+ + 2H_2O \qquad \text{Equation 2}$$

4.2 Experimental

4.2.1 Materials

Stainless steel filters (1.4404/316L) from GKN Sinter Metals are used, consisting of 65 wt% Fe, 19 wt% Cr, 12 wt% Ni, with traces of Mo and Si. These filters consist of a three-dimensional structure with an average pore size of 50 μm and a BET surface area of 0.14 m^2/g (Figure 1) [17]. Rectangular samples of 16x36 mm (5 mm thick) are cut from the as-received stainless steel filter by electrical discharge machining (Agiecut Challenge 2).

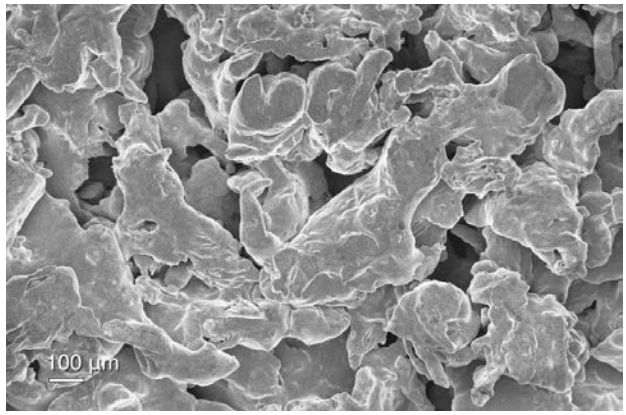

Figure 1: Low magnification SEM picture of as-received stainless steel filter

CNF agglomerates (MF-C150, Carbon Nanotube & Fiber 21) are used, containing individual fibers of 80-150 nm in diameter and a purity of >80%, with <20% amorphous carbon and <2% Ni/Fe. As-received these CNFs agglomerates have an average size of 150 µm, which are separated into three size fractions (65, 110 and 140 µm) by wet sieving [16] the CNFs dispersed in ethanol, using three sieve mesh sizes (80, 150 and 250 µm).

Palladium(II)2,4-pentanedionate (Pd 34.7%, Alfa Aesar) is used for deposition of Pd particles. Nitrogen (99.999%, Linde), air (home-produced) and hydrogen (99.999%, Linde) were used for calcination and reduction of the Pd-complex.

Sodium nitrite (>99%, Merck), hydrogen (99.999%, Linde) and nitrogen (99.999%, Linde) were used in milli-Q water (home-produced) for nitrite hydrogenation testing.

4.2.2 Characterization

Pd loading is determined with XRF in an ARL Advant'X spectrometer. The available total surface area is determined through N_2 adsorption measured with a Micromeretics Tristar 3000. The average agglomerate size of CNFs is measured by laser light diffraction in a Mastersizer 2000 from Malvern Instruments. HR-SEM pictures were obtained in a Zeiss Merlin Scanning Electron Microscope equipped with an EDX detector.

4.2.3 Pd deposition

CNF agglomerates are impregnated with Pd through wet impregnation with palladium(II)2,4-pentanedionate in toluene. To achieve about 1.3 wt% Pd on 0.14 g CNFs, 4 mg palladium acetylacetonate was dissolved into 80 ml toluene. The CNFs are introduced into the solution in a vacuum rotary evaporator for typically 6 h at 65 °C. After impregnation the samples are dried in a vacuum furnace overnight. Finally, the CNF agglomerates with palladium are calcined at 250 °C for 2 h in 100 ml/min air, followed by reduction at 250 °C for 1 h in 50% H_2 in N_2, total flow rate 100 ml/min.

4.2.4 Preparation immobilized CNF layers

Formation of layers of immobilized CNF agglomerates is achieved in a home-designed filtration set-up. For immobilization 30 or 60 mg CNF agglomerates are suspended in 15 ml of ethanol. A layer of the CNF agglomerates is formed by filtration, *i.e.* removal of the ethanol through the stainless steel filter. The immobilization procedure is discussed in more detail in previous published work [16], for this study layers were produced with 400 mbar pressure drop during filtration-deposition.

4.2.5 Catalytic activity testing for nitrite hydrogenation

The CNF layer, like a conventional washcoat, can be used in two different regimes. First, the liquid feed can be flown through the CNF layer, mimicking a membrane contactor reactor. Second, the liquid feed can be flown over the CNF layer, mimicking the use of a washcoat on a dense support. To enable testing in these two modes of operation, two set-ups were designed, shown in Figure 2.

In the flow-through set-up the liquid flow passes from the bottom chamber (height 6.5 mm, volume ~$4 \cdot 10^{-6}$ m^3) through the porous filter to the small funnel on top. Introduction of the liquid feed from two introduction points makes the liquid flow inside the reactor more homogeneous. These experiments will be called ‘flow-through’ experiments.

The flow-over set-up is designed to use the same filters with the same dimensions, but the liquid flow is channeled in a flow chamber (height 6.5 mm, volume ~$4 \cdot 10^{-6}$ m^3) to pass over the external surface of the CNF layer on top of the filter. The top of the

chamber is transparent, which enables checking absence of any trapped air bubbles, ensuring full and homogeneous use of the CNF layer. These will be called 'flow-over' experiments.

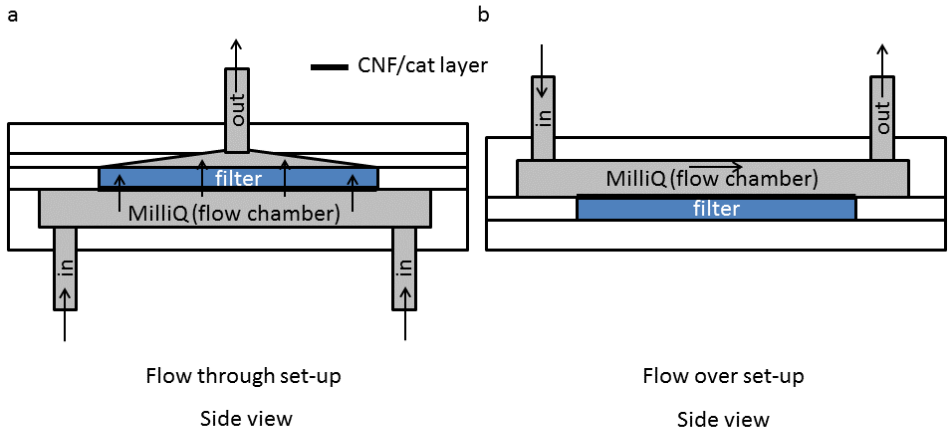

Figure 2: Schematic overview of a) flow-through and b) flow-over set-up used

Catalytic activity for nitrite hydrogenation was measured at room temperature in one of the reactors as described above using 0.22 mmol/L NO_2^- as a starting solution, saturating the solution with 0.5 atm H_2, resulting in 0.39 mmol/L H_2. This solution is not buffered. Immobilized CNF layers of usually 30 mg CNFs are tested, although 60 mg CNFs are tested to see the influence of the layer thickness on the diffusion limitations. Flow rates of 0.5 – 5 ml/min were used for the introduced nitrite solution.

Nitrite (NO_2^-) and ammonium (NH^{4+}) concentrations are measured with an ion chromatograph (Dionex, ICS 1000). NO_2^- conversion and NH^{4+} selectivity are calculated from these measurements, assuming ammonium is the only by-product [18, 19].

4.3 Results

4.3.1 BET

BET analysis of N2 physisorption data for Pd on CNFs, calcined at 400 °C resulted in a total surface area of 35.7 m^2/g.

4.3.2 CNF agglomerates

As received CNF agglomerates were separated into three fractions, using the wet sieving method. The resulting fractions exhibit average particle sizes of 65 µm, 110 µm and 140 µm (Figure 3).

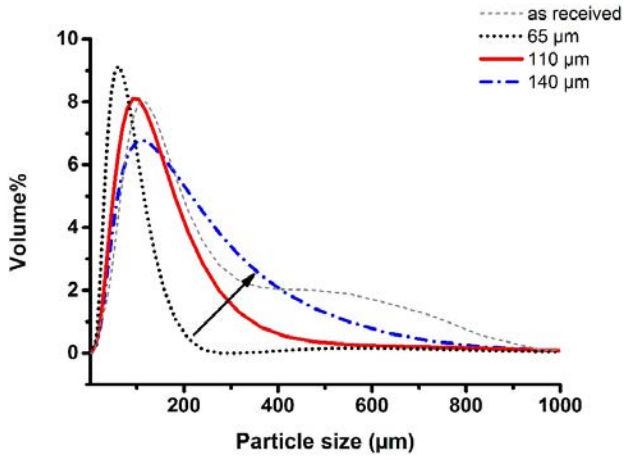

Figure 3: Volume averaged particle size distributions of as received CNF agglomerates and the three selected size fractions, according to laser light diffraction, measured in ethanol

4.3.3 Catalytic testing

Catalytic testing was performed continuously for up to 35 hours, measuring the same flow rate at the start and at the end of the measurement. This shows no decrease in the nitrite conversion, therefore it is assumed there is no degradation or loss of the Pd catalyst particles.

4.3.3.1 Effect of CNF particle size (Flow-through)

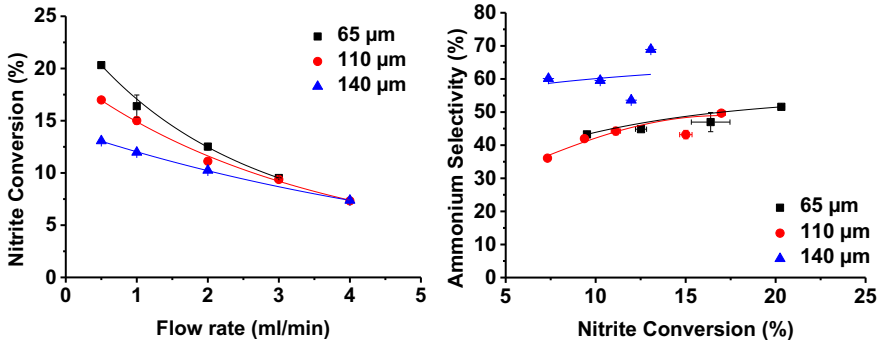

Figure 4 a) Influence of CNF particle size and flow rate on resulting nitrite conversion with 1.3 wt% Pd on 30 mg CNFs, b) influence of CNF particle size and conversion on ammonium selectivity

Figure 4 shows the effect of flow rate on nitrite conversion and selectivity to ammonium in flow-through mode for three CNF particle sizes. In all cases conversion decreases with increasing flow rate, as would be expected based on residence time. It can be clearly seen that the nitrite conversion decreases with increasing particle size. CNF particles of 65 µm and 110 µm result in similar ammonium selectivities when compared at constant conversion. However, bigger particles (140 µm) clearly show higher ammonium selectivity.

4.3.3.2 CNF particles loading

Two flow patterns i.e. flow-through and flow over the CNF layer are tested, details can be found in the Experimental section.

Flow-through

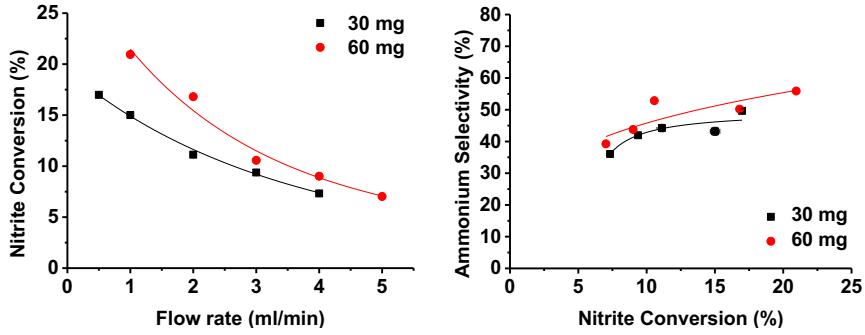

Figure 5 a) Influence of CNF particle loading and flow rate on nitrite conversion with 1.3 wt% Pd on CNF particles of 110 µm, b) influence of CNF particles loading and nitrite conversion on ammonium selectivity

Figure 5 shows the effect of flow rate on nitrite conversion and selectivity to ammonium for two different catalyst loadings in flow-through mode, tested for 110 µm CNF particles. Decreasing conversions with increasing flow rate, as discussed above, are expected. As can be seen, increase in catalyst loading results in only a relatively small increase in conversion (Figure 5a) and a slight increase in ammonium selectivity (Figure 5b).

Flow-over

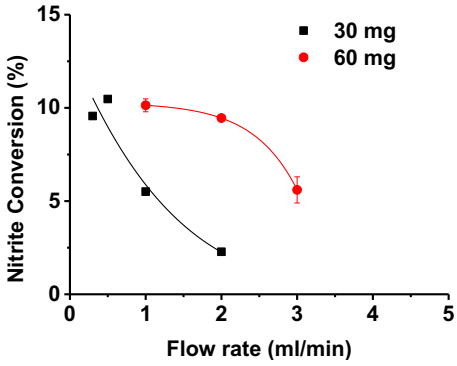

Figure 6 Influence of CNF particles loading and flow rate on nitrite conversion, with 1.3 wt% Pd on CNFs particles of 110µm

Figure 6 shows the effect of flow rate on nitrite conversion for two different catalyst loadings in flow-over mode. Catalyst loading (30 and 60 mg) and particle size (110µm) were similar to the flow-through tests above in Figure 5. It can be seen clearly that the conversion is significantly lower for flow-over experiments compared to flow-through experiments (Figure 5a), for both catalyst loadings.

4.4 Discussion

All experiments were performed with 0.217 mmol/L NO_2^- and 0.39 mmol/L H_2, resulting in maximal conversion of 21% and 28% for NO_2^- and H_2, respectively. Thus, the experiments are done under, or close to, differential conditions (conversions <15%). The maximal change in pH, due to consumption of H^+ during one experiment (Equation 1 and 2), is from 7 to 9.8. The variation in the final pH between all experiments reported is in the window between 9.3 and 9.8. In literature increasing pH is shown to result in decreasing activity and increasing ammonium selectivity [20, 21]. These effects are minor in this pH window compared to the differences reported in this study.

In all cases an increase in flow rate results in lower conversions. This confirms expectations; when the contact time with the catalyst particles is shorter, the conversion decreases.

4.4.1 Particle size

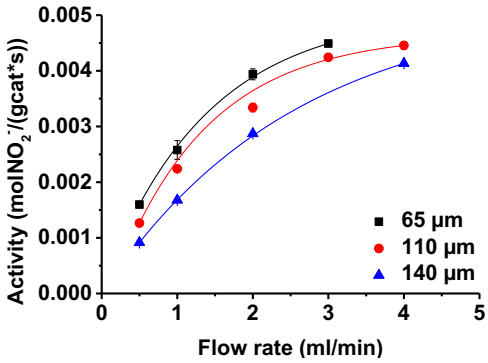

Figure 7 Influence of CNF particle size and flow rate on activity per gram catalyst with 1.3 wt% Pd on 30 mg CNFs of 110 µm in flow-through mode

Figure 7 shows the influence of particle size as well as flow rate on the catalyst activity per gram catalyst, calculated based on the data in Figure 4a. Clearly, activity per gram catalyst increases with increasing flow rate, suggesting significant concentration gradients at the external surface of the CNF particles. Increasing flow rates would decrease the thickness of the stagnant layer, and thus the external concentration gradient. Also, the activity increases with decreasing particle size, which

can be attributed to both internal as well as external concentration gradients. The effect of the flow rate suggests that external mass transfer limitation is dominant under the conditions applied. Figure 4b shows high ammonium selectivity for the biggest particles (140 µm), whereas both smaller particle sizes resulted in identical selectivity at constant conversion. The particle size distribution for the 140 µm fraction (Figure 3) shows a wider distribution, compared to the smaller fractions, with more large particles present. These larger particles are determining for the decrease in activity shown in Figure 7. High H_2 concentration as well as high pH are both favorable for ammonium formation. The observation that smaller particles show lower ammonium selectivity than larger particles suggests that transport limitation of nitrite and/or protons is dominant over transport limitation of hydrogen.

4.4.2 CNF particles loading

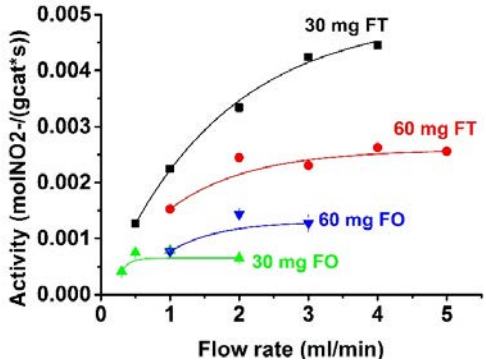

Figure 8 Influence of CNF particles loading and flow rate on activity per gram catalyst with 1.3 wt% Pd on CNFs particles of 110 µm; in flow-through (FT) and flow-over (FO) mode

Figure 8 shows the effect of the amount of catalyst used on the activity per gram catalyst, for both modes of operation, i.e. flow-through and flow-over. These experiments were done with relatively small particles (110 µm) to minimize the diffusion limitations as discussed above.

Clearly, flow-over experiments result in lower activity than flow-through experiments, suggesting more diffusion limitations in the flow-over experiments. This agrees well with the fact that the diffusion length in flow-through mode is equal to the

radius of the catalyst particles (55 micrometer), whereas the diffusion length in flow-over mode is equal to the thickness of the catalyst layer, varying between 450 and 800 micrometer.

The effects of amount of catalyst in Figure 8 are counter intuitive, both for flow-over and flow-through operation. In flow-through mode, the activity per gram decreases significantly when increasing the thickness of the catalyst layer, whereas a constant value would be expected. The effect is certainly too large to be attributed to differences in conversion level as the experiments are performed close to differential conditions. Even more surprising is the observation that the activity per gram increases with increasing amount of catalyst in flow-over mode; in this case a decrease was anticipated if the system would be determined by diffusion limitations in the layer.

We tentatively assign both effects to changes in the morphology of the CNF layer when increasing the catalyst amount. We showed in previous work [16] that the density of the CNF layer increases with the thickness of the layer. Inhomogeneity in the layer thickness can therefore easily cause tunneling of liquid through relatively porous thin patches in the layer, causing inhomogeneous liquid distribution and low conversion in flow-through mode. On the other hand, such uneven distribution of catalyst over the layer would also cause increased surface roughness of the external surface of the catalyst layer. This contributes to increased activity in flow-over mode.

Normally the extent of internal and external diffusion limitations can be evaluated through the Thiele modulus/Weisz-Prater criterion and the Carberry number respectively. Unfortunately for this system we were unable to determine the porosity due to the CNFs being too brittle for Hg porosimetry. In addition, Hg porosimetry and N_2 adsorption assume a classical pore system of certain sizes, our CNF layer mimics the inverse structure of such a classical pore structure, therefore the usually applied theory cannot be used. Measurements are further complicated by the porous filter structure used as the support for the CNF layer. Rough estimation of the porosity by calculating the volume from density and weight and comparing this with the actual occupied volume is not possible because of the penetration of the CNFs into the pores of the filter. Another unknown factor is the Pd particle size, despite various efforts to

determine this through chemisorption. Tortuosity has not been measured, but can be estimated as 1 because of the extremely open structure of the CNF particles.

In summary, we demonstrated that a catalytic reactor with immobilized CNF-supported Pd catalyst indeed shows catalytic activity, but that efficient catalyst use needs further optimization.

4.5 Conclusions

In this study an immobilized layer of CNF agglomerates, loaded with 1.3 wt% Pd, is catalytically tested in nitrite hydrogenation. It is observed that activity per gram catalyst increases with decreasing particle size, pointing to both internal and external mass transfer limitation. Furthermore, activity increases with increasing flow rate, indicating that external diffusion limitations are dominating.

Flow-through experiments clearly result in higher activity compared to flow-over experiments for identical layers (both layer thickness and particle size). This we assigned to stronger diffusion limitations in flow-over experiments as the diffusion length is much larger (450 to 800 micrometer) compared to flow-through experiments (particle radius 55 micrometer).

Counter intuitive results for increasing amount of catalyst are tentatively assigned to changes in the morphology of the CNF layer. Inhomogeneity in thin CNF layers causes maldistribution and tunneling of the liquid in flow-through mode. Concurrent increase of the roughness of the outer surface enhances activity in flow-over mode.

Acknowledgements

This work took place within the framework of the Institute for Sustainable Process Technology (ISPT). The authors gratefully acknowledge Dr. Irina Simakova from the Boreskov Institute of Catalysis for making XRF available, ing. Bert Geerdink for essential assistance in designing the set-ups, Mark Smithers for SEM micrographs and Karin Altena-Schildkamp and ing. Cindy Huiskes for performing N_2 adsorption experiments.

[1] F. Kapteijn, T. A. Nijhuis, J. J. Heiszwolf, and J. A. Moulijn, "New non-traditional multiphase catalytic reactors based on monolithic structures," *Catalysis Today,* vol. 66, pp. 133-144, 3/30/ 2001.

[2] K. Pangarkar, T. J. Schildhauer, J. R. van Ommen, J. Nijenhuis, F. Kapteijn, and J. A. Moulijn, "Structured Packings for Multiphase Catalytic Reactors," *Industrial & Engineering Chemistry Research,* vol. 47, pp. 3720-3751, 2008/05/01 2008.

[3] T. Boger, A. K. Heibel, and C. M. Sorensen, "Monolithic Catalysts for the Chemical Industry," *Industrial & Engineering Chemistry Research,* vol. 43, pp. 4602-4611, 2004/08/01 2004.

[4] M. Grasemann, A. Renken, M. Kashid, and L. Kiwi-Minsker, "A novel compact reactor for three-phase hydrogenations," *Chemical Engineering Science,* vol. 65, pp. 364-371, 2010.

[5] B. Averill, J. Moulijn, R. van Santen, and P. van Leeuwen, *Catalysis: An Integrated Approach: An Integrated Approach* vol. 123: Elsevier, 1999.

[6] T. A. Nijhuis, M. T. Kreutzer, A. C. J. Romijn, F. Kapteijn, and J. A. Moulijn, "Monolithic catalysts as efficient three-phase reactors," *Chemical Engineering Science,* vol. 56, pp. 823-829, 2// 2001.

[7] S. Roy, T. Bauer, M. Al-Dahhan, P. Lehner, and T. Turek, "Monoliths as multiphase reactors: a review," *AIChE journal,* vol. 50, pp. 2918-2938, 2004.

[8] L. K.-M. P. Tribolet, "Palladium on carbon nanofibers grown on metallic filters as novel structured catalyst," *Catalysis Today,* vol. 2005, pp. 337-343, 2005.

[9] P. W. A. M. Wenmakers, J. van der Schaaf, B. F. M. Kuster, and J. C. Schouten, ""Hairy Foam": carbon nanofibers grown on solid carbon foam. A fully accessible, high surface area, graphitic catalyst support," *Journal of Materials Chemistry,* vol. 18, pp. 2426-2436, 2008.

[10] N. Jarrah, J. G. van Ommen, and L. Lefferts, "Development of monolith with a carbon-nanofiber-washcoat as a structured catalyst support in liquid phase," *Catalysis Today,* vol. 79–80, pp. 29-33, 4/30/ 2003.

[11] N. A. Jarrah, F. Li, J. G. van Ommen, and L. Lefferts, "Immobilization of a layer of carbon nanofibres (CNFs) on Ni foam: A new structured catalyst support," *Journal of Materials Chemistry,* vol. 15, pp. 1946-1953, 2005.

[12] J. K. Chinthaginjala, D. B. Thakur, K. Seshan, and L. Lefferts, "How Carbon-Nano-Fibers attach to Ni foam," *Carbon,* vol. 46, pp. 1638-1647, 11// 2008.

[13] S. Pacheco Benito and L. Lefferts, "The production of a homogeneous and well-attached layer of carbon nanofibers on metal foils," *Carbon,* vol. 48, pp. 2862-2872, 8// 2010.

[14] R. M. Tiggelaar, D. B. Thakur, H. Nair, L. Lefferts, K. Seshan, and J. G. E. Gardeniers, "Influence of thin film nickel pretreatment on catalytic thermal chemical vapor deposition of carbon nanofibers," *Thin Solid Films,* vol. 534, pp. 341-347, 2013.

[15] D. B. Thakur, R. M. Tiggelaar, J. G. E. Gardeniers, L. Lefferts, and K. Seshan, "Carbon nanofiber based catalyst supports to be used in microreactors: Synthesis and characterization," *Chemical Engineering Journal,* vol. 160, pp. 899-908, 6/15/ 2010.

[16] J. M. Roemers-van Beek, J. G. van Ommen, and L. Lefferts, "Immobilization of carbon nanofibers (CNFs) on a stainless steel filter as a catalyst support layer," *Catalysis Today,* vol. 301, pp. 134-140, 2018.

[17] G. S. Metals. Available: http://www.gkn.com/sintermetals/media/Brochures Library/Capabilities - Porous Metal Filters/GKN Filter Technology SIKA-R IS AS EN.pdf, last accessed November 2016

[18] S. Hörold, K. D. Vorlop, T. Tacke, and M. Sell, "Development of catalysts for a selective nitrate and nitrite removal from drinking water," *Catalysis Today,* vol. 17, pp. 21-30, 1993/05/26/ 1993.

[19] S. Hörold, T. Tacke, and K. D. Vorlop, "Catalytical removal of nitrate and nitrite from drinking water: 1. Screening for hydrogenation catalysts and influence of reaction conditions on activity and selectivity," *Environmental Technology,* vol. 14, pp. 931-939, 1993/10/01 1993.

[20] J. K. Chinthaginjala and L. Lefferts, "Support effect on selectivity of nitrite reduction in water," *Applied Catalysis B: Environmental,* vol. 101, pp. 144-149, 2010/11/22/ 2010.

[21] S. D. Ebbesen, B. L. Mojet, and L. Lefferts, "Effect of pH on the Nitrite Hydrogenation Mechanism over Pd/Al2O3 and Pt/Al2O3: Details Obtained with ATR-IR Spectroscopy," *The Journal of Physical Chemistry C,* vol. 115, pp. 1186-1194, 2011/02/03 2011.

Chapter 5

Conclusions and Recommendations

The work as shown in this thesis revolves around the central idea of a novel support structure using carbon nanofibers (CNFs) to enable reversible catalyst loading. The design of the novel support structure, including a binder layer of grown CNFs, raised some questions about the initiation of CNF growth from polycrystalline metal. Therefore the first part of this thesis focusses on more fundamental questions about CNF growth initiation. After that, in the second part, we produce a model of the novel support structure, showing the feasibility of this support structure under operating conditions and the possibility of removal of deactivated catalyst from the reactor. In the last part we test the model support structure in nitrite hydrogenation in two different flow designs. The results are evaluated in terms of the diffusion limitations this design is subject to.

5.1 CNF growth initiation

In **Chapter 2** initiation of CNF growth is studied on polycrystalline nickel. Previous work in our group has shown the initiation on reduced nickel (under 25000 Pa C_2H_4) occurs through NiC_3, but nickel oxide initiates CNF growth too fast to observe its initial stages. Nickel oxide reduces to nickel nuclei, but an open question, as posed by Jarrah *et al.* [1], remains if these nickel nuclei form NiC_3 particles. To be able to study this CNF growth initiation on nickel oxide in more detail, we inhibit the CNF growth by using extremely low ethylene concentrations (50 Pa). This is conducted both under atmospheric conditions through extreme dilution of ethylene and under low pressure conditions through introduction of very low quantities of ethylene in an ESEM chamber.

Reduced samples were tested under these extreme dillutions for comparison with previous work in our group. As shown in Chapter 2.3.1, the reduced samples showed only few scattered CNFs under extremely dilluted C_2H_4 at atmospheric conditions (Chapter 2, Figure 2), or in the ESEM no CNF growth at all. We attribute this to the fast diffusion of carbon to the bulk of the Ni foam in comparison to the slow supply of carbon through the low pressure carbon containing gas. This demonstrates the inhibition of the CNF growth, slowing down the CNF growth initiation.

On oxidized nickel samples this study shows that NiO is still present when CNF growth initiates, as shown in Chapter 2.3.3.2. This nickel oxide is hypothesized to

isolate the Ni nanoparticles, forming during reduction of the NiO layer, from the bulk Ni. Through this isolation, C diffusion to the bulk and/or sintering of the Ni nanoparticles with the polycrystalline nickel in the foam are prevented. No NiC_3 could be observed due to the extremely low carbon concentrations used.

As discussed in Chapter 2.4, at present time it is impossible to determine the exact function of the isolating NiO layer. To distinguish between the C diffusion to the bulk Ni and the sintering of the Ni nanoparticles, information on both structure changes below the surface, in the NiO layer (a 'bulk' process) and CNF growth (surface process) is needed. The problem here is that very localized analysis is needed inside the 'bulk' of a sample coupled to, but observed seperately from, a phenomenon observed at the surface, preferably on a larger scale. This can not be done with only one characterization technique. To continue the microscopic experiments of Chapter 2 a coupling of for instance *in-situ* TEM with *in-situ* SEM could add valuable information.

During unsuccesful CNF growth experiments in the ESEM some interesting phenomena were observed. Under certain gas compositions in the ESEM chamber we observed oscillations of dark contrast patches. This indicates carbon precipitation and afterwards dissolving into the nickel surface under a constant gas composition. Also precipitation patterns of carbon on polycrystalline nickel foam were observed *in-situ*, following grain boundaries and not crossing grain boundaries, as shown in Chapter 2, SI Movie 1, during the ESEM experiments. Continuation of these experiments with more focus on the link with graphene growth seems promising for fundamental research on the interaction between Ni and carbon.

Conducting CNF growth experiments with extremely low ethylene concentrations directly on the stainless steel filters used in Chapter 3 and 4 proved more complex than anticipated. Stainless steel consists mainly of iron (65 wt%), but also 12 wt% Ni. CNF growth under atmospheric conditions, as shown in Chapter 3, shows metal particles in the tips of the CNFs. SEM-EDX analysis showed these are Fe particles. CNF growth on stainless steel is much slower (carbon deposition in mg/cm^2h) than on nickel, as shown for metal foils by Pacheco et al. [2]. Under the extremely diluted gas pressures presented in Chapter 2 CNF growth on stainless steel is not achieved at all. Therefore it would be interesting to study CNF growth from

polycrystalline nickel alloyed with increasing amounts of iron, to observe the balance between faster CNF growth from nickel particles and slower CNF growth from iron particles. This could also be studied at atmospheric pressure with higher ethylene concentrations. In the case of ESEM experiments, this would quickly hit operational limits, at least for enabling *in-situ* characterization.

5.2 Reversible catalyst loading

In **Chapter 3** a model of the novel catalyst support structure is achieved and tested for stability under operational conditions. In the original idea a 3D open foam structure was envisioned as support structure. In this study this is simplified to a filter, effectively reducing the system to the 2D surface of a porous structure. On this surface an immobilized CNF layer can be achieved as a filter cake.

The as-received CNF agglomerates were separated into three fractions before layers were deposited. As discussed in Chapter 3.3.2, the 150μm fraction is selected for its reproducible immobilized layers and abundant availability after separation. This fraction consists of particles in the range of 30-500 μm, with an (volume) average particle size of 150 μm.

The immobilized CNF layer consists of 25 mg of CNFs of the 150μm fraction. This layer is tested for stability in a home-designed set-up where MilliQ water is flown through a chamber on top of the substrate, subjecting the immobilized CNF agglomerates layer to a shear force. In Chapter 3.3.5 (Figure 8) we show that the immobilized CNF layer is a stable catalyst support layer up to 0.18 m/s flow over the layer. This also shows the immobilized CNF layer can be removed by increasing shear force at flow rates above 0.18 m/s. At high flow rates (>0.7 m/s) almost all the CNFs are removed (>85%), and we anticipate that total removal will be achieved at even higher flowrates.

In Chapter 3.3.6 it is shown that an increase in pressure drop during immobilization increases the stability of the CNF layer (Figure 10). This indicates increased adherence between the surface of the filter and the CNF agglomerates layer. During flow tests, pieces of the entire immobilized CNFs layer are removed from the filter, leaving only bare filter surface (Figure 9). This shows the interaction between the

CNF agglomerates and the stainless steel surface is weaker than the interaction between CNF agglomerates within the layer.

Permeability of the CNF layer depends on the particle size of the CNF agglomerates, shown in Chapter 3.3.4. Repetitive exposure to the 90 mbar pressure drop during permeability tests results in densification of the CNF layer, also depending on the particles size of the CNFs. However this densification has no effect on the stability of the immobilized CNF layer.

This shows that the penetration of the CNF agglomerates into the pore mouths of the filter is the determining factor for the stability of the immobilized CNF layer. As shown in Chapter 3.3.6, higher pressure drop during deposition results in higher stability of the CNF layer, this is caused by deeper penetration of the CNF agglomerates into the pore mouths while the CNF layer is deposited. The stability of the CNF layer is not influenced by densification. The difference is that the CNF layer before the densification tests has already been established and the CNF particles are already interacting with each other. During the densification tests the entire layer only gets compressed, but is not pushed deeper into the pores.

The addition of a binder layer consisting of CNFs grown directly from (and thus anchored to) the stainless steel filter is explored to manipulate the bonding between the stainless steel surface and the CNF agglomerates. Originally these two types of CNFs, both grown and deposited agglomerates, were theorized to have the same kind of interaction with each other as occurs between the CNF agglomerates. Since the grown CNFs are attached to the stainless steel surface this would provide extra anchorage for the CNF agglomerates. Strong attachment of CNFs to nickel foam is known [3, 4], so the attachment between the two different types of CNFs is easier to break than the attachment of the grown CNFs to the stainless steel surface. This is similar to the principle of Velcro [5], where you can attach two layers and tear them apart again without diminishing the capability to bond again. This enables specific removal of only the CNF agglomerates.

However, in Chapter 3.3.7 this binder layer of grown CNFs is shown to decrease the stability of the immobilized CNF layer. This grown CNF layer decreases the surface roughness of the stainless steel filter, apparently weakening the interaction between the

CNF agglomerates and the stainless steel filter. This means that surface roughness is dominant over entanglement of CNF agglomerates with the grown CNF layer for stability of the immobilized CNF layer.

A thorough study of the removal and re-application of the immobilized CNF layer is recommended to explore the feasibility of the repeated reversible loading on the same support structure. Removal of the immobilized CNF layer can be achieved not only through an increase of the shear force flow rate but also by back flushing. Initial tests have been conducted on back flush through the stainless steel filter and removal rates of the CNF layer seem promising (>92%).

Stainless steel as metal support was chosen because of its ability to grow CNFs directly from the support. As the grown CNF layer has a negative effect on stability, as shown in Chapter 3.3.7, structured supports that do not have any capability to grow CNFs directly become more attractive. Therefore an exploration of alternative foam substrates, like carbon based filter or ceramic filter, is recommended.

This model system is a simplification and seems to meet the necessary criteria for a future application (in terms of layer stability and removability). However, an exploration of the above described, original idea with a 3D system is still very interesting. A possible next step between 2D and 3D would be to have a highly porous support with a gradient in the pore size, shown in Figure 1, where the CNF agglomerates can be loaded inside the porous structure through filtration like in Chapter 3. In Chapter 3 an increase in layer thickness leads to less stability. However if the CNFs are immobilized inside the porous structure an increase in loading of the CNF agglomerates (with catalyst particles) would be possible, without decreasing the stability. This is not fully 3D, as the interaction with the porous structure during immobilization is still not 3D. This would necessitate a few changes compared to the current 2D model. During operation, in a reactor as shown in Chapter 3, Figure 12, it would be necessary to use a flow through design, because flow over would not use the entire catalyst layer. For removal it would be necessary to use back-flush operation. After this, functionalization of the inner surface of the porous structure could be explored to really fully make the step to a 3D immobilization step.

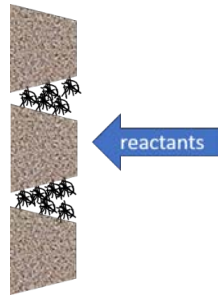

Figure 1 Graphical representation of a porous structured support with a gradient in pore size, CNFs immobilized inside the pores.

Further work is needed and many variables (e.g. different porous supports, loading inside the structure, pore/particles size balance) can still be explored to develop this concept and enable implementation in real operational catalytic reactors. At the end of this Chapter an idea for a reactor design using this structured support can be found.

5.3 Nitrite hydrogenation

In Chapter 4 the model catalyst support as described in Chapter 3 is tested in catalytic nitrite hydrogenation as a model reaction. The CNF agglomerates are loaded with 1.3 wt% Pd before immobilization of the CNF agglomerates. All experiments are done at or close to differential conditions. In all cases increasing flow rates show decreasing conversions; shorter contact time with the catalyst particles decrease conversions, as can be expected. However, when converting to activity per gram catalyst, increasing flow rates show increasing activity per gram catalyst.

Decreasing particles size of the CNF agglomerates results in increasing activity per gram catalyst (Chapter 4.4.1, Figure 8), indicating mass transfer limitations, which could be both internal and external. The increasing activity per gram catalyst with increasing flow rates, indicate that external diffusion limitations are dominant.

Two different operation regimes are tested; flow through the Pd-loaded, immobilized CNF layer and flow over the surface of the Pd-loaded, immobilized CNF layer. Identical layers with the same layer thickness and particle size were compared for both flow-over and flow-through experiments. Flow-through experiments clearly result in higher activity compared to flow-over experiments, as was shown in Chapter

4.4.2, Figure 9. This is not surprising as the diffusion length in flow-over experiments (450 to 800 μm) is much larger than in flow-through experiments (55 μm), thus showing stronger diffusion limitations.

As discussed in Chapter 4.4.2, at first glance the effect of an increased amount of Pd-loaded CNF agglomerates seems counter intuitive. However we assign this (tentatively) to morphological differences in the CNF agglomerates layer due to the immobilization method. As demonstrated in Chapter 3, an increase in amount of CNF agglomerates results in a denser layer and thus stronger deposition forces. This results in higher susceptibility towards maldistribution and tunneling caused by inhomogeneities in the CNF agglomerates layer. In flow-through mode this results in a significant decrease in activity per gram catalyst, because the CNF layer is only partially used due to maldistribution and tunneling. However, in flow-over mode the increased surface roughness at the external surface of the CNF agglomerates layer enhances activity per gram catalyst, by offering additional contact surface.

Initial nitrite hydrogenation tests were conducted on a CNF layer directly grown on the stainless steel filter, as the layer discussed as a binder layer in Chapter 3. In Chapter 3 we determined these growth catalyst particles are Fe particles, based on SEM with EDX. These Fe particles are reactive, as shown in Figure 2, in nitrite hydrogenation without addition of any other catalyst particles, even without H_2 (Figure 2b). This has also been shown previously by Aran *et al.* [6]. Three reduction reaction have been suggested in literature.

$$3Fe^0 + NO_2^- + 8H^+ \rightarrow 3Fe^{2+} + NH_4^+ + 2H_2O \qquad \text{Equation 1}$$

$$3Fe^0 + 2NO_2^- + 8H^+ \rightarrow 3Fe^{2+} + N_2 + 4H_2O \qquad \text{Equation 2}$$

$$Fe^0 + NO_2^- + 6H_2O \rightarrow 3Fe(OH)_2 + NH_4^+ + 2OH^- \qquad \text{Equation 3}$$

In this research the addition of a second reactive metal particle, Fe, in addition to the Pd we are using as catalyst, is an unwanted complication making observations less clear. In Chapter 3 we concluded the use of a grown CNF binder layer has only disadvantages for this specific system. The elimination of this binder layer also means there are no longer Fe particles present, this made for clearer observations. However,

for future practical applications it should be noted that this reactivity of Fe in nitrite hydrogenation has a positive, though very temporary, effect on both conversion and ammonium selectivity.

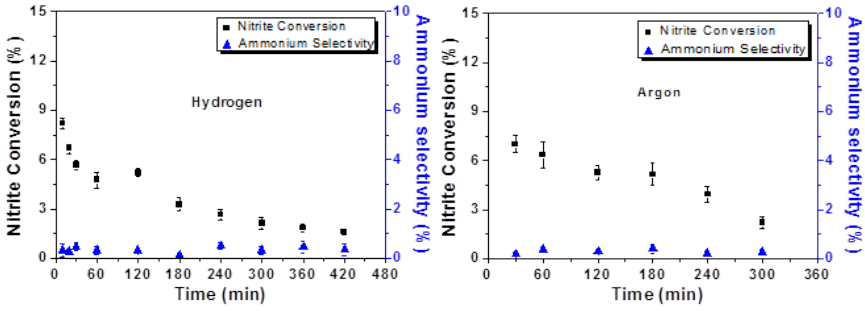

Figure 2 Nitrite conversion and ammonium selectivity after reaction with Fe particles resulting from CNF growth on stainless steel filter over time, tested using 1 ml/min of 0.22 mmol/L NO_2^- as a starting solution, saturating the solution with a) 1 atm H_2, resulting in 0.78 mmol/L H_2 and b) 1 atm Ar, resulting in 0.78 mmol/L Ar

The availability of H_2 at the catalyst surface is an important factor in the ammonium selectivity achieved in nitrite hydrogenation, as also discussed by Brunet-Espinosa et al. [7] for a porous membrane reactor filled with Pd/CNF. The lower the available H_2, the lower the ammonium selectivity. Therefore we studied the effect of the hydrogen concentration on nitrite conversion and ammonium selectivity for a CNF layer consisting of 30 mg CNFs of the 110 μm fraction loaded with 1.3 wt% Pd, in a flow through experiment. This is the same sample as used in Chapter 4.4.2 Figure 9.

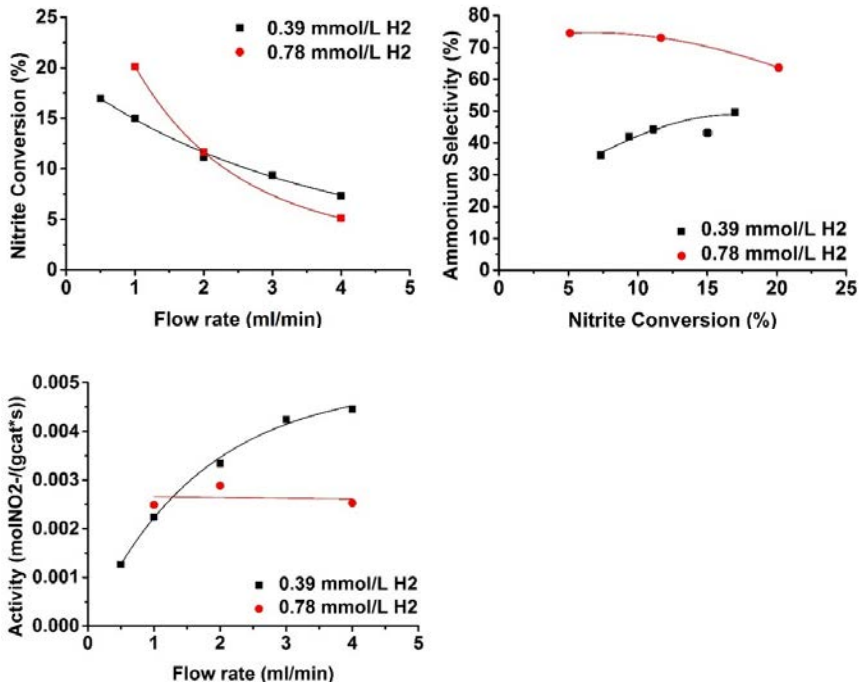

Figure 3 a) Influence of H_2 pre-saturation pressure and flow rate on nitrite conversion in flow-through, with 1.3 wt% Pd on 30 mg CNFs particles of 110 μm b) Influence of H_2 pressure and nitrite conversion on ammonium selectivity c) Influence of H_2 pressure and flow rate on activity per gram catalyst

Increase in H_2 concentration results in a clear increase in ammonium selectivity, as can be seen from Figure 3b, which is exactly as would be expected from literature. Surprising however is the activity as shown in Figure 3c. Doubling the hydrogen saturation to 0.78 mmol/L H_2 results in an independence of the activity on the flow rate. This means for the higher H_2 concentration there is an abundance of H_2 and the reaction rate does not depend on H_2 diffusion, but this does not agree with the lower activity as shown in Figure 3c. This independence of the flow rate is different from all previously shown results at lower H_2 concentration. In the case of lower H_2 concentration the activity becomes much larger. This is strange as the same amount H_2 is available at higher concentration. It could be that H_2 is choking the catalyst particles in such abundance, though with the very open CNF layer structure, small diffusion lengths in 110 μm particles and small size of H_2 this seems unlikely.

A likely explanation would seem that the maldistribution as described in Chapter 4 causes artefacts in our measurements. However these results have proven to be reproducible. The layers are produced through identical procedure, which would mean the extent of maldistribution as described in Chapter 4 should be identical. In one experiment we even conducted both experiments with 0.39 and 0.78 mmol/L H_2 in sequence on the same sample. These results match the individual experiments. This leads us to believe that, although we cannot explain this phenomenon right now, it is a phenomenon and not an artifact. Further investigation into this conundrum is advised as hydrogen concentration is an important factor in process design for both the catalyst properties and the reactor design.

A cross-over, as shown in Figure 4, between membrane microreactors as discussed by Brunet-Espinosa et al. [7] and the immobilized CNF layer as discussed in this thesis would be interesting as a continuation of this work. For this crossover an increase in membrane reactor size would be needed, to enable deposition of the CNF agglomerates. Combining the membrane reactor design with immobilization of CNF agglomerates is a simplification in preparation; replacing two metal-deposition steps and a CNF growth step by a deposition step of Pd/CNF agglomerates. If the membrane layer as discussed for the membrane reactors is first deposited on the outside, this could act as the ‘pore gradient’ we suggested above. The CNF agglomerates would be deposited on the inside by a driving force through the porous reactor wall. This means the PDMS membrane as discussed by Brunet-Espinosa et al. [7] would have to be replaced by a water-permeable membrane. This would also open up the possibility of recycling the Pd/CNF phase from the membrane reactor (through backflushing). Finding a balance between reactor size and Pd/CNF agglomerate size to create a feasible commercial reactor design will be a challenge, but arguably the biggest challenge will be on how to deposit the CNF layer uniformly on all sides of a long, round tube.

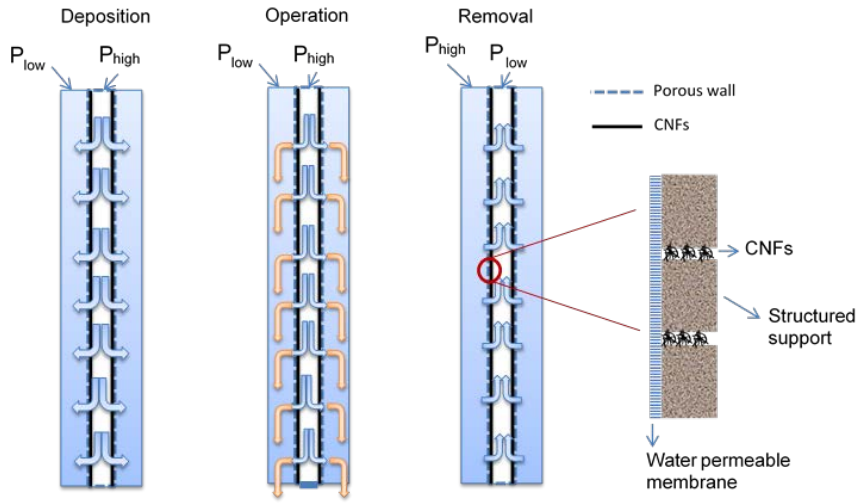

Figure 4 Schematic representation of suggested design of a reactor with a cross-over between membrane microreactors and immobilized CNF layer.

References

[1] N. A. Jarrah, J. G. van Ommen, and L. Lefferts, "Mechanistic aspects of the formation of carbon-nanofibers on the surface of Ni foam: A new microstructured catalyst support," *Journal of Catalysis,* vol. 239, pp. 460-469, 4/25/ 2006.

[2] S. Pacheco Benito and L. Lefferts, "The production of a homogeneous and well-attached layer of carbon nanofibers on metal foils," *Carbon,* vol. 48, pp. 2862-2872, 8// 2010.

[3] N. A. Jarrah, F. Li, J. G. van Ommen, and L. Lefferts, "Immobilization of a layer of carbon nanofibres (CNFs) on Ni foam: A new structured catalyst support," *Journal of Materials Chemistry,* vol. 15, pp. 1946-1953, 2005.

[4] J. Chinthaginjala, D. Thakur, K. Seshan, and L. Lefferts, "How carbon-nano-fibers attach to Ni foam," *Carbon,* vol. 46, pp. 1638-1647, 2008.

[5] G. De Mestral, "Velvet type fabric and method of producing same," US 2717437 A, 1955.

[6] H. Aran, S. P. Benito, M. Luiten-Olieman, S. Er, M. Wessling, L. Lefferts*, et al.*, "Carbon nanofibers in catalytic membrane microreactors," *Journal of membrane science,* vol. 381, pp. 244-250, 2011.

[7] R. Brunet Espinosa, D. Rafieian, R. G. H. Lammertink, and L. Lefferts, "Carbon nano-fiber based membrane reactor for selective nitrite hydrogenation," *Catalysis Today,* vol. 273, pp. 50-61, 2016/09/15/ 2016.

Summary

The work in this thesis explores a novel catalyst support design. In this design a macro-porous basis is used to immobilize a layer of carbon nanofibers (CNFs) agglomerates with the possible addition of a grown CNF binder layer. The synthesis of this grown CNF binder layer poses additional fundamental questions on CNF growth. The produced catalyst support is tested for activity and selectivity in a fast heterogeneous reaction, in this case nitrite hydrogenation in liquid phase.

In **Chapter 2** fundamental questions on the initiation of CNF growth on polycrystalline nickel are explored. The CNF growth is slowed down by using very low partial pressures of ethylene, aiming to observe the initiation. These experiments were performed under atmospheric pressure with extremely diluted ethylene (50 Pa), coupled to *ex-situ* characterization in high-resolution Scanning Electron Microscopy, X-ray diffraction and Raman spectroscopy. Additionally, *in-situ* experiments were conducted under low pressure conditions in an Environmental Scanning Electron Microscopy (ESEM) introducing very low quantities of ethylene in the chamber.

For reduced samples, atmospheric experiments showed very little CNFs and ESEM experiments showed even no CNFs at all. This is attributed to diffusion of C to the bulk of the Ni-foam preventing Ni_3C formation as a precursor of Ni nanoparticles, the CNF growth catalyst particles. CNF growth was significant on oxidized samples, but clearly slowed down by using extremely low ethylene pressure. It is shown that an isolating layer of unreduced NiO is needed between the Ni bulk and the Ni nanoparticles resulting from gradual reduction of the NiO layer, to enable CNF growth. This isolating NiO layer is hypothesized to prevent C diffusion to the bulk and/or sintering of the Ni nanoparticles with the polycrystalline nickel in the foam. At present time distinguishing between these two hypotheses is impossible.

In **Chapter 3** a catalyst support structure is produced by immobilizing a layer of CNF agglomerates on a stainless steel filter through filtration. By optimizing various parameters (*e.g.* CNF particle size, amount of CNFs used, pressure drop used) an immobilized CNF layer, stable at relatively low shear force flows (<0.18 m/s), is produced. The immobilized CNF layer can be removed by increasing the flow rate further, this enables selective removal of the catalyst particles after deactivation.

Removal of the CNF agglomerates takes place in pieces of the entire layer. This shows that the attachment of the entire layer to the surface of the stainless steel filter determines the stability of the CNF layer. Attachment between the CNF aggregates is apparently stronger than attachment to the filter. Different ways to increase attachment of the immobilized CNF layer to the stainless steel filter are attempted, *e.g.* increased pressure drop, densification, an additional binder layer. It is shown that both surface roughness of the filter on micro-scale and penetration of CNF agglomerates in the pore mouths of the stainless steel filter determine the stability of the CNF layer.

In **Chapter 4**, a Pd-loaded, immobilized CNF agglomerates layer on a stainless steel filter is tested for catalytic hydrogenation of nitrite. Activity and selectivity in nitrite hydrogenation is studied by varying several parameters, *e.g.* CNF particle size, CNF particles loading, flow regime. Flowing a H_2 saturated nitrite solution through the Pd-CNF layer results in higher reaction rates compared to flowing over the layer. This demonstrates that flow-over mode is subject to mass transfer limitations due to the relatively long diffusion distance in the Pd-CNF layer, compared to flow-through mode. Varying the CNF particle size shows external diffusion limitations at the surface of the individual CNF agglomerates dominate in flow-through mode.

In **Chapter 5** recommendations are made for future work, among others a reactor design using immobilized CNFs is proposed.

Samenvatting

Het werk in deze thesis verkent een nieuw katalysator drager ontwerp. In dit ontwerp wordt een macro-poreuze basis gebruikt voor de immobilisatie van een laag koolstof nanovezels (CNFs) agglomeraten, met mogelijk de toevoeging van een gegroeide CNF bindlaag. De synthese van deze gegroeide CNF bindlaag roept fundamentele vragen op over de CNF groei. De geproduceerde katalysator drager wordt getest op activiteit en selectiviteit in een snelle heterogene reactie, in dit geval nitriet hydrogenatie.

In **Hoofdstuk 2** worden fundamentele vragen over de initiatie van CNF groei op polykristallijn nikkel behandeld. CNF groei is vertraagd door gebruik van een zeer verlaagde ethyleen druk, met als doel de observatie van de initiatie. Deze experimenten werden uitgevoerd onder extreem verdund ethyleen (50 Pa), gekoppeld aan *ex-situ* karakterisering in hoge resolutie Scanning Electron Microscopy, X-ray diffractie and Raman spectroscopie. Daarnaast zijn *in-situ* experimenten uitgevoerd bij lage druk in een Environmental Scanning Electron Microscopy (ESEM), waarbij zeer lage ethyleen hoeveelheden in de kamer worden geintroduceerd.

Gereduceerd nikkel schuim laat in het geval van atmosferische experimenten erg weinig CNFs zien en in het geval van ESEM experimenten zijn er zelfs helemaal geen CNFs gevonden. Dit wordt toegewezen aan diffusie van C naar de bulk van het nikkel schuim, waardoor formatie van Ni_3C wordt voorkomen. Ni_3C is de voorloper van Ni nanodeeltjes, de groei katalysator voor CNF groei. Op geoxideerde samples is de CNF groei significant, maar wel duidelijk vertraagd door het gebruik van een extreem lage ethyleen druk. Er wordt getoond dat een isolerende laag van ongereduceerd NiO nodig is tussen de Ni bulk en de Ni nanodeeltjes, die ontstaan door geleidelijke reductie van de NiO laag, om CNF groei mogelijk te maken. Deze isolerende laag wordt verondersteld om C diffusie naar de bulk en/of sinteren van de Ni nanodeeltjes met het

polykristallijne nikkel in het schuim te voorkomen. Op dit moment is het niet mogelijk onderscheid te maken tussen deze twee hypotheses.

In **Hoofdstuk 3** wordt een katalysator drager geproduceerd door immobilisatie van een laag CNF agglomeraten op een roestvrij staal filter door middel van filtratie. Door optimalisatie van diverse parameters (bijv. CNF deeltjes grootte, hoeveelheid gebruikte CNFs, gebruikte drukval) is een geïmmobiliseerde CNF laag geproduceerd, die stabiel is bij relatief kleine afschuifkrachten (stroomsnelheden <0.18 m/s). De geïmmobiliseerde CNF laag kan worden verwijderd door de stroomsnelheid op te voeren, dit maakt selectieve verwijdering van katalysator deeltjes, na deactivering, mogelijk.

Verwijdering van de CNF agglomeraten vind plaats in stukken van de hele laag. Dit laat zien dat de hechting van de hele laag aan het oppervlak van het roestvrij staal filter de stabiliteit van de CNF laag bepaalt. De hechting tussen de CNF agglomeraten onderling is blijkbaar sterker dan de hechting aan het filter. Er zijn verschillende manieren geprobeerd om deze hechting te verbeteren, bijv. hogere drukval, verdichting, een extra bindlaag. Er wordt getoond dat zowel de oppervlakte ruwheid van het filter op macro-schaal als de indringdiepte van CNF agglomeraten in de poriemonden van het roestvrij staal filter bepalend zijn voor de stabiliteit van de CNF laag.

In **Hoofdstuk 4**, wordt een met Pd beladen, geïmmobiliseerde CNF agglomeraten laag op een roestvrij staal filter getest voor katalytische hydrogenatie van nitriet. Activiteit en selectiviteit in nitriet hydrogenatie worden bestudeerd door meerdere parameters te variëren, bijv. CNF deeltjes grootte, hoeveelheid gebruikte CNFs, stroomrichting. Het stromen van een met H_2 gesatureerde nitriet oplossing door de Pd-CNF laag resulteert in hogere activiteit dan stroming over de laag. Dit demonstreert dat de ‘flow-over mode’ onderhevig is aan massa transport limiteringen door de relatief lange diffusielengte in de Pd-CNF laag, vergeleken met de ‘flow-through mode’. Variatie van de CNF deeltjesgrootte laat zien dat in de ‘flow-through mode’ externe diffusielimiteringen aan het oppervlak van de individuele CNF agglomeraten dominant zijn.

In **hoofdstuk 5** worden aanbevelingen gedaan voor toekomstig werk, inclusief een voorstel voor een reactor ontwerp dat gebruik maakt van geïmmobiliseerde CNFs.

List of publications

Articles

- J.M. Roemers-van Beek, J.G. van Ommen, L. Lefferts; *Immobilization of carbon nanofibers (CNFs) on a stainless steel filter as a catalyst support layer*, Catalysis Today 301, pp 134-140, https://doi.org/10.1016/j.cattod.2017.05.031

- J.M. Roemers-van Beek, Z.J. Wang, A. Rinaldi, M.G. Willinger, L. Lefferts, *Initiation of Carbon Nanofiber Growth on Polycrystalline Nickel Foam at Low Ethylene Pressure*, Submitted to ChemCatChem

- J.M. Roemers-van Beek, J. Zhu, J.G. van Ommen, L. Lefferts, *Hydrogenation of nitrite on Pd supported on immobilized CNF agglomerates on a stainless steel filter*, In preparation

Oral presentations

- J.M. van Beek, L. Lefferts, "The Velcro effect: A dual-layered carbon nanofiber (CNF) support for reversible catalyst loading", 4th International Conference on Structured Catalysts and Reactors (ICOSCAR-4), September 25-27 2013, Beijing, China

- J.M. van Beek, J. Zhu, L. Lefferts, "A novel CNF support layer for reversible loading of catalyst particles", XVth Netherlands Catalysis and Chemistry Conference (NCCC XV), March 10-12 2014, Noordwijkerhout, The Netherlands

- J.M. van Beek, Z.J. Wang, M.G. Willinger, L. Lefferts, "Initiation of carbon nanofiber (CNF) growth from polycrystalline nickel foams", XVIth Netherlands Catalysis and Chemistry Conference (NCCC XVI), March 02-04 2015, Noordwijkerhout, The Netherlands

Poster presentations

- J.M. van Beek, D.B. Thakur, L. Lefferts**,** "Using carbon nanofiber (dis)entanglement for reversible catalyst loading", MESA+-day, September 27th 2011, Enschede, The Netherlands

- J.M. van Beek, D.B. Thakur, L. Lefferts**,** "Using carbon nanofiber (dis)entanglement for reversible catalyst loading", Netherlands Process Technology Symposium (NPS11), October 24-26 2011, Arnhem, The Netherlands

- Zhu-Jun Wang, Gisela Weinberg, Qiang Zhang, Achim Klein-Hoffmann, Robert Weatherup, Joline van Beek, Marc Georg Willinger, Robert Schlögl, "In situ characterizations of metal assisted chemical vapor deposition for growth of mono- and few layer graphene", 2nd International Symposium on Advanced Electron Microscopy for Catalysis and Energy Storage Materials (EmCat2012), February 5-8 2012, Berlin, Germany

- J.M. van Beek, D.B. Thakur, L. Lefferts**,** "Using carbon nanofiber (dis)entanglement for reversible catalyst loading", XIIIth Netherlands Catalysis and Chemistry Conference (NCCC XIII), March 05-07 2012, Noordwijkerhout, The Netherlands

- J.M. van Beek, D.B. Thakur, L. Lefferts**,** "Creating a dual-layered carbon nanofiber (CNF) support for reversible catalyst loading", Carbon in Catalysis Conference (CarboCat-V), June 28-30 2012, Bressanone-Brixen, Italy

- J.M. van Beek, D.B. Thakur, L. Lefferts**,** "Creating a dual-layered carbon nanofiber (CNF) support for reversible catalyst loading", XIVth Netherlands Catalysis and Chemistry Conference (NCCC XIV), March 11-13 2013, Noordwijkerhout, The Netherlands

- J. Zhu, J.M. van Beek, L. Lefferts, "Nitrite Hydrogenation using Pd on a Novel Carbon Nanofiber Support in a Structured Reactor", XVth Netherlands Catalysis and Chemistry Conference (NCCC XV), March 10-12 2014, Noordwijkerhout, The Netherlands

- J. Zhu, J.M. van Beek, L. Lefferts, “Nitrite Hydrogenation using Pd on a Novel Carbon Nanofiber Support in a Structured Reactor”, Netherlands Process Technology Symposium (NPS14), November 03-05 2014, Arnhem, The Netherlands

- J.M. van Beek, J. Zhu, L. Lefferts, “A novel CNF support layer for reversible loading of structured reactor with catalyst particles”, 9th International Symposium on Catalysis in Multiphase Reactors (CAMURE-9), December 7-10 2014, Lyon, France

- J.M. van Beek, J. Zhu, L. Lefferts, “A novel CNF support layer for reversible loading of structured reactor with catalyst particles”, MESA+-day, September 28th 2015, Enschede, The Netherlands

- J.M. Roemers-van Beek, Z.J. Wang, A. Rinaldi, M.G. Willinger, L. Lefferts, “Initiation of Catalytic Carbon Nanofiber Growth on Polycrystalline Nickel Foam as Catalyst Support Material”, EuropaCat, August 27-31 2017 Florence, Italy

Acknowledgements

This PhD has been a loooong journey, so these acknowledgements will also include a long list of people, please bear with me .

I would like to start with thanking everyone who was directly involved in the work of this thesis.

First of all, I want to thank Leon for giving me this opportunity and for never giving up on this thesis (although we came close sometimes). Jan, thank you for the support during my writing phase and for your ever-present optimism, I liked our discussions a lot. Jie, thanks for joining my project and conducting lots of experiments, sometimes even around the clock. You showed me and the group quite a bit of Chinese culture. Marc, thank you for the fruitful cooperation and the nice stays I had in Berlin. I am very pleased and honored that you were able to join my promotion committee as well. Zhu-Jun, thanks for your cooperation, expertise and the long hours in the ESEM room. Ali I am glad you reinforced our cooperation with your expertise and knowledge.

When I started out as a PhD I had lots of help from Vijay at a time when he was finishing his own PhD and adjusting to life as a Post-Doc. Thanks for your valuable advice and guidance. Arie, you are the man of the wild idea which sparked the hypothesis on which this PhD was started. Thanks for your ever present laugh and positive attitude.

Of course all this work would have been impossible if not for all the technical support I received. Bert you truly are the walking technical encyclopedia of our group on anything equipment or computer related. Karin is the mistress of lab supplies, lab cleanings and analysis. Tom helps anywhere he can and is a wizard with the XRF. Without the three of you I would never have made it, or at least not with my sanity intact. Thanks for all the nice talks, diners and games.

I would also like to thank the involved students, Gijs and Wouter, for their contributions. I hope I was able to teach you something, I certainly learned from you guys.

Over the years I've known quite some CPM-ers, please forgive me if I've missed someone.

Thank you Seshan for your positive and levelheaded attitude, it was a pleasure to get to know you. Barbara I loved your laugh and your singing. Sabine, Lidy and Jacqueline, thanks for your support and the nice coffee breaks. Maaike thanks for being you; your optimism and involvement were missed for a long time after you left. Thanks for the talks and the support, I hope you're still enjoying your CPM-kookboek. Dorothy, thanks for your support in the last challenging bits. It's amazing how fast I get replies sometimes. Ruben, thank you for the fun discussions about anything and everything, not in the least badminton, Oktoberfests and CNFs. Louise our talks at the coffee table, amongst others about walking, were always a pleasure.

Our office has been a pretty special place for me for quite some time. For four years I've been able to share it with Shilpa, Yingnan and Arturo. These were the best times! The companionship in our office was quite strong. Shilpa you're a good friend, we've shared quite a bit and I'm very pleased to call you my paranymph. We've always enjoyed our diner and games nights with you and James and I hope to be having lots more of those. Yingnan, I don't quite recognize that timid and quiet guy that arrived in 2010 anymore, but I sure love the guy you've become. It was amazing to see you, Yin and Milo earlier this year. Arturo, you're such a hard-working guy; if there was someone there when I came in the office at midnight, it was often you. But you always kept laughing (and teasing), which was much appreciated.

Roger (for once I'll write to you in English), we did not only share the CNFs field, but also our love for board games. I'm delighted you've agreed to be my paranymph. We would love to meet up with you, Maria and Ayla again soon for some nice diner and games evenings. We wish you lots of luck in your endeavors. Kamilla, I enjoyed your company at the coffee table, conferences and courses, you were always a positive presence. Chau we've often talked about food and gardening and I've shared your fresh Vietnamese spring rolls recipe with many people; everyone loves it! Rao and Masoud

we've often had nice times at courses and conferences, I especially remember our Schiermonnikoog walk in the snow and some games nights. Kaisa, I've enjoyed your company at the coffee table and our diners.

There's the 'older' PhDs and postdocs, I've had the pleasure of meeting Gacia, Kumar, Berta, Davide, Patrick, Igor, Inga and Zjelko. Even though some of them were already in the last stressful stages of their CPM stays, I got many sound advices. We had lots of social events, making sure the group feels like a group. Thanks for making me feel at home when I only just arrived.

Then there's the people I had a bit more overlap with. Sergio, who supervised my MSc assignment and taught me lots about CNFs. Son, who always aimed to please everyone. Marijana with her laugh, we had some quite important and open talks. Dennis, who drove the two of us all the way to north Italy, all in one day. Chris, who (rightfully) questioned everything, sometimes quite frank. Cristina with her ever-present smile and great humour. José with his 'active sites' and all-around fun attitude. Songbo, the good guy and 'Ganbei'-king. Thanks guys for making my time in CPM a memorable time.

The CPM-spirit is assured with the newer additions to our group. Tushar, my 'new' office mate. Guido, who always knows where to party. Reza, who loved meeting Evelien and unfortunately already left again. Rolf who joined as a master student working with CNFs and now has become my successor as 'the only Dutch PhD'. And Jimmy, Pengyu and Maria, who I've talked little with but heard a lot about. I'm sure you guys are doing a great job in keeping up the borrels and CPM-events.

Last but not least (on the professional side) I've also enjoyed working with Taha; we always had great discussions about CNFs and I was pleased to join your work for a bit. I would also like to thank Mark Smithers for the countless hours spent at the HR-SEM looking at fibers, strange phenomena and stainless steel and talking about sports and music. I would also like to thank the whole ISPT/HESTRE team for supporting me financially, administratively and with input and suggestions for the experimental work.

Ok done with the professional acknowledgments, now on with the private part.

First of all I would like to thank all my friends for always encouraging me and believing in me. There's quite a large group of you so thanking everyone individually is probably not a good idea, I'll do that in person some time soon. I'll just quickly sum everyone up here. Maïsha; Miriam and Jeroen; Soubhik and Jorien; Rikkert and Martha; Matthias and Marjolein; Pieter, Elly and Lotte; Susanne, Nora, Hugo and Evi; Rick, Debbie, Olivier and Thomas; Bouwe, Marloes, Elise and Owen; Jeroen and Yasira; Jeroen and Marion; Anke and Mike; Annelies and Lennard; Ivo; Maarten, Katharina and Lina; and Harm and Katharina. Some of you have experienced what a PhD is about, some of you are chemists, some like board games, or tea or nice food. Some have offered to read my thesis, others have been there for me to talk to during the difficult and stressful times of my PhD. All of you bring something unique to the mix and I hope to count you among my friends for years and years to come.

Of course the support from my family has been invaluable over the years. Sometimes it was quite hard to explain, that you work at the University, but you're still a student, you hope to 'pass' your defence, but you already finished your study. Everyone has always been very interested and supportive, even if it became confusing or if I had things on my mind nobody could understand. I have been very fortunate not only with my own family but also with my in-laws, Bert, Lily, Stephan and everyone further removed, who asked the right questions and overlooked the confusing answers.

My own family not only got me here but also extensively took the time to get to know my crazy PhD world. Han, my father, who gave me the beta genes and has been a constant support in logic and deduction. Gerwi, my mother, from whom I get the drive for social interaction and organizing fun stuff and who was proof reader of my thesis. And Karina, who shares so many of my interests, although she made the mistake of going into physics instead of chemistry, and was an invaluable support.

And last but most important of all Arnout and Evelien. Arnout the foundation upon which I build, whose support means the world to me and who I'm going to grow old with. And Evelien who has rocked my world for the past 2+ years and who has even joined me in meetings with Leon . She's an incredible little girl.